CHAPTER 4 DESIGN AND ANALYSIS

Page

4.1 INTRODUCTION

The concept of designing a material to yield a desired set of properties has received impetus from the growing acceptance of composite materials. Inclusion of material design in the structural design process has had a significant effect on that process, particularly upon the preliminary design phase. In this preliminary design, a number of materials will be considered, including materials for which experimental materials property data are not available. Thus, preliminary material selection may be based on analytically-predicted properties. The analytical methods are the result of studies of micromechanics, the study of the relationship between effective properties of composites and the properties of the composite constituents. The inhomogeneous composite is represented by a homogeneous anisotropic material with the effective properties of the composite.

The purpose of this chapter is to provide an overview of techniques for analysis in the design of composite materials. Starting with the micromechanics of fiber and matrix in a lamina, analyses through simple geometric constructions in laminates are considered.

A summary is provided at the end of each section for the purpose of highlighting the most important concepts relative to the preceding subject matter. Their purpose is to reinforce the concepts, which can only fully be understood by reading the section.

The analysis in this chapter deals primarily with symmetric laminates. It begins with a description of the micromechanics of basic lamina properties and leads into classical laminate analysis theory in an arbitrary coordinate system. It defines and compares various failure theories and discusses the response of laminate structures to more complex loads. It highlights considerations of translating individual lamina results into predicted laminate behavior. Furthermore, it covers loading situations and structural responses such as buckling, creep, relaxation, fatigue, durability, and vibration.

4.2 BASIC LAMINA PROPERTIES AND MICROMECHANICS

The strength of any given laminate under a prescribed set of loads is probably best determined by conducting a test. However, when many candidate laminates and different loading conditions are being considered, as in a preliminary design study, analysis methods for estimation of laminate strength become desirable. Because the stress distribution throughout the fiber and matrix regions of all the plies of a laminate is quite complex, precise analysis methods are not available. However, reasonable methods do exist which can be used to guide the preliminary design process.

Strength analysis methods may be grouped into different classes, depending upon the degree of detail of the stresses utilized. The following classes are of practical interest:

1. Laminate level. Average values of the stress components in a laminate coordinate system are utilized.

2. Ply, or lamina, level. Average values of the stress components within each ply are utilized.

3. Constituent level. Average values of the stress components within each phase (fiber or matrix) of each ply are utilized.

4. Micro-level. Local stresses of each point within each phase are utilized.

Micro-level stresses could be used in appropriate failure criteria for each constituent to determine the external loads at which local failure would initiate. However, the uncertainties, due to departures from the assumed regular local geometry and the statistical variability of local strength make such a process impractical.

At the other extreme, laminate level stresses can be useful for translating measured strengths under single stress component tests into anticipated strength estimates for combined stress cases. However this procedure does not help in the evaluation of alternate laminates for which test data do not exist.

Ply level stresses are the commonly used approach to laminate strength. The average stresses in a given ply are used to calculate first ply failure and then subsequent ply failure leading to laminate failure. The analysis of laminates by the use of a ply-by-ply model is presented in Section 4.3 and 4.4.

Constituent level, or phase average stresses, eliminate some of the complexity of the micro-level stresses. They represent a useful approach to the strength of a unidirectional composite or ply. Micromechanics provides a method of analysis, presented in Section 4.2, for constituent level stresses. Micromechanics is the study of the relations between the properties of the constituents of a composite and the effective properties of the composite. Starting with the basic constituent properties, Sections 4.2 through 4.4 develop the micromechanical analysis of a lamina and the associated ply-by-ply analysis of a laminate.

4.2.1 Assumptions

Several assumptions have been made for characterizing lamina properties.

4.2.1.1 Material homogeneity

Composites, by definition, are heterogeneous materials. Mechanical analysis proceeds on the assumption that the material is homogeneous. This apparent conflict is resolved by considering homogeneity on microscopic and macroscopic scales. Microscopically, composite materials are certainly heterogeneous. However, on the macroscopic scale, they appear homogeneous and respond homogeneously when tested. The analysis of composite materials uses effective properties which are based on the average stress and average strain.

4.2.1.2 Material orthotropy

Orthotropy is the condition expressed by variation of mechanical properties as a function of orientation. Lamina exhibit orthotropy as the large difference in properties between the 0° and 90° directions. If a material is orthotropic, it contains planes of symmetry and can be characterized by four independent elastic constants.

4.2.1.3 Material linearity

Some composite material properties are nonlinear. The amount of nonlinearity depends on the property, type of specimen, and test environment. The stress-strain curves for composite materials are frequently assumed to be linear to simplify the analysis.

4.2.1.4 Residual stresses

One consequence of the microscopic heterogeneity of a composite material is the thermal expansion mismatch between the fiber and the matrix. This mismatch causes residual strains in the lamina after curing. The corresponding residual stresses are often assumed not to affect the material's stiffness or its ability to strain uniformly.

4.2.2 Fiber composites: physical properties

A unidirectional fiber composite (UDC) consists of aligned continuous fibers which are embedded in a matrix. The UDC physical properties are functions of fiber and matrix physical properties, of their volume fractions, and perhaps also of statistical parameters associated with fiber distribution. The fibers have, in

general, circular cross-sections with little variability in diameter. A UDC is clearly anisotropic since properties in the fiber direction are very different from properties transverse to the fibers.

Properties of interest for evaluating stresses and strains are:

Elastic properties
Viscoelastic properties - static and dynamic
Thermal expansion coefficients
Moisture swelling coefficients
Thermal conductivity
Moisture diffusivity

A variety of analytical procedures may be used to determine the various properties of a UDC from volume fractions and fiber and matrix properties. The derivations of these procedures may be found in References 4.2.2(a) and (b).

4.2.2.1 Elastic properties

The elastic properties of a material are a measure of its stiffness. This information is necessary to determine the deformations which are produced by loads. In a UDC, the stiffness is provided by the fibers; the role of the matrix is to prevent lateral deflections of the fibers. For engineering purposes, it is necessary to determine such properties as Young's modulus in the fiber direction, Young's modulus transverse to the fibers, shear modulus along the fibers and shear modulus in the plane transverse to the fibers, as well as various Poisson's ratios. These properties can be determined in terms of simple analytical expressions.

The effective elastic stress-strain relations of a typical transverse section of a UDC, based on average stress and average strain, have the form:

$$\begin{aligned}
\bar{\sigma}_{11} &= n^*\bar{\varepsilon}_{11} + \ell^*\bar{\varepsilon}_{22} + \ell^*\bar{\varepsilon}_{33} \\
\bar{\sigma}_{22} &= \ell^*\bar{\varepsilon}_{11} + (k^* + G_2^*)\bar{\varepsilon}_{22} + (k^* - G_2^*)\bar{\varepsilon}_{33} \qquad \text{4.2.2.1(a)} \\
\bar{\sigma}_{33} &= \ell^*\bar{\varepsilon}_{11} + (k^* - G_2^*)\bar{\varepsilon}_{22} + (k^* + G_2^*)\bar{\varepsilon}_{33}
\end{aligned}$$

$$\begin{aligned}
\bar{\sigma}_{12} &= 2G_1^*\bar{\varepsilon}_{12} \\
\bar{\sigma}_{23} &= 2G_2^*\bar{\varepsilon}_{23} \qquad \text{4.2.2.1(b)} \\
\bar{\sigma}_{13} &= 2G_1^*\bar{\varepsilon}_{13}
\end{aligned}$$

with inverse

$$\begin{aligned}
\bar{\varepsilon}_{11} &= \frac{1}{E_1^*}\bar{\sigma}_{11} - \frac{\nu_{12}^*}{E_1^*}\bar{\sigma}_{22} - \frac{\nu_{12}^*}{E_1^*}\bar{\sigma}_{33} \\
\bar{\varepsilon}_{22} &= -\frac{\nu_{12}^*}{E_1^*}\bar{\sigma}_{11} + \frac{1}{E_2^*}\bar{\sigma}_{22} - \frac{\nu_{23}^*}{E_2^*}\bar{\sigma}_{33} \qquad \text{4.2.2.1(c)} \\
\bar{\varepsilon}_{33} &= -\frac{\nu_{12}^*}{E_1^*}\bar{\sigma}_{11} - \frac{\nu_{23}^*}{E_2^*}\bar{\sigma}_{22} + \frac{1}{E_2^*}\bar{\sigma}_{33}
\end{aligned}$$

where an asterisk (*) denotes effective values. Figure 4.2.2.1 illustrates the loadings which are associated with these properties.

The effective modulus k^* is obtained by subjecting a specimen to the average state of stress $\bar{\varepsilon}_{22} = \bar{\varepsilon}_{33}$ with all other strains vanishing in which case it follows from Equations 4.2.2.1(a) that

$$(\bar{\sigma}_{22} + \bar{\sigma}_{33}) = 2k^*(\bar{\varepsilon}_{22} + \bar{\varepsilon}_{33}) \qquad \text{4.2.2.1(d)}$$

Unlike the other properties listed above, k^* is of little engineering significance but is of considerable analytical importance.

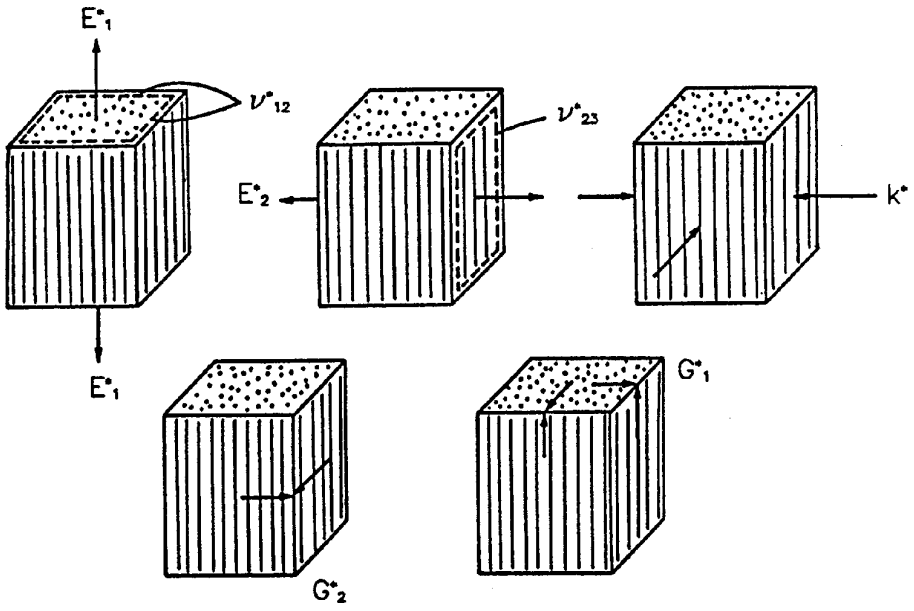

FIGURE 4.2.2.1 *Basic loading to define effective elastic properties.*

Only five of the properties in Equations 4.2.2.1(a-c) are independent. The most important interrelations of properties are:

$$n^* = E_1^* + 4k^*\nu_{12}^{*2} \qquad 4.2.2.1(e)$$

$$\ell^* = 2k^*\nu_{12}^* \qquad 4.2.2.1(f)$$

$$\frac{4}{E_2^*} = \frac{1}{G_2^*} + \frac{4\nu_{12}^{*2}}{E_1^*} \qquad 4.2.2.1(g)$$

$$\frac{2}{1-\nu_{23}^*} = 1 + \frac{k^*}{\left(1+4k^*\dfrac{\nu_{23}^{*2}}{E_1^*}\right)G_2^*} \qquad 4.2.2.1(h)$$

$$G_2^* = \frac{E_2^*}{2(1+\nu_{23}^*)} \qquad 4.2.2.1(i)$$

Computation of effective elastic moduli is a very difficult problem in elasticity theory and only a few simple models permit exact analysis. One type of model consists of periodic arrays of identical circular fibers, e.g., square periodic arrays or hexagonal periodic arrays (References 4.2.2.1(a) - (c)). These models are analyzed by numerical finite difference or finite element procedures. Note that the square array is not a suitable model for the majority of UDCs since it is not transversely isotropic.

The composite cylinder assemblage (CCA) permits exact analytical determination of effective elastic moduli (Reference 4.2.2.1(d)). Consider a collection of composite cylinders, each with a circular fiber core and a concentric matrix shell. The size of the cylinders may vary but the ratio of core radius to shell radius is held constant. Therefore, the matrix and fiber volume fractions are the same in each composite cylinder. One strength of this model is the randomness of the fiber placement, while an undesirable feature is the large variation of fiber sizes. It can be shown that the latter is not a serious concern.

The analysis of the CCA gives closed form results for the effective properties, $k^*, E_1^*, \nu_{12}^*, n^*, \ell^*$ and G_1^* and closed bounds for the properties G_2^*, E_2^*, and ν_{23}^*. Such results will now be listed for isotropic fibers with the necessary modifications for transversely isotropic fibers (References 4.2.2(a) and 4.2.2.1(e)).

$$k^* = \frac{k_m(k_f+G_m)v_m + k_f(k_m+G_m)v_f}{(k_f+G_m)v_m + (k_m+G_m)v_f} = k_m + \frac{v_f}{\frac{1}{(k_f-k_m)} + \frac{v_m}{(k_m+G_m)}} \qquad 4.2.2.1(j)$$

$$E_1^* = E_m v_m + E_f v_f + \frac{4(\nu_f-\nu_m)^2 v_m v_f}{\frac{v_m}{k_f} + \frac{v_f}{k_m} + \frac{1}{G}} \simeq E_m v_m + E_f v_f \qquad 4.2.2.1(k)$$

The last is an excellent approximation for all UDC.

$$\nu_{12}^* = \nu_m v_m + \nu_f v_f + \frac{(\nu_f-\nu_m)\left(\frac{1}{k_m}-\frac{1}{k_f}\right)v_m v_f}{\frac{v_m}{k_f} + \frac{v_f}{k_m} + \frac{1}{G_m}} \qquad 4.2.2.1(l)$$

$$G_1^* = G_m \frac{G_m v_m + G_f(1+v_f)}{G_m(1+v_f) + G_f v_m} = G_m + \frac{v_f}{\frac{1}{(G_f-G_m)} + \frac{v_m}{2G_m}} \qquad 4.2.2.1(m)$$

As indicated earlier in the CCA analysis for G_2^* does not yield a result but only a pair of bounds which are in general quite close (References 4.2.2(a), 4.2.2.1(d,e)). A preferred alternative is to use a method of approximation which has been called the Generalized Self Consistent Scheme (GSCS). According to this method, the stress and strain in any fiber is approximated by embedding a composite cylinder in the effective fiber composite material. The volume fractions of fiber and matrix in the composite cylinder are those of the entire composite. Such an analysis has been given in Reference 4.2.2(b) and results in a quadratic equation for G_2^*. Thus,

$$A\left(\frac{G_2^*}{G_m}\right)^2 + 2B\left(\frac{G_2^*}{G_m}\right) + C = 0 \qquad 4.2.2.1(n)$$

where

$$A = 3\nu_f\nu_m^2(\gamma-1)(\gamma+\eta_f) + [\gamma\eta_m + \eta_f\eta_m - (\gamma\eta_m - \eta_f)\nu_f^3][\nu_f\eta_m(\gamma-1) - (\gamma\eta_m+1)] \qquad 4.2.2.1(o)$$

$$B = -3\nu_f\nu_m^2(\gamma-1)(\gamma+\eta_f) + \frac{1}{2}[\gamma\eta_m + (\gamma-1)\nu_f + 1][(\eta_m-1)(\gamma+\eta_f) - 2(\gamma\eta_m - \eta_m)\nu_f^3] + \frac{\nu_f}{2}(\eta_m+1)(\gamma-1)[\gamma + \eta_f + (\gamma\eta_m - \eta_f)\nu_f^3] \qquad 4.2.2.1(p)$$

$$C = 3\nu_f\nu_m^2(\gamma-1)(\gamma+\eta_f) + [\gamma\eta_m + (\gamma-1)\nu_f + 1][\gamma + \eta_f + (\gamma\eta_m - \eta_f)\nu_f^3] \qquad 4.2.2.1(q)$$

$$\gamma = G_f / G_m \qquad 4.2.2.1(r)$$

$$\eta_m = 3 - 4\nu_m \qquad 4.2.2.1(s)$$

$$\eta_f = 3 - 4\nu_f \qquad 4.2.2.1(t)$$

To compute the resulting E_2^* and ν_{23}^*, use Equations 4.2.2.1(g-h). It is of interest to note that when the GSCS approximation is applied to those properties for which CCA results are available (see above Equations 4.2.2.1(j-m)), the CCA results are retrieved.

For transversely isotropic fibers, the following modifications are necessary (References 4.2.2(a) and 4.2.2.1(e)):

For k^*	k_f is the fiber transverse bulk modulus
For E_1^*, ν_{12}^*	$E_f = E_{1f}$
	$\nu_f = \nu_{1f}$
	k_f as above
For G_1^*	$G_f = G_{1f}$
For G_2^*	$G_f = G_{2f}$
	$\eta_f = 1 + 2G_{2f}/k_f$

Numerical analysis of the effective elastic properties of the hexagonal array model reveals that the values are extremely close to those predicted by the CCA/GSCS models as given by the above equations. The results are generally in good to excellent agreement with experimental data.

The simple analytical results given here predict effective elastic properties with sufficient engineering accuracy. They are of considerable practical importance for two reasons. First, they permit easy determination of effective properties for a variety of matrix properties, fiber properties, volume fractions, and environmental conditions. Secondly, they provide the only approach known today for experimental determination of carbon fiber properties.

For purposes of laminate analysis, it is important to consider the plane stress version of the effective stress-strain relations. Let x_3 be the normal to the plane of a thin unidirectionally-reinforced lamina. The plane stress condition is defined by

$$\bar{\sigma}_{33} = \bar{\sigma}_{13} = \bar{\sigma}_{23} = 0 \qquad 4.2.2.1(u)$$

Then from Equations 4.2.2.1(b-c)

$$\begin{aligned} \bar{\varepsilon}_{11} &= \frac{1}{E_1^*}\bar{\sigma}_{11} - \frac{\nu_{12}^*}{E_2^*}\bar{\sigma}_{22} \\ \bar{\varepsilon}_{22} &= \frac{\nu_{12}^*}{E_1^*}\bar{\sigma}_{11} + \frac{1}{E_2^*}\bar{\sigma}_{22} \qquad 4.2.2.1(v) \\ 2\bar{\varepsilon}_{12} &= \frac{\bar{\sigma}_{12}}{G_1^*} \end{aligned}$$

The inversion of Equation 4.2.2.1(v) gives

$$\begin{aligned} \bar{\sigma}_{11} &= C_{11}^*\bar{\varepsilon}_{11} + C_{12}^*\bar{\varepsilon}_{22} \\ \bar{\sigma}_{22} &= C_{12}^*\bar{\varepsilon}_{11} + C_{22}^*\bar{\varepsilon}_{22} \qquad 4.2.2.1(w) \\ \bar{\sigma}_{12} &= 2G_2^*\bar{\varepsilon}_{12} \end{aligned}$$

where

$$\begin{aligned} C_{11}^* &= \frac{E_1^*}{1 - \nu_{12}^{*2}E_2^*/E_1} \\ C_{12}^* &= \frac{\nu_{12}^* E_2^*}{1 - \nu_{12}^{*2}E_2^*/E_1} \qquad 4.2.2.1(x) \\ C_{22}^* &= \frac{E_2^*}{1 - \nu_{12}^{*2}E_2^*/E_1} \end{aligned}$$

For polymer matrix composites, at the usual 60% fiber volume fraction, the square of ν_{12}^* is close enough to zero to be neglected and the ratio of E_2^*/E_1^* is approximately 0.1 - 0.2. Consequently, the following approximations are often useful.

$$C_{11}^* \approx E_1^* \qquad C_{12}^* \approx \nu_{12}^* E_2^* \qquad C_{22}^* \approx E_2^* \qquad 4.2.2.1(y)$$

4.2.2.2 Viscoelastic properties

The simplest description of time-dependence is linear viscoelasticity. Viscoelastic behavior of polymers manifests itself primarily in shear and is negligible for isotropic stress and strain. This implies that the elastic stress-strain relation

$$\sigma_{11} + \sigma_{22} + \sigma_{33} = 3\,K(\varepsilon_{11} + \varepsilon_{22} + \varepsilon_{33}) \qquad 4.2.2.2(a)$$

where K is the three-dimensional bulk modulus, remains valid for polymers. When a polymeric specimen is subjected to shear strain ε_{12}° which does not vary with time, the stress needed to maintain this shear strain is given by

$$\sigma_{12}(t) = 2\,G(t)\varepsilon_{12}^{\circ} \qquad 4.2.2.2(b)$$

and $G(t)$ is defined as the shear relaxation modulus. When a specimen is subjected to shear stress, σ_{12}°, constant in time, the resulting shear strain is given by

$$\varepsilon_{12}(t) = \frac{1}{2}g(t)\sigma_{12}^{\circ} \qquad 4.2.2.2(c)$$

and $g(t)$ is defined as the shear creep compliance.

Typical variations of relaxation modulus $G(t)$ and creep compliance $g(t)$ with time are shown in Figure 4.2.2.2. These material properties change significantly with temperature. The relaxation modulus decreases with increasing temperature and the creep compliance increases with increasing temperature, which implies that the stiffness decreases as the temperature increases. The initial value of these properties at "time-zero" are denoted G_o and g_o and are the elastic properties of the matrix. If the applied shear strain is an arbitrary function of time, commencing at time-zero, Equation 4.2.2.2(b) is replaced by

$$\sigma_{12}(t) = 2\,G(t)\varepsilon_{12}(0) + 2\int_o^t G(t-t')\frac{d\varepsilon_{12}}{dt'}dt' \qquad 4.2.2.2(d)$$

Similarly, for an applied shear stress which is a function of time, Equation 4.2.2.2(c) is replaced by

$$\varepsilon_{12}(t) = \frac{1}{2}g(t)\sigma_{12}(0) + \frac{1}{2}\int_o^t g(t-t')\frac{d\sigma_{12}}{dt'}dt' \qquad 4.2.2.2(e)$$

The viscoelastic counterpart of Young's modulus is obtained by subjecting a cylindrical specimen to axial strain ε_{11}° constant in space and time. Then

$$\sigma_{11}(t) = E(t)\varepsilon_{11}^{\circ} \qquad 4.2.2.2(f)$$

and $E(t)$ is the Young's relaxation modulus. If the specimen is subjected to axial stress, σ_{11}°, constant is space and time, then

$$\varepsilon_{11}(t) = e(t)\sigma_{11}^{\circ} \qquad 4.2.2.2(g)$$

and $e(t)$ is Young's creep compliance. Obviously $E(t)$ is related to K and $G(t)$, and $e(t)$ is related to k and $g(t)$. (See Reference 4.2.2.2(a).)

The basic problem is the evaluation of the effective viscoelastic properties of a UDC in terms of matrix viscoelastic properties and the elastic properties of the fibers. (It is assumed that the fibers themselves do not exhibit any time-dependent properties.) This problem has been resolved in general fashion in References 4.2.2.2(b) and (c). Detailed analysis shows that the viscoelastic effect in a UDC is significant only for axial shear, transverse shear, and transverse uniaxial stress.

For any of average strains $\bar{\varepsilon}_{22}, \bar{\varepsilon}_{23}, \text{and}\,\bar{\varepsilon}_{12}$ constant in time, the time-dependent stress response will be

$$\begin{aligned} \bar{\sigma}_{22}(t) &= E_2^*(t)\bar{\varepsilon}_{22} \\ \bar{\sigma}_{23}(t) &= 2\,G_2^*(t)\bar{\varepsilon}_{23} \\ \bar{\sigma}_{12}(t) &= 2\,G_1^*(t)\bar{\varepsilon}_{12} \end{aligned} \qquad 4.2.2.2(h)$$

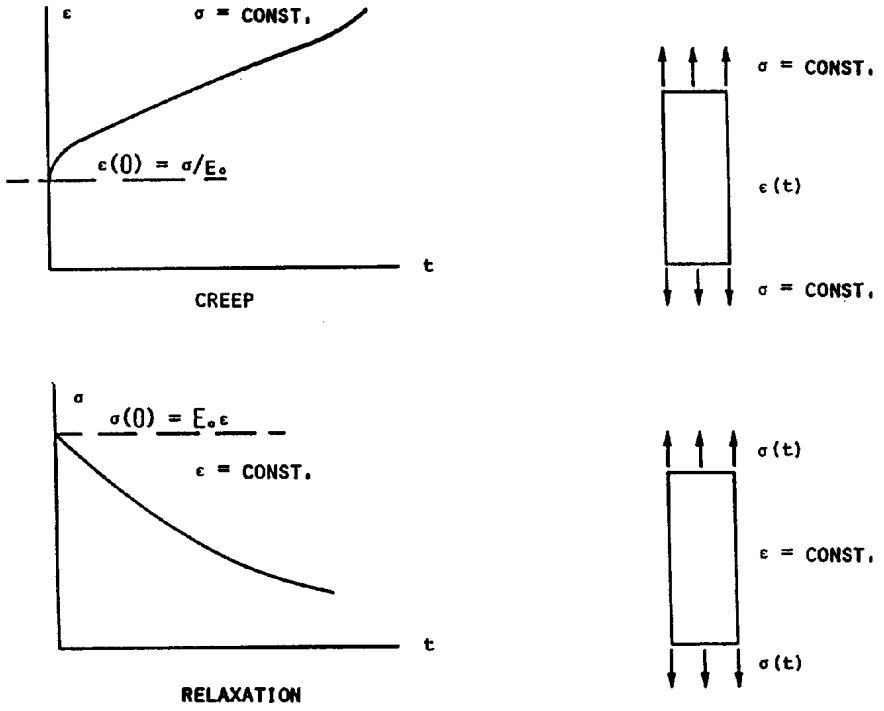

FIGURE 4.2.2.2 *Typical viscoelastic behavior.*

For any of stresses $\bar{\sigma}_{22}, \bar{\sigma}_{23}$, and $\bar{\sigma}_{12}$ constant in time, the time-dependent strain response will be

$$\begin{aligned} \bar{\varepsilon}_{22}(t) &= e_2^*(t)\bar{\sigma}_{22} \\ \bar{\varepsilon}_{23}(t) &= \frac{1}{2} g_2^*(t)\bar{\sigma}_{23} \\ \bar{\varepsilon}_{12}(t) &= \frac{1}{2} g_1^*(t)\bar{\sigma}_{12} \end{aligned} \qquad 4.2.2.2(i)$$

where material properties in Equations 4.2.2.2(h) are effective relaxation moduli and the properties in Equations 4.2.2.2(i) are effective creep functions. All other effective properties may be considered elastic. This implies in particular that if a fiber composite is subjected to stress $\bar{\sigma}_{11}(t)$ in the fiber direction, then

$$\begin{aligned} \bar{\sigma}_{11}(t) &\approx E_1^* \bar{\varepsilon}_{11}(t) \\ \bar{\varepsilon}_{22}(t) = \bar{\varepsilon}_{33}(t) &\approx \nu_{12}^* \bar{\varepsilon}_{11}(t) \end{aligned} \qquad 4.2.2.2(j)$$

where E_1^* and ν_{12}^* are the elastic results of Equations 4.2.2.2(k) with matrix properties taken as initial (elastic) matrix properties. Similar considerations apply to the relaxation modulus k^*.

The simplest case of the viscoelastic properties entering into Equations 4.2.2.2(h-i) is the relaxation modulus $G_1^*(t)$ and its associated creep compliance $g_1^*(t)$. A very simple result has been obtained for fibers which are infinitely more rigid than the matrix (Reference 4.2.2(a)). For a viscoelastic matrix, the results reduce to

$$G_l^*(t) = G_m(t)\frac{1+v_f}{1-v_f}$$
$$g_l^*(t) = g_m(t)\frac{1-v_f}{1+v_f} \qquad 4.2.2.2(k)$$

This results in an acceptable approximation for glass fibers in a polymeric matrix and an excellent approximation for boron fibers in a polymeric matrix. However, the result is not applicable to the case of carbon or graphite fibers in a polymeric matrix since the axial shear modulus of these fibers is not large enough relative to the matrix shear modulus. In this case, it is necessary to use the correspondence principle mentioned above (References 4.2.2(a) and 4.2.2.2(b)). The situation for transverse shear is more complicated and involves complex Laplace transform inversion. (Reference 4.2.2.2(c)).

All polymeric matrix viscoelastic properties such as creep and relaxation functions are significantly temperature dependent. If the temperature is known, all of the results from this section can be obtained for a constant temperature by using the matrix properties at that temperature. At elevated temperatures, the viscoelastic behavior of the matrix may become nonlinear. In this event, the UDC will also be nonlinearly viscoelastic and all of the results given here are not valid. The problem of analytical determination of nonlinear properties is, of course, much more difficult than the linear problem (See Reference 4.2.2.2(d)).

4.2.2.3 Thermal expansion and moisture swelling

The elastic behavior of composite materials discussed in Section 4.2.2.1 is concerned with externally applied loads and deformations. Deformations are also produced by temperature changes and by absorption of moisture in two similar phenomena. A change of temperature in a free body produces thermal strains while moisture absorption produces swelling strains. The relevant physical parameters to quantify these phenomena are thermal expansion coefficients and swelling coefficients.

Fibers have significantly smaller thermal expansion coefficients than do polymeric matrices. The expansion coefficient of glass fibers is 2.8 x 10^{-6} in/in/F° (5.0 x 10^{-6} m/m/C°) while a typical epoxy value is 30 x 10^{-6} in/in/F° (54 x 10^{-6} m/m/C°). Carbon and graphite fibers are anisotropic in thermal expansion. The expansion coefficients in the fiber direction are extremely small, either positive or negative of the order of 0.5 x 10^{-6} in/in/F° (0.9 x 10^{-6} m/m/C°). To compute these stresses, it is necessary to know the thermal expansion coefficients of the layers. Procedures to determine these coefficients in terms of the elastic properties and expansion coefficients of component fibers and matrix are discussed in this section.

When a laminate absorbs moisture, there occurs the same phenomenon as in the case of heating. Again, the swelling coefficient of the fibers is much smaller than that of the matrix. Free swelling of the layers cannot take place and consequently internal stresses develop. These stresses can be calculated if the UDC swelling coefficients are known.

Consider a free cylindrical specimen of UDC under uniform temperature change ΔT. Neglecting transient thermal effects, the stress-strain relations (Equation 4.2.2.1(c)) assume the form

$$\bar{\varepsilon}_{11} = \frac{1}{E_1^*}\bar{\sigma}_{11} - \frac{\nu_{12}^*}{E_1^*}\bar{\sigma}_{22} - \frac{\nu_{12}^*}{E_1^*}\bar{\sigma}_{33} + \alpha_1^*\Delta T$$
$$\bar{\varepsilon}_{22} = -\frac{\nu_{12}^*}{E_1^*}\bar{\sigma}_{11} + \frac{1}{E_2^*}\bar{\sigma}_{22} - \frac{\nu_{23}^*}{E_2^*}\sigma_{33} + \alpha_2^*\Delta T \qquad 4.2.2.3(a)$$
$$\bar{\varepsilon}_{33} = -\frac{\nu_{12}^*}{E_1^*}\bar{\sigma}_{11} - \frac{\nu_{23}^*}{E_2^*}\bar{\sigma}_{22} + \frac{1}{E_2^*}\bar{\sigma}_{33} + \alpha_2^*\Delta T$$

where

α_1^* - effective axial expansion coefficient

α_2^* - effective transverse expansion coefficient

It has been shown by Levin (Reference 4.2.2.3(a)) that there is a unique mathematical relationship between the effective thermal expansion coefficients and the effective elastic properties of a two-phase composite. When the matrix and fibers are isotropic

$$\alpha_1^* = \alpha_m + \frac{\alpha_f - \alpha_m}{\frac{1}{K_f} - \frac{1}{K_m}}\left[\frac{3(1-2\nu_{12}^*)}{E_1^*} - \frac{1}{K_m}\right]$$

$$\alpha_2^* = \alpha_m + \frac{\alpha_f - \alpha_m}{\frac{1}{K_f} - \frac{1}{K_m}}\left[\frac{3}{2k^*} - \frac{3(1-2\nu_{12}^*)}{E_1^*} - \frac{1}{K_m}\right] \qquad 4.2.2.3(b)$$

where

α_m, α_f - matrix, fiber isotropic expansion coefficients

K_m, K_f - matrix, fiber three-dimensional bulk modulus

E_1^*, ν_{12}^*, k^* - effective axial Young's modulus, axial Poisson's ratio, and transverse bulk modulus

These equations are suitable for glass/epoxy and boron/epoxy. They have also been derived in References 4.2.2.3(b) and (c). For carbon and graphite fibers, it is necessary to consider the case of transversely isotropic fibers. This complicates the results considerably as shown in Reference 4.2.2.1(c) and (e).

Frequently thermal expansion coefficients of the fibers and matrix are functions of temperature. It is not difficult to show that Equations 4.2.2.3(b) remain valid for temperature-dependent properties if the elastic properties are taken at the final temperature and the expansion coefficients are taken as secant at that temperature.

To evaluate the thermal expansion coefficients from Equation 4.2.2.3(b) or (c), the effective elastic properties, k^*, E_1^*, and ν_{12}^* must be known. These may be taken as the values predicted by Equations 4.2.2.1(j-l) with the appropriate modification when the fibers are transversely isotropic. Figures 4.2.2.3(a) and (b) shows typical plots of the effective thermal expansion coefficients of graphite/epoxy.

When a composite with polymeric matrix is placed in a wet environment, the matrix will begin to absorb moisture. The moisture absorption of most fibers used in practice is negligible; however, aramid fibers alone absorb significant amounts of moisture when exposed to high humidity. The total moisture absorbed by an aramid/epoxy composite, however, may not be substantially greater than other epoxy composites.

When a composite has been exposed to moisture and sufficient time has elapsed, the moisture concentration throughout the matrix will be uniform and the same as the boundary concentration. It is customary to define the specific moisture concentration c by

$$c = C/\rho \qquad 4.2.2.3(c)$$

where ρ is the density. The swelling strains due to moisture are functions of Δc and the swelling coefficients, β_{ij}

$$\varepsilon_{ij} = \beta_{ij}\Delta c \qquad 4.2.2.3(d)$$

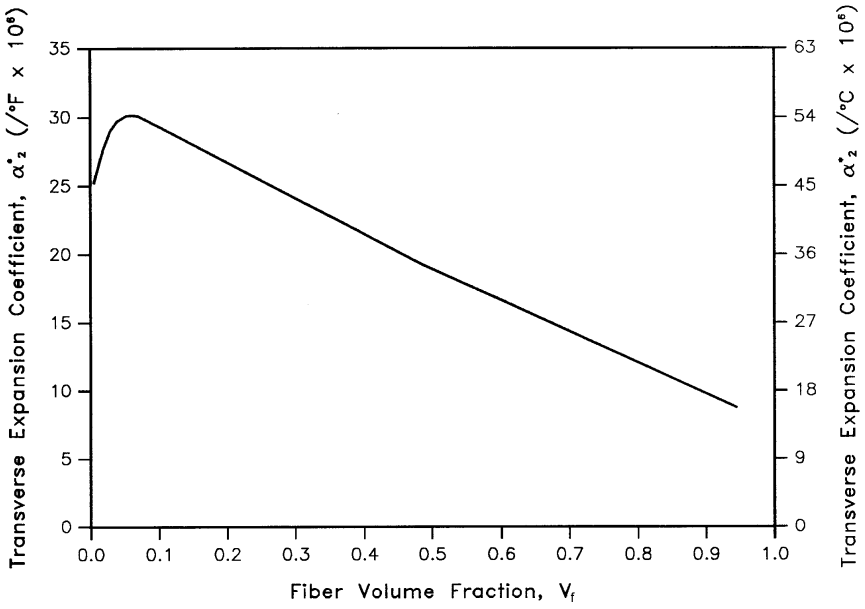

FIGURE 4.2.2.3(a) *Effect of fiber volume on thermal expansion for representative carbon/epoxy composite. E_{lf} 50 Msi (340 GPa).*

If there are also mechanical stresses and strains, then the swelling strains are superposed on the latter. This is exactly analogous to the thermoelastic stress-strain relations of an isotropic material. The effective swelling coefficients β^*_{ij} are defined by the average strains produced in a free sample subjected to a uniform unit change of specific moisture concentration in the matrix. For discussions of other aspects of moisture absorption, both transient and steady state, see References 4.2.2.3(d) and (e).

Finally, simultaneous moisture swelling and thermal expansion, or hygrothermal behavior can be considered. The simplest approach is to assume that the thermal expansion strains and the moisture swelling strains can be superposed. For a free specimen,

$$\bar{\varepsilon}_{11} = \alpha^*_1 \Delta T + \beta^*_1 \Delta c$$
$$\bar{\varepsilon}_{22} = \bar{\varepsilon}_{33} = \alpha^*_2 \Delta T + \beta^*_2 \Delta c \qquad 4.2.2.3(e)$$

In this event, the matrix elastic properties in Equations 4.2.2.3(a) and (b) may be functions of the final temperature and moisture concentration. This dependence must be known to evaluate $\alpha^*_1, \alpha^*_2, \beta^*_1,$ and β^*_2 in Equation 4.2.2.3(e).

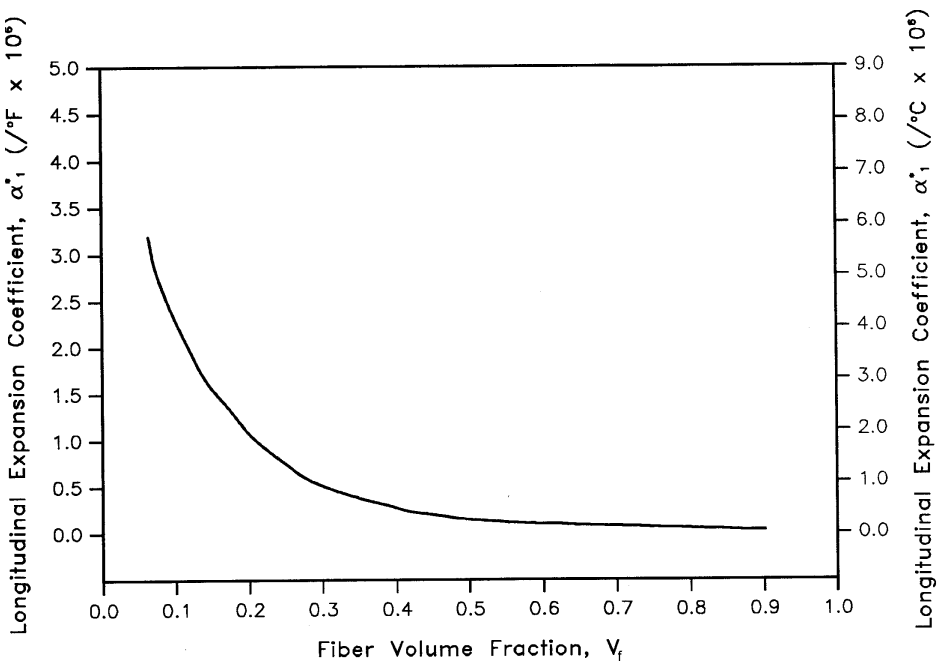

FIGURE 4.2.2.3(b) *Effect of fiber volume on thermal expansion for representative carbon/epoxy composite.* E_{lf} *= 50 Msi (340 GPa).*

4.2.2.4 Thermal conduction and moisture diffusion

The thermal conduction analysis has many similarities with the analyses for moisture diffusion, as well as electrical conduction, and dielectric and magnetic properties. Since these conductivity problems are governed by similar equations, the results can be applied to each of these areas.

Let $T(x)$ be a steady state temperature field in a homogeneous body. The temperature gradient is given by

$$H_i = \frac{\partial T}{\partial x_i} \qquad 4.2.2.4(a)$$

and the heat flux vector by

$$D_i = \mu_{ij} H_j \qquad 4.2.2.4(b)$$

where μ_{ij} is the conductivity tensor. It may be shown (Reference 4.2.2(a)) that for isotropic matrix and fibers, the axial conductivity μ_l^* is given by

$$\mu_l^* = \mu_m v_m + \mu_f v_f \qquad 4.2.2.4(c)$$

and for transversely isotropic fibers

$$\mu_l^* = \mu_m v_m + \mu_{Lf} v_f \qquad 4.2.2.4(d)$$

where μ_{lf} is the longitudinal conductivity of the fibers. The results of Equations 4.2.2.4(c) and (d) are valid for any fiber distribution and any fiber cross-section.

The problem of transverse conductivity is mathematically analogous to the problem of longitudinal shearing (Reference 4.2.2(a)). All results for the effective longitudinal shear modulus G_1^* can be interpreted as results for transverse effective conductivity μ_2^*. In particular, for the composite cylinder assemblage model

$$\mu_2^* = \mu_m \left[\frac{\mu_m v_m + \mu_f (1 + v_f)}{\mu_m (1 + v_f) + \mu_f v_m} \right]$$
$$= \mu_m + \frac{v_f}{\frac{1}{(\mu_f - \mu_m)} + \frac{v_m}{2\mu_m}} \qquad 4.2.2.4(e)$$

These results are for isotropic fibers. For carbon and graphite fibers μ_f should be replaced by the transverse conductivity μ_{2f} of the fibers (Reference 4.2.2.1(e)). As in the elastic case, there is reason to believe that Equation 4.2.2.4(e) accurately represents all cases of circular fibers which are randomly distributed and not in contact. Again the hexagonal array numerical analysis results coincide with the number predicted by Equation 4.2.2.4(e).

To interpret the results for the case of moisture diffusivity, the quantity μ_m is interpreted as the diffusivity of the matrix. Since moisture absorption of fibers is negligible, μ_f is set equal to zero. The results are then

$$\mu_1^* = \mu_m v_m$$
$$\mu_2^* = \mu_m \frac{v_m}{1 + v_f} \qquad 4.2.2.4(f)$$

These equations describe the moisture diffusivity of a composite material.

4.2.3 Fiber composites: strength and failure

The mathematical treatment of the relationships between the strength of a composite and the properties of its constituents is considerably less developed than the analysis for the other physical property relationships discussed in Section 4.2.2. Failure is likely to initiate in a local region due to the influence of the local values of constituent properties and the geometry in that region. This dependence upon local characteristics of high variability makes the analysis of the composite failure mechanisms much more complex than the analyses of the physical properties previously discussed.

Because of the complexity of the failure process, it may be desirable to regard the strength of a unidirectional fiber composite subjected to a single principal stress component as a quantity to be measured experimentally, rather than deduced from constituent properties. Such an approach may well be the practical one for fatigue failure of these composites. Indeed, the issue of determining the degree to which heterogeneity should be considered in the analysis of composite strength and failure is a matter for which there exists a considerable degree of difference of opinion. At the level of unidirectional composites, it is well to examine the effects upon failure of the individual constituents to develop an understanding of the nature of the possible failure mechanisms. This subject is discussed in the following sections. The general issue of the approach to failure analysis is treated further in laminate strength and failure.

The strength of a fiber composite clearly depends upon the orientation of the applied load with respect to the direction in which the fibers are oriented as well as upon whether the applied load is tensile or compressive. The following sections present a discussion of failure mechanisms and composite-constituent property relations for each of the principal loading conditions.

4.2.3.1 Axial tensile strength

One of the most attractive properties of advanced fiber composites is high tensile strength. The simplest model for the tensile failure of a unidirectional fiber composite subjected to a tensile load in the fiber

direction is based upon the elasticity solution of uniform axial strain throughout the composite. Generally, the fibers have a lower strain to failure than the matrix, and composite fracture occurs at the failure strain of the fibers alone. This results in a composite tensile strength, F_l^{tu}, given by:

$$F_l^{tu} = v_f F_f^{tu} + v_m \sigma_m^t \qquad 4.2.3.1$$

where F_f^{tu} - the fiber tensile strength

σ_m^t - the stress in the matrix at a strain equal to the fiber failure strain

The problem with this approach is the variability of the fiber strength. Non-uniform strength is characteristic of most current high-strength fibers. There are two important consequences of a wide distribution of individual fiber strengths. First, all fibers will not be stressed to their maximum value simultaneously. Secondly, those fibers which break earliest during the loading process will cause perturbations of the stress field near the break, resulting in localized high fiber-matrix interface shear stresses. These shear stresses transfer the load across the interface and also introduce stress concentrations into adjacent unbroken fibers.

The stress distribution at each local fiber break may cause several possible failure events to occur. The shear stresses may cause a crack to progress along the interface. If the interface is weak, such propagation can be extensive. In this case, the strength of the composite material may differ only slightly from that of a bundle of unbonded fibers. This undesirable mode of failure can be prevented by a strong fiber-matrix interface or by a soft ductile matrix which permits the redistribution of the high shear stresses. When the bond strength is high enough to prevent interface failure, the local stress concentrations may cause the fiber break to propagate through the matrix, to and through adjacent fibers. Alternatively, the stress concentration in adjacent fibers may cause one or more of such fibers to break before failure of the intermediate matrix. If such a crack or such fiber breaks continue to propagate, the strength of the composite may be no greater than that of the weakest fiber. This failure mode is defined as a weakest link failure. If the matrix and interface properties are of sufficient strength and toughness to prevent or arrest these failure mechanisms, then continued load increases will produce new fiber failures at other locations in the material. An accumulation of dispersed internal damage results.

It can be expected that all of these effects will occur before material failure. That is, local fractures will propagate for some distance along the fibers and normal to the fibers. These fractures will initiate and grow at various points within the composite. Increasing the load will produce a statistical accumulation of dispersed damage regions until a sufficient number of such regions interact to provide a weak surface, resulting in composite tensile failure.

4.2.3.1.1 Weakest link failure

The weakest link failure model assumes that a catastrophic mode of failure is produced with the occurrence of one, or a small number of, isolated fiber breaks. The lowest stress at which this type of failure can occur is the stress at which the first fiber will break. The expressions for the expected value of the weakest element in a statistical population (e.g., Reference 4.2.3.1.1(a)) have been applied by Zweben (Reference 4.2.3.1.1(b)) to determine the expected stress at which the first fiber will break. For practical materials in realistic structures, the calculated weakest link failure stress is quite small and, in general, failure cannot be expected in this mode.

4.2.3.1.2 Cumulative weakening failure

If the weakest link failure mode does not occur, it is possible to continue loading the composite. With increasing stress, fibers will continue to break randomly throughout the material. When a fiber breaks, there is a redistribution of stress near the fracture site. The treatment of a fiber as a chain of links is appropriate to the hypothesis that fracture is due to local imperfections. The links may be considered to have a statistical strength distribution which is equivalent to the statistical flaw distribution along the fibers.

Additional details for this model are given in References 4.2.3.1.1(a) and 4.2.3.1.2. The cumulative weakening model does not consider the overstress on adjacent fibers or the effect of adjacent laminae.

4.2.3.1.3 Fiber break propagation failure

The effects of stress perturbations on fibers adjacent to broken fibers are significant. The load concentration in the fibers adjacent to a broken fiber increases the probability that a second fiber will break. Such an event will increase the probability of additional fiber breaks, and so on. The fiber break propagation mode of failure was studied by Zweben (Reference 4.2.3.1.1(b)). The occurrence of the first fracture of an overstressed fiber was proposed as a measure of the tendency for fiber breaks to propagate, and, hence, as a failure criterion for this mode. Although the first multiple break criterion may provide good correlations with experimental data for small volumes of material, it gives very low failure stress predictions for large volumes of material. Additional work in this area can be found in References 4.2.3.1.3(a) and (b).

4.2.3.1.4 Cumulative group mode failure

As multiple broken fiber groups grow, the magnitude of the local axial shear stress increases and axial cracking can occur. The cumulative group mode failure model (Reference 4.2.3.1.4) includes the effects of the variability of fiber strength, load concentrations in fibers adjacent to broken fibers, and matrix shear failure or interfacial debonding which will serve to arrest the propagating cracks. As the stress level increases from that at which fiber breaks are initiated to that at which the composite fails, the material will have distributed groups of broken fibers. This situation may be considered as a generalization of the cumulative weakening model. In practical terms, the complexity of this model limits its use.

Each of these models has severe limitations for the quantitative prediction of tensile strength. However, the models show the importance of variability of fiber strength and matrix stress-strain characteristics upon composite tensile strength.

4.2.3.2 Axial compressive strength

Both strength and stability failures must be considered for compressive loads applied parallel to the fibers of a unidirectional composite. Microbuckling is one proposed failure mechanism for axial compression (Reference 4.2.3.2(a)). Small wave-length micro-instability of the fibers occurs in a manner analogous to the buckling of a beam on an elastic foundation. It can be demonstrated that this instability can occur even for a brittle material such as glass. Analyses of this instability were performed independently in References 4.2.3.2(b) and (c). The energy method for evaluation of the buckling stress has been used for these modes. This procedure considers the composite as stressed to the buckling load. The strain energy in this compressed but straight pattern (extension mode) is then compared to an assumed buckling deformation pattern (shear mode) under the same load. The change in strain energy in the fiber and the matrix can be compared to the change in potential energy associated with the shortening of the distance between the applied loads at the ends of the fiber. The condition for instability is given by equating the strain energy change to the work done by the external loads during buckling.

The results for the compressive strength, F_l^{cu}, for the extension mode is given by

$$F_l^{cu} = 2\,v_f\sqrt{\frac{v_f\ E_m E_f}{3(1-v_f)}} \qquad 4.2.3.2(a)$$

The result for the shear mode is

$$F_l^{cu} = \frac{G_m}{1-v_f} \qquad 4.2.3.2(b)$$

The compressive strength of the composite is plotted as a function of the fiber volume fraction, v_f, in Figure 4.2.3.2 for E-glass fibers embedded in an epoxy matrix. The compressive strength of glass-reinforced plastic, with a fiber volume fraction of 0.6 to 0.7, is on the order of 460 to 600 ksi (3100 to 4100 MPa). Values of this magnitude do not appear to have been measured for any realistic specimens. However, the achievement of a strength of half a million psi in a composite of this type would require an average short-

ening greater than 5%. For the epoxy materials used in this calculation, such a shortening would result in a decrease in the effective shear stiffness of the matrix material since the proportional limit of the matrix would be exceeded. Hence, it is necessary to modify the analysis to consider the inelastic deformation of the matrix. As a first approximation, the matrix modulus in Equations 4.2.3.2(a) and (b) can be replaced by a reduced modulus. A more general result can be obtained by modeling the matrix as an elastic, perfectly plastic material. For this matrix, the secant value at each axial strain value may be assumed to govern the instability. These assumptions (Reference 4.2.3.2(d)) yield the following result for the shear mode:

$$F_1^{cu} = \sqrt{\frac{v_f E_f F^{cpl}}{3(1 - v_f)}} \qquad 4.2.3.2(c)$$

where F^{cpl} is the matrix yield stress level.

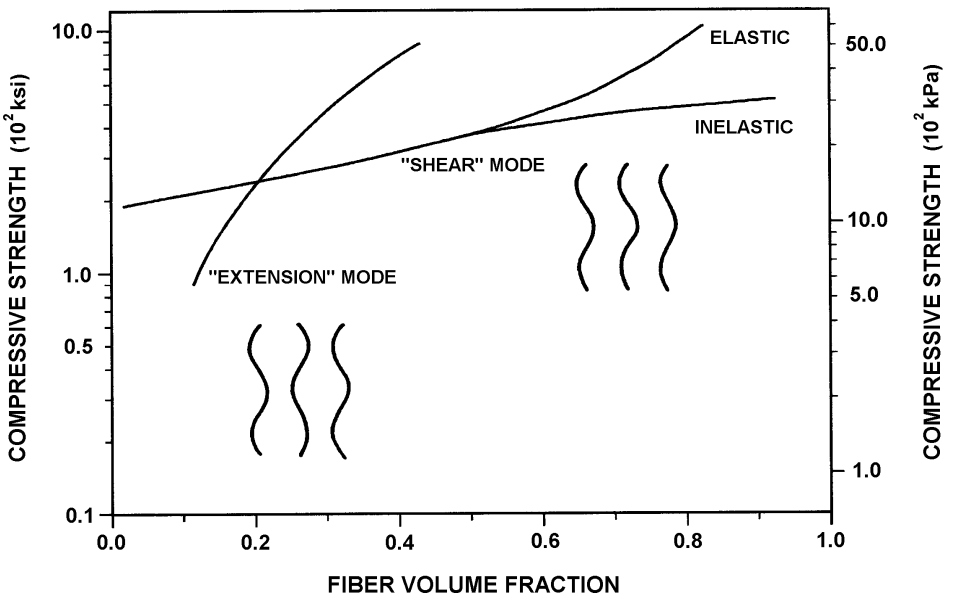

FIGURE 4.2.3.2 *Compressive strength of glass-reinforced epoxy composite.*

For the generally dominant shear mode, the elastic results of Equation 4.2.3.2(b) are independent of the fiber modulus, yet the compressive strength of boron/epoxy is much greater than that of glass/epoxy composites. One hypothesis to explain this discrepancy, is that use of the stiffer boron fibers yields lower matrix strains and less of a strength reduction due to inelastic effects. Thus, the results of Equation 4.2.3.2(c) show a ratio of $\sqrt{6}$ or 2.4 for the relative strengths of boron compared to glass fibers in the same matrix.

All of the analytical results above indicate that compressive strength is independent of fiber diameter. Yet different diameter fibers may yield different compressive strengths for composites because large diameter fibers such as boron (0.005 inch, 0.13 mm D) are better collimated than small diameter fibers, such as glass (0.0004 in, 0.010 mm D). For small diameter fibers, such as aramid and carbon, local out-of-straightness can introduce matrix shear stresses, cause fiber debonding, and produce lower instability stress levels (References 4.2.3.2(e) and 4.2.2.1(d)). Carbon and aramid fibers are anisotropic and have extremely low axial shear moduli. As a result, the elastic buckling stress in the shear mode is reduced to:

$$F^{ccr} = \frac{G_m}{1 - v_f(1 - G_m / G_{lf})} \qquad 4.2.3.2(d)$$

where G_{lf} is the fiber longitudinal shear modulus (Reference 4.2.3.2(e)). For high fiber shear moduli, this equation reduces to Equation 4.2.3.2(b).

Another failure mechanism for oriented polymeric fibers such as aramid fibers (Reference 4.2.3.2(e)) is a kink-band formation at a specific angle to the direction of compressive stress. The formation of kink-bands is attributed to the fibrillar structure of the highly anisotropic fiber and poor fiber shear strength. Breakup of the fiber into very small diameter fibrils results in degradation of shear stiffness and hence the compressive strength.

The results of the compressive strength analyses indicate that for the elastic case, the matrix Young's modulus is the dominant parameter. For the inelastic case, however, there are strength limitations which depend both upon the fiber modulus and upon the matrix strength. For some materials, performance is limited by a matrix yield strength at a given fiber modulus. For other materials, a gain in compressive strength can be achieved by improving the matrix modulus.

4.2.3.3 Matrix mode strength

The remaining failure modes of interest are transverse tension and compression and axial shear. For each of these loading conditions, material failure can occur without fracture of the fibers, hence the terminology "matrix-dominated" or "matrix modes of failure". Micromechanical analyses of these failure modes are complex because the critical stress states are in the matrix, are highly non-uniform, and are very dependent upon the local geometry. As a result, it appears that the most fruitful approaches will be those that consider average states of stress.

There are two types of shearing stresses which are of interest for these matrix-dominated failures: (1) in a plane which contains the filaments, and (2) in a plane normal to the filaments. In the first case, the filaments provide very little reinforcement to the composite and the shear strength depends on the shear strength of the matrix material. In the second case, some reinforcement may occur; at high volume fractions of filaments, the reinforcement may be substantial. It is important to recognize that filaments provide little resistance to shear in any surfaces parallel to them.

The approach to shear failure analysis is to consider that a uniaxial fibrous composite is comprised of elastic-brittle fibers embedded in an elastic-perfectly plastic matrix. For the composite, the theorems of limit analysis of plasticity (e.g., References 4.2.3.3(a) and (b)) may be used to obtain upper and lower bounds for a composite limit load (Reference 4.2.3.3(c)). The limit load is defined as the load at which the matrix yield stress permits composite deformation to increase with no increase in load. The failure strength of a ductile matrix may be approximated by this limit load.

4.2.4 Strength under combined stress

It is possible to apply the micro-mechanical models for failure described above, to combined stresses in the principal directions. Little work of this type has been done however. Generally the strengths in principal directions have been used in a failure surface for a homogeneous, anisotropic material for estimation of strength under combined loads. The understanding of failure mechanisms resulting from the above micro-mechanical models can be used to define the general form of failure surface to be utilized. This approach is outlined in the following sections.

Knowledge of the different failure mechanisms and quantitative experimental data for a UDC under single stress components can be used to formulate practical failure criteria for combined stresses. Plane stress failure criteria are discussed below with references also given for more complicated stress systems. The stresses considered are averaged over a representative volume element. The fundamental assumption is that there exists a failure criterion of the form:

$$F(\sigma_{11},\sigma_{22},\sigma_{12}) = 1 \qquad 4.2.4(a)$$

which characterizes the failure of the UDC. The usual approach to construction of a failure criterion is to assume a quadratic form in terms of stress or strain since the quadratic form is the simplest form which can adequately describe the experimental data. The various failure criteria which have been proposed all use coefficients based on experimental information such as ultimate stresses under single load components (References 4.2.4(a) - (d)). For example, the general quadratic version of Equation 4.2.4(a) for plane stress would be:

$$\begin{aligned} &C_{11}\sigma_{11}^2 + C_{22}\sigma_{22}^2 + C_{66}\sigma_{12}^2 + 2C_{12}\sigma_{11}\sigma_{22} + 2C_{16}\sigma_{11}\sigma_{12} \\ &+2C_{26}\sigma_{22}\sigma_{12} + C_1\sigma_{11} + C_2\sigma_{22} + C_6\sigma_{12} = 1 \end{aligned} \qquad 4.2.4(b)$$

The material has different strengths in uniaxial, longitudinal, and transverse tension and compression. Evidently the shear strength is not affected by the sign of the shear stress. It follows that all powers of shear stress in the failure criterion must be even. Consequently, the criterion simplifies to

$$C_{11}\sigma_{11}^2 + C_{22}\sigma_{22}^2 + C_{66}\sigma_{12}^2 + 2C_{12}\sigma_{11}\sigma_{22} + C_1\sigma_{11} + C_2\sigma_{22} = 1 \qquad 4.2.4(c)$$

The ultimate stresses under single component stress conditions for each of σ_{11}, σ_{22}, and σ_{12} determine the constants for the failure criterion.

$$\begin{aligned} C_{11} &= \frac{1}{F_1^{tu}F_1^{cu}} \qquad C_{22} = \frac{1}{F_2^{tu}F_2^{cu}} \\ C_1 &= \frac{1}{F_1^{tu}} - \frac{1}{F_1^{cu}} \qquad C_2 = \frac{1}{F_2^{tu}} - \frac{1}{F_2^{cu}} \\ C_{66} &= \frac{1}{(F_1^{su})^2} \end{aligned} \qquad 4.2.4(d)$$

However, C_{12} cannot be determined from the single component ultimate stresses. Biaxial stress tests must be performed to determine this coefficient. Frequently, the coefficient is established by relating Equation 4.2.4(c) to the Mises-Henky yield criterion for isotropic materials, yielding

$$C_{12} = -\frac{1}{2}(C_{11}C_{22})^{1/2} \qquad 4.2.4(e)$$

The above failure criterion is the two-dimensional version of the Tsai-Wu criterion (Reference 4.2.4(c)). Its implementation raises several problems; the most severe of these is that the failure criterion ignores the diversity of failure modes which are possible.

The identification of the different failure modes of a UDC can provide physically more realistic, and also simpler, failure criteria (Reference 4.2.4(e)). Testing a polymer matrix UDC reveals that tensile stress in the fiber direction produces a jagged, irregular failure surface. Tensile stress transverse to the surface produces a smooth, straight failure surface (See Figures 4.2.4(a) and (b)). Since the carrying capacity deterioration in the tensile fiber mode is due to transverse cracks and the transverse stress σ_{22} has no effect on such cracks, it is assumed that the plane tensile fiber mode is only dependent on the stresses σ_{11} and σ_{12}.

For compressive σ_{11}, failure is due to fiber buckling in the shear mode and the transverse stress σ_{22} has little effect on the compressive failure. In this *compressive fiber mode*, failure again depends primarily on σ_{11}. The dependence on σ_{12} is not known and arguments may be made for and against including it in the failure criterion.

For tension transverse to the fibers, the *tensile matrix mode*, failure occurs by a sudden crack in the fiber direction as shown in Figure 4.2.4(b). Since stress in the fiber direction has no effect on a crack in the fiber direction, this failure mode is dependent only on σ_{22} and σ_{12}.

For compressive stress transverse to the fibers, failure occurs on some plane parallel to the fibers, but not necessarily normal to σ_{22}. This *compressive matrix mode* is produced by normal stress and shear stress on the failure plane. Again, the stress σ_{11} does not effect this failure.

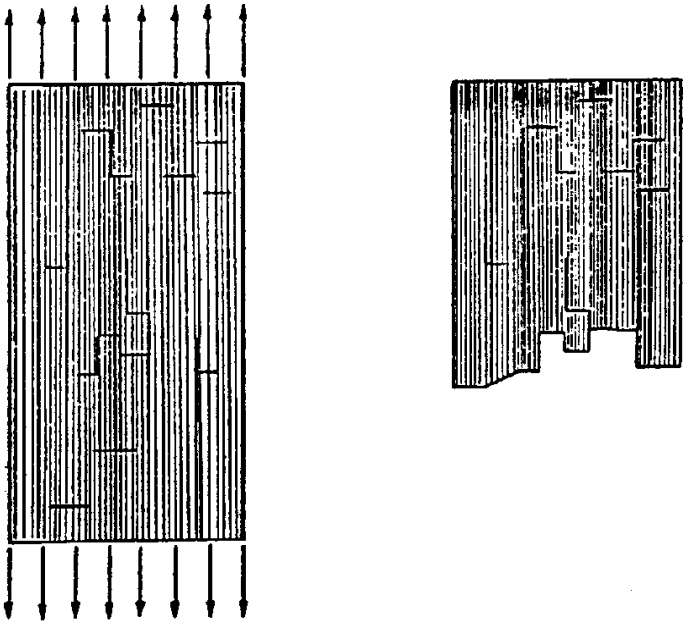

FIGURE 4.2.4(a) *Tensile fiber failure mode.*

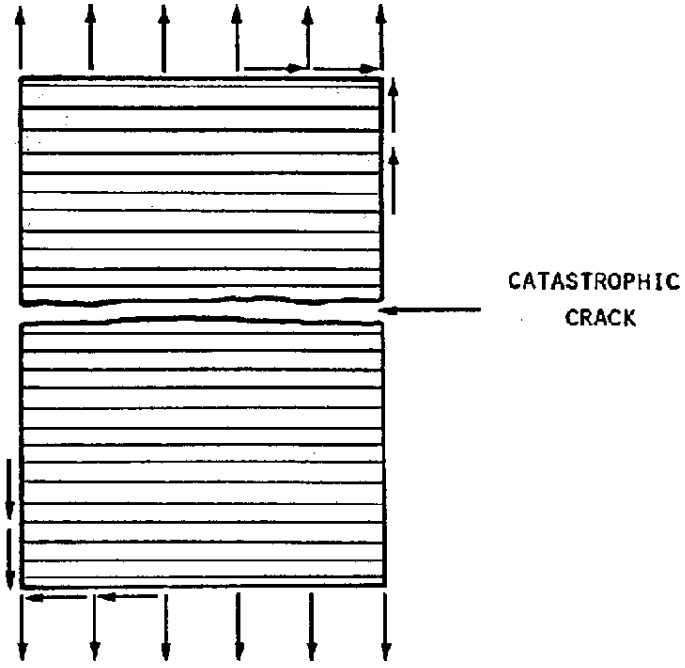

FIGURE 4.2.4(b) *Tensile matrix failure mode.*

Each of the failure modes described can be modeled separately by a quadratic polynomial (Reference 4.2.4(e)). This approach provides four individual failure criteria. Note the choice of stress components included in each of these criteria, and the particular mathematical form used, are subjects which are not yet fully resolved. The following criteria appear to a reasonable set with which the different modes of failure can be handled separately.

Fiber modes

Tensile

$$\left(\frac{\sigma_{11}}{F_1^{tu}}\right)^2+\left(\frac{\sigma_{12}}{F_{12}^{su}}\right)^2=1 \qquad 4.2.4(f)$$

Compressive

$$\left(\frac{\sigma_{11}}{F_1^{cu}}\right)^2+\left(\frac{\sigma_{12}}{F_{12}^{su}}\right)^2=1 \qquad 4.2.4(g)$$

Matrix modes

Tensile

$$\left(\frac{\sigma_{22}}{F_2^{tu}}\right)^2+\left(\frac{\sigma_{12}}{F_{12}^{su}}\right)^2=1 \qquad 4.2.4(h)$$

Compressive

$$\left(\frac{\sigma_{22}}{2F_{23}^{su}}\right)^2+\left[\left(\frac{F_2^{cu}}{2F_{23}^{su}}\right)^2-1\right]\left(\frac{\sigma_{22}}{F_2^{cu}}\right)+\left(\frac{\sigma_{12}}{F_{12}^{su}}\right)^2=1 \qquad 4.2.4(i)$$

Note that F_2^{cu} in Equation 4.2.4(i) should be taken as the absolute value. The ultimate transverse shear stress, $\sigma_{23}=F_{23}^{su}$, is very difficult to measure. A reasonable approximation for this quantity is the ultimate shear stress for the matrix. For any given state of stress, one each of Equations 4.2.4(f) and (g) and Equations 4.2.4(h) and (i) are chosen according to the signs of σ_{11} and σ_{22}. The stress components are introduced into the appropriate pair and whichever criterion is satisfied first is the operative criterion.

The advantages are Equations 4.2.4(f) - (i) are:

1. The failure criteria are expressed in terms of single component ultimate stresses. No biaxial test results are needed.

2. The failure mode is identified by the criterion which is satisfied first.

The last feature is of fundamental importance for analysis of fiber composite structural elements, since it permits identification of the nature of initial damage. Moreover, in conjunction with a finite element analysis, it is possible to identify the nature of failure in elements, modify their stiffnesses accordingly, and proceed with the analysis to predict new failures.

4.2.5 Summary

- Composite strength analysis is most commonly performed, by industry, on the macromechanics level given that the analysis of composite materials uses effective lamina properties based on average stress and strain.

- Ply level stresses are the commonly used approach to laminate strength analysis.

- Lamina stress/strain is influenced by many properties of interest, but is dominated by mechanical load and environmental sensitivity.

- Stress-strain elastic behavior, in its simplest form, may be described as a function of a composite materials constitutive properties (i.e., E, G, ν, α).

- Several practical failure criteria exist today that: 1) depend upon cross-plied laminate coupon data to determine lamina stress/strain allowables and 2) identify the failure mode based on the allowable that is first exceeded by its stress/strain counterpart.

4.3 ANALYSIS OF LAMINATES

4.3.1 Lamina stress-strain relations

A laminate is composed of unidirectionally-reinforced laminae oriented in various directions with respect to the axes of the laminate. The stress-strain relations developed in the Section 4.2 must be transformed into the coordinate system of the laminate to perform the laminate stress-strain analysis. A new system of notation for the lamina elastic properties is based on x_1 in the fiber direction, x_2 transverse to the fibers in the plane of the lamina, and x_3 normal to the plane of the lamina.

$$\begin{aligned} E_1 &= E_1^* & \nu_{12} &= \nu_{12}^* \\ E_2 &= E_3 = E_2^* & \nu_{23} &= \nu_{23}^* \\ G_{12} &= G_1^* & G_{23} &= G_2^* \end{aligned} \qquad 4.3.1(a)$$

In addition, the laminae are now treated as effective homogeneous, transversely isotropic materials.

$$\begin{Bmatrix} \varepsilon_{11} \\ \varepsilon_{22} \\ \varepsilon_{33} \\ 2\varepsilon_{23} \\ 2\varepsilon_{13} \\ 2\varepsilon_{12} \end{Bmatrix} = \begin{bmatrix} \frac{1}{E_1} & \frac{-\nu_{12}}{E_1} & \frac{-\nu_{12}}{E_1} & 0 & 0 & 0 \\ \frac{-\nu_{12}}{E_1} & \frac{1}{E_2} & \frac{-\nu_{23}}{E_2} & 0 & 0 & 0 \\ \frac{-\nu_{12}}{E_1} & \frac{-\nu_{23}}{E_2} & \frac{1}{E_2} & 0 & 0 & 0 \\ 0 & 0 & 0 & \frac{1}{G_{23}} & 0 & 0 \\ 0 & 0 & 0 & 0 & \frac{1}{G_{12}} & 0 \\ 0 & 0 & 0 & 0 & 0 & \frac{1}{G_{12}} \end{bmatrix} \begin{Bmatrix} \sigma_{11} \\ \sigma_{22} \\ \sigma_{33} \\ \sigma_{23} \\ \sigma_{13} \\ \sigma_{12} \end{Bmatrix} \qquad 4.3.1(b)$$

It has become common practice in the analysis of laminates to utilize engineering shear strains rather than tensor shear strains. Thus the factor of two has been introduced into the stress-strain relationship of Equation 4.3.1(b).

The most important state of stress in a lamina is plane stress, where

$$\sigma_{13} = \sigma_{23} = \sigma_{33} = 0 \qquad 4.3.1(c)$$

since it occurs from both in-plane loading and bending at sufficient distance from the laminate edges. The plane stress version of Equation 4.3.1(b) is

$$\begin{Bmatrix} \varepsilon_{11} \\ \varepsilon_{22} \\ \varepsilon_{12} \end{Bmatrix} = \begin{bmatrix} \frac{1}{E_1} & \frac{-\nu_{12}}{E_1} & 0 \\ \frac{-\nu_{12}}{E_1} & \frac{1}{E_2} & 0 \\ 0 & 0 & \frac{1}{G_{12}} \end{bmatrix} \begin{Bmatrix} \sigma_{11} \\ \sigma_{22} \\ \sigma_{12} \end{Bmatrix} \qquad 4.3.1(d)$$

which may be written as

$$\{\varepsilon_\ell\} = [S]\{\sigma_\ell\} \qquad 4.3.1(e)$$

Here $[S]$, the compliance matrix, relates the stress and strain components in the principal material directions. These are called laminae coordinates and are denoted by the subscript ℓ.

Equation 4.3.1(d) relates the in-plane strain components to the three in-plane stress components. For the plane stress state, the three additional strains can be found to be

$$\varepsilon_{23} = \varepsilon_{13} = 0$$
$$\varepsilon_{33} = -\sigma_{11}\frac{\nu_{13}}{E_1} - \sigma_{22}\frac{\nu_{23}}{E_2} \qquad 4.3.1(f)$$

and the complete state of stress and strain is determined.

The relations 4.3.1(d) can be inverted to yield

$$\{\sigma_\ell\} = [S]^{-1}\{\varepsilon_\ell\} \qquad 4.3.1(g)$$

or

$$\{\sigma_\ell\} = [Q]\{\varepsilon_\ell\} \qquad 4.3.1(h)$$

The matrix $[Q]$ is defined as the inverse of the compliance matrix and is known as the reduced lamina stiffness matrix. Its terms can be shown to be

$$[Q] = \begin{bmatrix} Q_{11} & Q_{12} & 0 \\ Q_{12} & Q_{22} & 0 \\ 0 & 0 & Q_{66} \end{bmatrix} \qquad 4.3.1(i)$$

$$Q_{11} = \frac{E_1}{1-\nu_{12}^2\frac{E_2}{E_1}} \qquad Q_{12} = \frac{\nu_{12}E_2}{1-\nu_{12}^2\frac{E_2}{E_1}}$$
$$Q_{22} = \frac{E_2}{1-\nu_{12}^2\frac{E_2}{E_1}} \qquad Q_{66} = G_{12} \qquad 4.3.1(j)$$

In the notation for the $[Q]$ matrix, each pair of subscripts of the stiffness components is replaced by a single subscript according to the following scheme.

$$11 \to 1 \qquad 22 \to 2 \qquad 33 \to 3$$
$$23 \to 4 \qquad 31 \to 5 \qquad 12 \to 6$$

The reduced stiffness and compliance matrices 4.3.1(i) and (d) relate stresses and strains in the principal material directions of the material. To define the material response in directions other than these coordinates, transformation relations for the material stiffnesses are needed.

In Figure 4.3.1(a), two sets of coordinate systems are depicted. The 1-2 coordinate system corresponds to the principal material directions for a lamina, while the x-y coordinates are arbitrary and related to the 1-2 coordinates through a rotation about the axis out of the plane of the figure. The angle θ is defined as the rotation from the arbitrary x-y system to the 1-2 material system.

The transformation of stresses from the 1-2 system to the x-y system follows the rules for transformation of tensor components.

$$\begin{Bmatrix} \sigma_{xx} \\ \sigma_{yy} \\ \sigma_{xy} \end{Bmatrix} = \begin{bmatrix} m^2 & n^2 & -2mn \\ n^2 & m^2 & 2mn \\ mn & -mn & m^2-n^2 \end{bmatrix} \begin{Bmatrix} \sigma_{11} \\ \sigma_{22} \\ \sigma_{12} \end{Bmatrix} \qquad 4.3.1(k)$$

or

$$\{\sigma_x\} = [\theta]\{\sigma_\ell\} \qquad 4.3.1(l)$$

where $m = \cos\theta$, and $n = \sin\theta$. In these relations, the subscript x is used as shorthand for the laminate coordinate system.

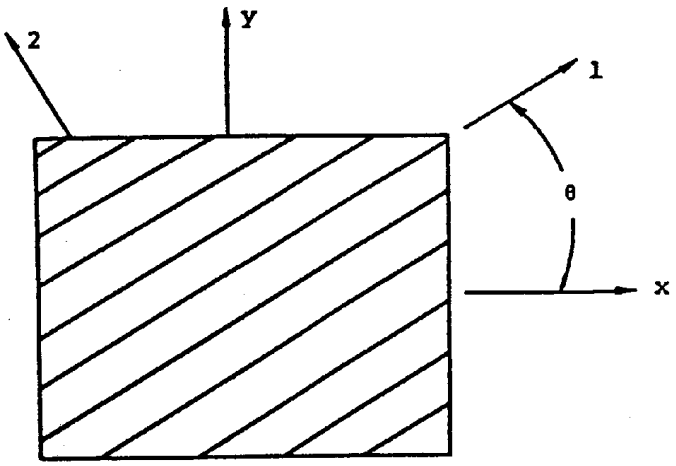

1, 2 Principal Material Coordinates
x, y Laminate, or Arbitrary Coordinates

FIGURE 4.3.1(a) *Coordinate systems.*

The same transformation matrix $[\theta]$ can also be used for the tensor strain components. However, since the engineering shear strains have been utilized, a different transformation matrix is required.

$$\begin{Bmatrix} \varepsilon_{xx} \\ \varepsilon_{yy} \\ 2\varepsilon_{xy} \end{Bmatrix} = \begin{bmatrix} m^2 & n^2 & -mn \\ n^2 & m^2 & mn \\ 2mn & -2mn & m^2 - n^2 \end{bmatrix} \begin{Bmatrix} \varepsilon_{11} \\ \varepsilon_{22} \\ 2\varepsilon_{12} \end{Bmatrix} \qquad 4.3.1(m)$$

or

$$\{\varepsilon_x\} = [\psi]\{\varepsilon_\ell\} \qquad 4.3.1(n)$$

Given the transformations for stress and strain to the arbitrary coordinate system, the relations between stress and strain in the laminate system can be determined.

$$\{\sigma_x\} = [\overline{Q}]\{\varepsilon_x\} \qquad 4.3.1(o)$$

The reduced stiffness matrix $[\overline{Q}]$ relates the stress and strain components in the laminate coordinate system.

$$[\overline{Q}] = [\theta][Q][\psi]^{-1} \qquad 4.3.1(p)$$

The terms within $[\overline{Q}]$ are defined to be

$$\begin{aligned}
\overline{Q}_{11} &= Q_{11}m^4 + Q_{22}n^4 + 2m^2n^2(Q_{12} + 2Q_{66}) \\
\text{Qbar}_{12} &= m^2n^2(Q_{11} + Q_{22} - 4Q_{66}) + (m^4 + n^4)Q_{12} \\
\overline{Q}_{16} &= [Q_{11}m^2 - Q_{22}n^2 - (Q_{12} + 2Q_{66})(m^2 - n^2)]mn \\
\overline{Q}_{22} &= Q_{11}n^4 + Q_{22}m^4 + 2m^2n^2(Q_{12} + 2Q_{66}) \\
\overline{Q}_{26} &= [Q_{11}n^2 - Q_{22}m^2 + (Q_{12} + 2Q_{66})(m^2 - n^2)]mn \\
\overline{Q}_{66} &= (Q_{11} + Q_{22} - 2Q_{12})m^2n^2 + Q_{66}(m^2 - n^2)^2 \\
\overline{Q}_{21} &= \overline{Q}_{12} \qquad \overline{Q}_{61} = \overline{Q}_{16} \qquad \overline{Q}_{62} = \overline{Q}_{26}
\end{aligned} \qquad 4.3.1(q)$$

where the subscript 6 has been retained in keeping with the discussion following Equation 4.3.1(j).

$$[\overline{Q}] = \begin{bmatrix} \overline{Q}_{11} & \overline{Q}_{12} & \overline{Q}_{16} \\ \overline{Q}_{21} & \overline{Q}_{22} & \overline{Q}_{26} \\ \overline{Q}_{16} & \overline{Q}_{26} & \overline{Q}_{66} \end{bmatrix} \qquad 4.3.1(r)$$

A feature of $[\overline{Q}]$ matrix which is immediately noticeable is that $[\overline{Q}]$ is fully-populated. The additional terms which have appeared in $[\overline{Q}]$, $\overline{Q}_{16}$ and $\overline{Q}_{26}$, relate shear strains to extensional loading and vice versa. This effect of a shear strain resulting from an extensional strain is depicted in Figure 4.3.1(b). From Equations 4.3.1(q), these terms are zero for θ equal to 0° or 90°. Physically, this means that the fibers are parallel or perpendicular to the loading direction. For this case, extensional-shear coupling does not occur for an orthotropic material since the loadings are in the principal directions. The procedure used to develop the transformed stiffness matrix can also be used to find a transformed compliance matrix.

$$\{\varepsilon_\ell\} = [S]\{\sigma_\ell\} \qquad 4.3.1(s)$$

$$\{\varepsilon_x\} = [\psi][S][\theta]^{-1}\{\sigma_x\} \qquad 4.3.1(t)$$

$$\{\varepsilon_x\} = [\overline{S}]\{\sigma_x\} \qquad 4.3.1(u)$$

Noting that the stress-strain relations are now defined in the laminate coordinate system, lamina stiffnesses can also be defined in this system. Thus, expanding the last of Equations 4.3.1(s) - (u):

$$\begin{Bmatrix} \varepsilon_{xx} \\ \varepsilon_{yy} \\ 2\varepsilon_{xy} \end{Bmatrix} = \begin{bmatrix} \overline{S}_{11} & \overline{S}_{12} & \overline{S}_{16} \\ \overline{S}_{21} & \overline{S}_{22} & \overline{S}_{26} \\ \overline{S}_{16} & \overline{S}_{26} & \overline{S}_{66} \end{bmatrix} \begin{Bmatrix} \sigma_{xx} \\ \sigma_{yy} \\ \sigma_{xy} \end{Bmatrix} \qquad 4.3.1(v)$$

The engineering constants for the material can be defined by specifying the conditions for an experiment. For $\sigma_{yy} = \sigma_{xy} = 0$, the ratio $\sigma_{xx} / \varepsilon_{xx}$ is Young's modulus in the x direction. For this same stress state, $-\varepsilon_{yy} / \varepsilon_{xx}$ is Poisson's ratio. In this fashion, the lamina stiffnesses in the coordinate system of Equations 4.3.1(s) - (u) are found to be:

$$E_x = \frac{1}{\overline{S}_{11}} \qquad E_y = \frac{1}{\overline{S}_{22}}$$

$$G_{xy} = \frac{1}{\overline{S}_{66}} \qquad \nu_{xy} = \frac{-\overline{S}_{21}}{\overline{S}_{11}} = \frac{-\overline{S}_{12}}{\overline{S}_{11}} \qquad 4.3.1(w)$$

It is sometimes desirable to obtain elastic constants directly from the reduced stiffnesses, $[\overline{Q}]$, by using Equations 4.3.1(o). In the general case where the $\overline{Q}_{ij}$ matrix is fully populated, this can be accomplished by using Equations 4.3.1(w) and the solution for $\overline{S}_{ij}$ as functions of $\overline{Q}_{ij}$ obtained from the inverse relationship of the two matrices. An alternative approach is to evaluate extensional properties for the case of zero shear strain. For single stress states and zero shear strain, the elastic constants in terms of the transformed stiffness matrix terms are:

$$E_x = \overline{Q}_{11} - \frac{\overline{Q}_{12}^2}{\overline{Q}_{22}}$$

$$E_y = \overline{Q}_{22} - \frac{\overline{Q}_{12}^2}{\overline{Q}_{11}} \qquad 4.3.1(x)$$

$$\nu_{xy} = \frac{\overline{Q}_{12}}{\overline{Q}_{22}} = \frac{\overline{Q}_{21}}{\overline{Q}_{22}}$$

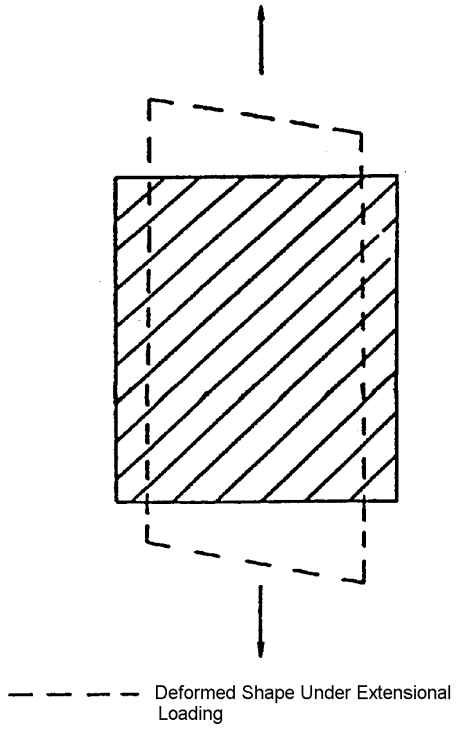

FIGURE 4.3.1(b) *Extensional-shear coupling.*

Also,

$$G_{xy} = \overline{Q}_{66}$$

From the terms in the $\left[\overline{Q}\right]$ matrix (Equation 4.3.1(q)) and the stiffness relations (Equation 4.3.1(x)), the elastic constants in an arbitrary coordinate system are functions of all the elastic constants in the principal material directions as well as the angle of rotation.

The variation of elastic modulus E_x with angle of rotation is depicted in Figure 4.3.1(c) for a typical graphite/epoxy material. For demonstration purposes, two different shear moduli have been used in generating the figure. The differences between the two curves demonstrate the effect of the principal material shear modulus on the transformed extensional stiffness. The two curves are identical at 0° and 90°, as expected since E_x is simply E_1 or E_2. Between these two endpoints, substantial differences are present. For the smaller shear modulus, the extensional stiffness is less than the E_2 value from approximately 50° to just less than 90°. For these angles, the material stiffness is more strongly governed by the principal material shear modulus than by the transverse extensional modulus. The curves of Figure 4.3.1(c) can also be used to determine the modulus E_y by simply reversing the angle scale.

With the transformed stress-strain relations, it is now possible to develop an analysis for an assemblage of plies, i.e., a laminate.

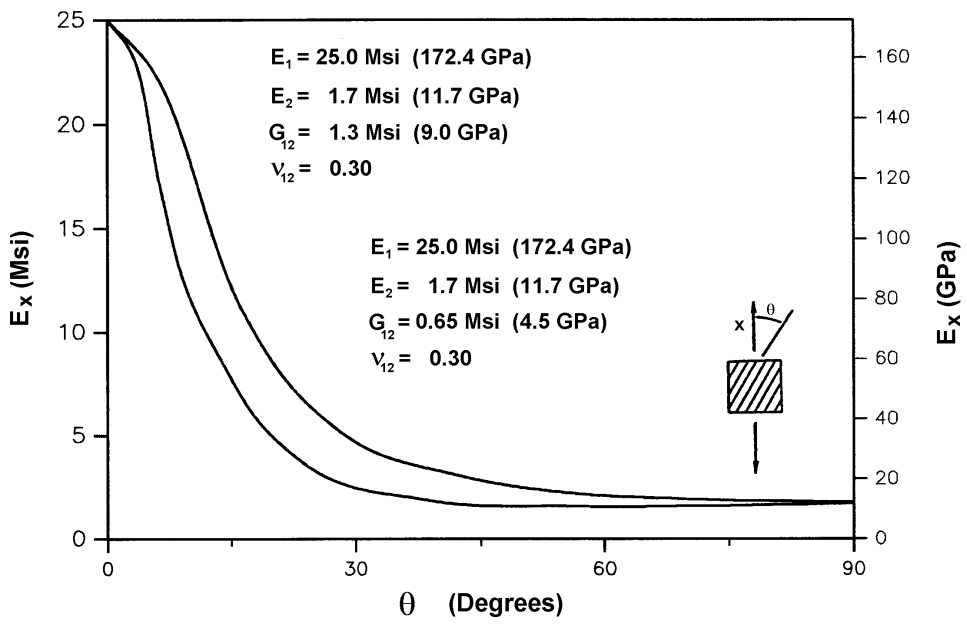

FIGURE 4.3.1(c) *Variation of E_x with angle and G_{12} for typical graphite/epoxy materials.*

4.3.2 Lamination theory

The development of procedures to evaluate stresses and deformations of laminates is crucially dependent on the fact that the thickness of laminates is much smaller than the in-plane dimensions. Typical thickness values for individual plies range between 0.005 and 0.010 inch (0.13 and 0.25 mm). Consequently, laminates using from 8 to 50 plies are still generally thin plates and, therefore, can be analyzed on the basis of the usual simplifications of thin plate theory.

In the analysis of isotropic thin plates it has become customary to analyze the cases of in-plane loading and bending separately. The former case is described by plane stress elastic theory and the latter by classical plate bending theory. This separation is possible since the two loadings are uncoupled for symmetric laminates; when both occur, the results are superposed.

The classical assumptions of thin plate theory are:

1. The thickness of the plate is much smaller than the in-plane dimensions;
2. The shapes of the deformed plate surface are small compared to unity;
3. Normals to the undeformed plate surface remain normal to the deformed plate surface;
4. Vertical deflection does not vary through the thickness; and
5. Stress normal to the plate surface is negligible.

On the basis of assumptions (2) - (4), the displacement field can be expressed as:

$$\begin{aligned} u_z &= u_z^{\circ}(x,y) \\ u_x &= u_x^{\circ}(x,y) - z\frac{\partial u_z}{\partial x} \\ u_y &= u_y^{\circ}(x,y) - z\frac{\partial u_z}{\partial y} \end{aligned} \qquad 4.3.2(a)$$

with the x-y-z coordinate system defined in Figure 4.3.2(a). These relations (Equation 4.3.2(a)) indicate that the in-plane displacements consist of a mid-plane displacement, designated by the superscript (°),

plus a linear variation through the thickness. The two partial derivatives are bending rotations of the mid-surface. The use of assumption (4) prescribes that u_z does not vary through the thickness.

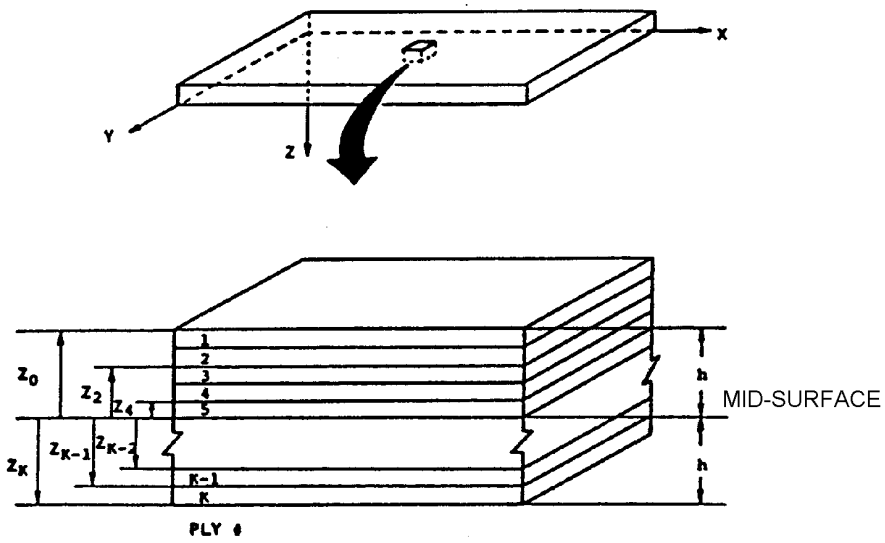

FIGURE 4.3.2(a) *Laminate construction.*

The linear strain displacement relations are

$$\varepsilon_{xx} = \frac{\partial u_x}{\partial x} \qquad \varepsilon_{yy} = \frac{\partial u_y}{\partial y}$$
$$\varepsilon_{xy} = \frac{1}{2}\left(\frac{\partial u_x}{\partial y} + \frac{\partial u_y}{\partial x}\right) \qquad 4.3.2(b)$$

and performing the required differentiations yields

$$\varepsilon_{xx} = \overset{\circ}{\varepsilon}_{xx} + z\kappa_{xx}$$
$$\varepsilon_{yy} = \overset{\circ}{\varepsilon}_{yy} + z\kappa_{yy} \qquad 4.3.2(c)$$
$$2\varepsilon_{xy} = 2\overset{\circ}{\varepsilon}_{xy} + 2z\kappa_{xy}$$

or

$$\{\varepsilon_x\} = \{\overset{\circ}{\varepsilon}\} + z\{\kappa\} \qquad 4.3.2(d)$$

where

$$\{\varepsilon^{\circ}\} = \begin{Bmatrix} \dfrac{\partial u_x^{\circ}}{\partial x} \\ \dfrac{\partial u_y^{\circ}}{\partial y} \\ \left[\dfrac{\partial u_x^{\circ}}{\partial y} + \dfrac{\partial u_y^{\circ}}{\partial x}\right] \end{Bmatrix} \qquad 4.3.2(e)$$

and

$$\{\kappa\} = \begin{pmatrix} \kappa_{xx} \\ \kappa_{yy} \\ \kappa_{xy} \end{pmatrix} = \begin{pmatrix} -\dfrac{\partial^2 u_z}{\partial x^2} \\ -\dfrac{\partial^2 u_z}{\partial y^2} \\ -2\dfrac{\partial^2 u_x}{\partial x \partial y} \end{pmatrix} \qquad 4.3.2(f)$$

The strain at any point in the plate is defined as the sum of a mid-surface strain $\{\varepsilon^\circ\}$, and a curvature $\{\kappa\}$ multiplied by the distance from the mid-surface.

For convenience, stress and moment resultants will be used in place of stresses for the remainder of the development of lamination theory (see Figure 4.3.2(b)). The stress resultants are defined as

$$\{N\} = \begin{pmatrix} N_{xx} \\ N_{yy} \\ N_{xy} \end{pmatrix} = \int_{-h}^{h} \{\sigma_x\}\, dz \qquad 4.3.2(g)$$

and the moment resultants are defined as

$$\{M\} = \begin{pmatrix} M_{xx} \\ M_{yy} \\ M_{xy} \end{pmatrix} = \int_{-h}^{h} \{\sigma_x\}\, z dz \qquad 4.3.2(h)$$

where the integrations are carried out over the plate thickness.

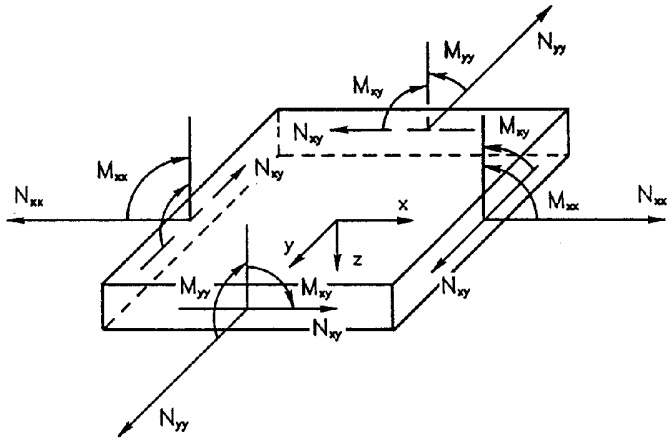

$$\{N\} = \int_{-h}^{h} \{\sigma_x\}\, dz$$

$$\{M\} = \int_{-h}^{h} \{\sigma_x\}\, z dz$$

FIGURE 4.3.2(b) *Stress and moment resultants.*

Noting Equations 4.3.1(o) and 4.3.2(c), relations between the stress and moment resultants and the mid-plane strains and curvatures can be written as

$$\{N\} = \int_{-h}^{h} \{\sigma_x\}\, dz = \int_{-h}^{h} \left[\overline{Q}\right](\{\varepsilon^\circ\} + z\{\kappa\})\, dz \qquad 4.3.2(i)$$

$$\{M\} = \int_{-h}^{h} \{\sigma_x\}\, z dz = \int_{-h}^{h} \left[\overline{Q}\right](\{\varepsilon^\circ\} + z\{\kappa\})\, z dz \qquad 4.3.2(j)$$

Since the transformed lamina stiffness matrices are constant within each lamina and the mid-plane strains and curvatures are constant with respect to the z-coordinate, the integrals in Equations 4.3.2(i) and (j) can be replaced by summations.

Introducing three matrices equivalent to the necessary summations, the relations can be written as

$$\{N\} = [A]\{\varepsilon^\circ\} + [B]\{\kappa\} \qquad 4.3.2(k)$$

$$\{M\} = [B]\{\varepsilon^\circ\} + [D]\{\kappa\} \qquad 4.3.2(l)$$

where the stiffness matrix is composed of the following 3x3 matrices:

$$[A] = \sum_{i=1}^{N} [\overline{Q}]^i (z_i - z_{i-1})$$

$$[B] = \frac{1}{2} \sum_{i=1}^{N} [\overline{Q}]^i (z_i^2 - z_{i-1}^2) \qquad 4.3.2(m)$$

$$[D] = \frac{1}{3} \sum_{i=1}^{N} [\overline{Q}]^i (z_i^3 - z_{i-1}^3)$$

where N is the total number of plies, z_i is defined in Figure 4.3.2(a) and subscript i denotes a property of the ith ply. Note that $z_i - z_{i-1}$ equals the ply thickness. Here the reduced lamina stiffnesses for the ith ply are found from Equations 4.3.2(k) and (l) using the principal properties and orientation angle for each ply in turn. Thus, the constitutive relations for a laminate have been developed in terms of stress and moment resultants.

Classical lamination theory has been used to predict the internal stress state, stiffness and dimensional stability of laminated composites (e.g., References 4.3.2(a) - (e)). The constitutive law for CLT couples extensional, shear, bending and torsional loads with strains and curvatures. Residual strains or warpage due to differential shrinkage or swelling of plies in a laminate have also been incorporated in lamination theory using an environmental load analogy (See Sections 4.3.3.3 and 4.3.3.4.). The combined influence of various types of loads and moments on laminated plate response can be described using the ABD matrix from Equations 4.3.2(k) and (l). In combined form:

$$\begin{bmatrix} N_x \\ N_y \\ N_{xy} \\ M_x \\ M_y \\ M_{xy} \end{bmatrix} = \begin{bmatrix} A_{11} & A_{12} & A_{16} & B_{11} & B_{12} & B_{16} \\ A_{12} & A_{22} & A_{26} & B_{12} & B_{22} & B_{26} \\ A_{16} & A_{26} & A_{66} & B_{16} & B_{26} & B_{66} \\ B_{11} & B_{12} & B_{16} & D_{11} & D_{12} & D_{16} \\ B_{12} & B_{22} & B_{26} & D_{12} & D_{22} & D_{26} \\ B_{16} & B_{26} & B_{66} & D_{16} & D_{26} & D_{66} \end{bmatrix} \begin{bmatrix} \varepsilon_x \\ \varepsilon_y \\ \varepsilon_{xy} \\ \kappa_x \\ \kappa_y \\ \kappa_{xy} \end{bmatrix} \qquad 4.3.2(n)$$

where N are loads, M are moments, ε are strains, κ are curvatures and

A_{ij} = extensional and shear stiffnesses
B_{ij} = extension-bending coupling stiffnesses
D_{ij} = bending and torsional stiffnesses

Several observations regarding lay-up and laminate stacking sequence (LSS) can be made with the help of Equation 4.3.2(n). These include:

(1) The stiffness matrix A_{ij} in Equation 4.3.2(n) is independent of LSS. Inversion of the stiffness matrix [ABD] yields the compliance matrix [A'B'D']. This inversion is necessary in order to calculate strains and curvatures in terms of loads and moments. The inversion results in a relationship between LSS and extension/shear compliances. However, this relationship is eliminated if the laminate is symmetric.

(2) Nonzero values of A_{16} and A_{26} indicates that there is extension/shear coupling (e.g., longitudinal loads will result in both extensional and shear strains). If a laminate is balanced A_{16} and A_{26} become zero, eliminating extension/shear coupling.

(3) Nonzero values of B_{ij} indicates that there is coupling between bending/twisting curvatures and extension/shear loads. Traditionally, these couplings have been suppressed for most applications by choosing an LSS that minimizes the values of B_{ij}. All values of B_{ij} become zero for symmetric laminates. Reasons for designing with symmetric laminates include structural dimensional stability requirements (e.g., buckling, environmental warping), compatibility of structural components at joints and the inability to test for strength allowables of specimens that have significant values of B_{ij}.

(4) In general, the values of D_{ij} are nonzero and strongly dependent on LSS. The average plate bending stiffnesses, torsional rigidity and flexural Poisson's ratio can be calculated per unit width using components of the compliance matrix [A'B'D'], i.e.,

$1/D'_{11}$ = bending stiffness about y-axis
$1/D'_{22}$ = bending stiffness about x-axis
$1/D'_{66}$ = torsional rigidity about x- or y-axis
$-D'_{12}/D'_{11}$ = flexural Poisson's ratio.

The D'_{16} and D'_{26} terms should also be included in calculations relating midplane curvatures to moments except when considering a special class of balanced, unsymmetric laminates.

(5) Nonzero values of D_{16} and D_{26} indicates that there is bending/twisting coupling. These terms will vanish only if a laminate is balanced and if, for each ply oriented at $+\theta$ above the laminate midplane, there is an identical ply (in material and thickness) oriented at $-\theta$ at an equal distance below the midplane. Such a laminate cannot be symmetric, unless it contains only 0° and 90° plies. Bending/twisting coupling can be minimized by alternating the location of $+\theta$ and $-\theta$ plies through the LSS (Section 4.6.5.2.2, Recommendation 5).

Additional information on laminate stacking sequence effects is found in Section 4.6.5.

4.3.3 Laminate properties

The relations between the mid-surface strains and curvatures and the membrane stress and moment resultants are used to calculate plate bending and extensional stiffnesses for structural analysis. The effects of orientation variables upon plate properties are also considered. In addition to the mechanical loading conditions treated thus far, the effects of temperature changes upon laminate behavior must be understood. Further, for polymeric matrix composites, high moisture content causes dimensional changes which can be described by effective swelling coefficients.

4.3.3.1 Membrane stresses

Recalling Equations 4.3.2(k) and (l) and noting that for symmetric laminates the [B] matrix is zero, the relations can be rewritten as

$$\begin{pmatrix} N_{xx} \\ N_{yy} \\ N_{xy} \end{pmatrix} = \begin{bmatrix} A_{11} & A_{12} & A_{16} \\ A_{12} & A_{22} & A_{26} \\ A_{16} & A_{26} & A_{66} \end{bmatrix} \begin{pmatrix} \varepsilon^{\circ}_{xx} \\ \varepsilon^{\circ}_{yy} \\ 2\,\varepsilon^{\circ}_{xy} \end{pmatrix} \qquad 4.3.3.1(a)$$

and

$$\begin{pmatrix} M_{xx} \\ M_{yy} \\ M_{xy} \end{pmatrix} = \begin{bmatrix} D_{11} & D_{12} & D_{16} \\ D_{12} & D_{22} & D_{26} \\ D_{16} & D_{26} & D_{66} \end{bmatrix} \begin{pmatrix} \kappa_{xx} \\ \kappa_{yy} \\ 2\,\kappa_{xy} \end{pmatrix} \qquad 4.3.3.1(b)$$

Since the extensional and bending behavior are uncoupled, effective laminate elastic constants can be readily determined. Inverting the stress resultant mid-plane strain relations yields

$$\{\varepsilon^{\circ}\} = [A]^{-1}\{N\} = [a]\{N\} \qquad 4.3.3.1(c)$$

from which the elastic constants are seen to be

$$E_x = \frac{1}{2\,h\,a_{11}} \qquad G_{xy} = \frac{1}{2\,h\,a_{66}}$$
$$E_y = \frac{1}{2\,h\,a_{22}} \qquad \nu_{xy} = -\frac{a_{12}}{a_{11}} \qquad 4.3.3.1(d)$$

where the divisor $2h$ corresponds to the laminate thickness.

Note that the [A] matrix is comprised of [Q] matrices from each layer in the laminate. It is obvious that the laminate elastic properties are functions of the angular orientation of the plies. This angular influence is illustrated in Figure 4.3.3.1 for a typical high modulus carbon/epoxy system which has the lamina properties listed in Table 4.3.3.1(a). The laminae are oriented in $\pm\theta$ pairs in a symmetric, balanced construction, creating what is called an angle-ply laminate.

The variation of shear modulus and Poisson's ratio are noteworthy in Figure 4.3.3.1. The shear modulus is equal to the unidirectional value for 0° and 90° and rises sharply to a maximum at 45°. The peak at 45° can be explained by noting that shear is equivalent to a combined state of tensile and compressive loads oriented at 45°. Thus, the shear loading on a $[\pm 45]_s$ laminate is equivalent to tensile and compressive loading on a $[0/90]_s$ laminate. Effectively, the fibers are aligned with the loading and, hence, with the large shear stiffness.

An even more interesting effect is seen in the variation of Poisson's ratio. The peak value in this example is greater than 1.5. In an isotropic material, this would be impossible. In an orthotropic material, the isotropic restriction does not hold and a Poisson's ratio greater than one is valid and realistic. In fact, large Poisson's ratios are typical for laminates constructed from unidirectional materials with the plies oriented at approximately 30°.

Because of the infinite variability of the angular orientation of the individual laminae, one would assume that a laminate having a stiffness which behaves isotropically in the plane of the laminate could be constructed by using many plies having small, equal differences in their orientation. It can be shown that a symmetric, quasi-isotropic laminate can be constructed with as few as six plies as a $[0/\pm 60]_s$ laminate. A general rule for describing a quasi-isotropic laminate states that the angles between the plies are equal to π / N, where N is an integer greater than or equal to 3, and there is an identical number of plies at each orientation in a symmetric laminate. For plies of a given material, all such quasi-isotropic laminates will have the same elastic properties, regardless of the value of N.

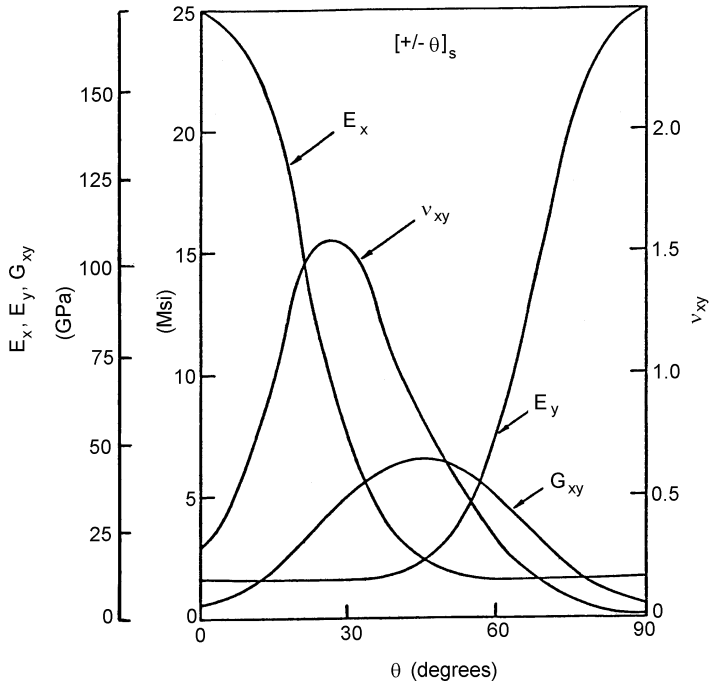

FIGURE 4.3.3.1 *Laminate elastic constants for high modulus carbon/epoxy.*

A quasi-isotropic laminate has in-plane stiffnesses which follow isotropic relationships

$$E_x = E_y = E_\theta \qquad 4.3.3.1(e)$$

where the subscript θ indicates any arbitrary angle. Additionally,

$$G_{xy} = \frac{E_x}{2(1+\nu_{xy})} \qquad 4.3.3.1(f)$$

There are two items which must be remembered about quasi-isotropic laminates. First and foremost, only the elastic in-plane properties are isotropic; the strength properties, in general, will vary with directions. The second item is that two equal moduli $E_x = E_y$ do not necessarily indicate quasi-isotropy, as demonstrated in Table 4.3.3.1(b). The first two laminates in Table 4.3.3.1(b) are actually the same (a $[0/90]_s$ laminate rotated 45° is a $[\pm 45]_s$ laminate). Note that the extensional moduli of these laminates are not the same and that the shear modulus of each laminate is not related to the extensional modulus and Poisson's ratio. For these laminates, the π/N relation has not been satisfied and they are not quasi-isotropic. The third laminate has plies oriented at 45° to each other but there are not equal numbers of plies at each angle. This laminate is also not quasi-isotropic.

This discussion of symmetric laminates has centered on membrane behavior. Symmetric laminates can be constructed which are very well behaved in the membrane sense. The bending behavior of symmetric laminates is considerably more complex, primarily due to the arrangement of plies through the thickness of the laminate.

TABLE 4.3.3.1(a) *Properties of a high-modulus carbon/epoxy lamina.*

E_1 = 25.0 Msi = 172 GPa	α_1 = 0.30x10^{-6} in/in/F° = 0.54x10^{-6} mm/mm/C°
E_2 = 1.7 Msi = 12 GPa	α_2 = 19.5x10^{-6} in/in/F° = 35.1x10^{-6} mm/mm/C°
G_{12} = 0.65 Msi = 4.5 GPa	
ν_{12} = 0.30	
ρ = 0.056 lb/in^3 = 1.55 g/cm^3	
F_1^{tu} = 110 ksi = 760 MPa	F_1^{cu} = 110 ksi = 760 MPa
F_2^{tu} = 4.0 ksi = 28 MPa	F_2^{cu} = 20.0 ksi = 138 MPa
F_{12}^{su} = 9.0 ksi = 62 MPa	
v_f = 0.6	t_R = 0.0052 in = 0.13 mm

TABLE 4.3.3.1(b) *Elastic properties of laminates.*

	$E_x = E_y$ Msi (GPa)	ν_{xy}	G_{xy} Msi (GPa)
$[0°/90°]_s$	13.4 (92.5)	0.038	0.65 (4.5)
$[\pm 45°]_s$	2.38 (16.4)	0.829	6.46 (44.5)
$[0°/90°/\pm 45°/-45°/90°/0°]_s$	11.0 (75.6)	0.213	2.59 (17.9)

4.3.3.2 Bending

The equations for bending analysis of symmetric laminates has been developed with the extensional analysis. The first complication that arises in the treatment of laminate bending deals with relationships between the extensional (A) and bending (D) elastic properties. In composite laminates, there is no direct relationship between extensional and bending stiffnesses, unlike the case of a homogeneous material where

$$D = \frac{A(2h)^2}{12} \qquad 4.3.3.2(a)$$

In determining the membrane stiffnesses (A), the position of the ply through the thickness of the laminate does not matter (Equation 4.3.2(m)). The relations for the bending stiffnesses are a function of the third power of the distance of the ply from the mid-surface. Therefore, the position of the plies with respect to the mid-surface is critical. The effects of ply position in a unit thickness laminate are shown in Table 4.3.3.2(a).

The three laminates shown in Table 4.3.3.2(a) are all quasi-isotropic. The membrane properties are isotropic and identical for each of the laminates. The bending stiffnesses can be seen to be a strong function of the thickness position of the plies. Additionally, bending stiffness calculations based on homogeneity (Equation 4.3.3.2) do not correspond to lamination theory calculations. Thus, the simple relations between extensional and bending stiffnesses are lost and lamination theory must be used for bending properties. Table 4.3.3.2(a) also demonstrates that quasi-isotropy holds only for extensional stiffnesses.

Another complication apparent in Table 4.3.3.2(a) involves the presence of the bending-twisting coupling terms, D_{16} and D_{26}. The corresponding extensional-shear coupling terms are zero because of the presence of pairs of layers at ±60° orientations. Noting that the bending-twisting terms can be of the same order of magnitude as the principal bending terms, D_{11}, D_{22}, and D_{66}, the bending-twisting effect can be severe. This effect can be reduced by the proper selection of stacking sequence.

Another example that shows how the laminate stacking sequence (LSS) can significantly affect composite behavior is the bending stiffness of a laminated beam with rectangular cross-section ($h \equiv$ laminate thickness). For the purpose of this example, define effective in-plane and bending moduli along the beam axis as

$$E_x = \frac{1}{A'_{11} h} \qquad 4.3.3.2(b)$$

$$E_x^b = \frac{12}{D'_{11} h^3} \qquad 4.3.3.2(c)$$

respectively. The relationship,

$$\Delta = \frac{E_x^b - E_x}{E_x} x100 \qquad 4.3.3.2(d)$$

provides a relative measure of the effect of LSS on beam bending stiffness. Bending moduli of laminated beams approach those of homogeneous beams as the number of plies increase provided that there is no preferential stacking of ply orientations through the thickness.

Table 4.3.3.2(b) shows lamination theory predictions of in-plane and effective bending moduli for beams with seven different LSS variations of a 16-ply, carbon/epoxy, quasi-isotropic lay-up.[1] Note that the in-plane moduli are independent of LSS because all lay-ups are symmetric. Bending moduli are shown to vary significantly above or below the in-plane moduli depending on preferential stacking of 0° plies towards the surface or center of the laminate, respectively.

In general, the relationship between effective bending moduli and stacking sequence can be more complex than that shown in Table 4.3.3.2(b). Predictions in the table assumed that the basic lamina moduli were constant (i.e., linear elastic behavior). Depending on material type and the degree of accuracy desired, this assumption may lead to poor predictions. Lamina moduli for graphite/epoxy have been shown to depend on environment and strain level. Since flexure results in a distribution of tension and compression strains through the laminate thickness, nonlinear elastic lamination theory predictions may be more appropriate.

The example from Table 4.3.3.2(b) shows a significant effect of LSS on bending moduli of laminated beams. Similarly, calculations with Equation 4.3.2(n) can be used to indicate that LSS has a strong influence on the bending behavior of laminated plates. However, the bending response of common structures may depend more on the resulting moment of inertia, I, for a given geometry than on LSS. This is particularly true for stringer geometries typically used to stiffen composite plates in aerospace structures.

Figure 4.3.3.2 illustrates how structural geometry of a beam section can overshadow the effects of LSS on bending. Web and flange members of each I-beam have LSS indicated in the legend of Figure

[1]The LSS used in Table 4.3.3.2(b) were chosen for illustrative purposes only and do not represent optimal LSS for a given application.

4.3.3.2[1] These LSS are the same as those used in Table 4.3.3.2(b). The ordinate axis of the figure indicates a percent difference between laminated and homogeneous beam calculations. As shown in Figure 4.3.3.2, the effect of LSS on the EI of an I-beam diminishes rapidly with increasing web height.

Additional information on laminate stacking sequence effects is found in Section 4.6.5.

TABLE 4.3.3.2(a) *Extensional and bending stiffnesses.*

	$[0/\pm60]_s$		$[\pm60/0]_s$		$[60/0/-60]_s$		Homogeneous Laminate	
A_{11}	1.05×10^{7}	(7.30×10^{10})	1.05×10^{7}	(7.30×10^{10})	1.05×10^{7}	(7.30×10^{10})	1.05×10^{7}	(7.30×10^{10})
A_{12}	3.42×10^{6}	(2.38×10^{10})	3.42×10^{6}	(2.38×10^{10})	3.42×10^{6}	(2.38×10^{10})	3.42×10^{6}	(2.38×10^{10})
A_{22}	1.05×10^{7}	(7.30×10^{10})	1.05×10^{7}	(7.30×10^{10})	1.05×10^{7}	(7.30×10^{10})	1.05×10^{7}	(7.30×10^{10})
A_{66}	3.55×10^{6}	(2.47×10^{10})	3.55×10^{6}	(2.47×10^{10})	3.55×10^{6}	(2.47×10^{10})	3.55×10^{6}	(2.47×10^{10})
D_{11}	1.55×10^{6}	(1.08×10^{10})	3.36×10^{5}	(2.34×10^{9})	7.42×10^{5}	(5.16×10^{9})	8.75×10^{5}	(6.09×10^{9})
D_{12}	1.50×10^{5}	(1.04×10^{9})	3.92×10^{5}	(2.73×10^{9})	3.12×10^{5}	(2.17×10^{9})	2.85×10^{5}	(1.98×10^{8})
D_{16}	4.74×10^{4}	(3.30×10^{8})	9.50×10^{4}	(6.61×10^{8})	1.42×10^{5}	(9.88×10^{8})	0.0	(0.0)
D_{22}	4.69×10^{5}	(3.26×10^{9})	1.20×10^{6}	(8.35×10^{9})	9.59×10^{5}	(6.67×10^{9})	8.75×10^{5}	(6.09×10^{9})
D_{26}	1.42×10^{5}	(9.88×10^{8})	2.81×10^{5}	(1.95×10^{9})	4.22×10^{5}	(2.94×10^{9})	0.0	(0.0)
D_{66}	1.63×10^{5}	(1.13×10^{9})	4.04×10^{5}	(2.81×10^{9})	3.23×10^{5}	(2.25×10^{9})	2.96×10^{5}	(2.06×10^{9})

Lamina properties are from Table 4.3.3.1(a); unit thickness laminate.

[A] lb/in (N/m) [D] in-lb (N/m)

[1]The LSS used in Figure 4.3.3.2 were chosen for illustrative purposes only and do not represent optimal LSS for a given application.

TABLE 4.3.3.2(b) *Stiffness predictions for seven different LSS for 16-ply, quasi-isotropic, carbon/epoxy, laminated beams.*

Stacking Sequence	In-plane Modulus E_x		Bending Modulus E_x^b		Percent Difference Δ
	Msi	GPa	Msi	GPa	%
$[0_2/(\pm45)_2/90_2]_s$	7.67	52.9	12.8	88.2	67
$[0/\pm45/90]_{2s}$	7.67	52.9	10.1	69.6	32
$[\pm45/0_2/\pm45/90_2]_s$	7.67	52.9	7.80	53.8	1.7
$[\pm45/0/90]_{2s}$	7.67	52.9	6.51	44.9	-15
$[(\pm45)_2/0_2/90_2]_s$	7.67	52.9	4.45	30.7	-42
$[(\pm45)_2/90_2/0_2]_s$	7.67	52.9	3.42	23.6	-55
$[90_2/(\pm45)_2/0_2]_s$	7.67	52.9	3.25	22.4	-58

Properties for T300/934 (V_f = 0.63): E_{11} = 20.0 Msi (138 GPa), E_{22} = 1.4 Msi (9.7 Gpa), G_{12} = 0.65 Msi (4.5 Gpa), ν_{12} = 0.31, Ply Thickness = 0.0056 in. (0.14 mm)

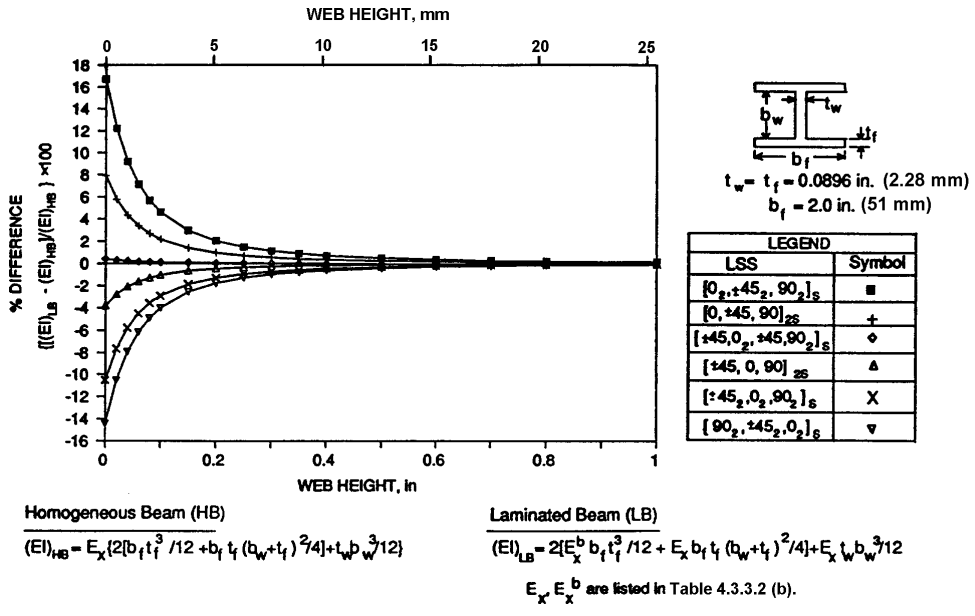

FIGURE 4.3.3.2 *Laminated and homogeneous EI calculations for an I-beam stringer geometry with variable web height.*

4.3.3.3 Thermal expansion

As the use of composite materials becomes more commonplace, they are subjected to increasingly severe mechanical and environmental loading conditions. With the advent of high temperatures in systems, the range of temperatures over which composite systems can be used has increased. The response of laminates to temperature and moisture, as well as to applied loads, must be understood. Previously, laminate extensional and bending stiffnesses were determined; in this section laminate conductivities and expansion coefficients will be defined.

To determine the laminate thermal expansion coefficients and thermally-induced stresses quantitatively, begin at the ply level. The thermoelastic relations for strain in the principal material directions are

$$\{\varepsilon_\ell\} = \{\varepsilon_\ell^{\mathrm{M}}\} + \{\alpha_\ell\}\Delta\mathrm{T} \qquad 4.3.3.3(a)$$

or

$$\{\varepsilon_\ell\} = \{\varepsilon_\ell^{\mathrm{M}}\} + \{\varepsilon_\ell^{\mathrm{T}}\} \qquad 4.3.3.3(b)$$

where

$\{\varepsilon_\ell^{\mathrm{M}}\}$ = strain induced by stress

The change in temperature is represented by $\Delta\mathrm{T}$ and the vector $\{\alpha_\ell\}$ represents the free thermal expansion coefficients of a ply. The individual components are

$$\{\alpha_\ell\} = \begin{pmatrix} \alpha_1 \\ \alpha_2 \\ 0 \end{pmatrix} \qquad 4.3.3.3(c)$$

The thermal strains, $\{\alpha_\ell\}\Delta\mathrm{T}$, are the lamina free thermal expansions, which produce no stress in an unconstrained lamina. The thermal expansion coefficients α_1 and α_2 are the effective thermal expansion coefficients α_1^* and α_2^* of the unidirectional composite.

Substituting for the mechanical strain terms in Equation 4.3.3.3(a) and inverting yields

$$\{\sigma_\ell\} = [\mathrm{Q}]\{\varepsilon_\ell\} - \{\Gamma_\ell\}\Delta\mathrm{T} \qquad 4.3.3.3(d)$$

where

$$\{\Gamma_\ell\} = [\mathrm{Q}]\{\alpha_\ell\}$$

The components in the thermal stress coefficient vector $\{\Gamma_\ell\}$ are

$$\{\Gamma_\ell\} = \begin{Bmatrix} \dfrac{\mathrm{E}_1\alpha_1 + \nu_{12}\,\mathrm{E}_2\,\alpha_2}{\Delta} \\ \dfrac{\mathrm{E}_2\,\alpha_2 + \nu_{12}\,\mathrm{E}_1\alpha_1}{\Delta} \\ 0 \end{Bmatrix} \qquad 4.3.3.3(e)$$

where

$$\Delta = 1 - \frac{\mathrm{E}_2}{\mathrm{E}_1}\nu_{12}^2$$

The vector $\{\Gamma_\ell\}\Delta\mathrm{T}$ physically represents a correction to the stress vector which results from the full constraint of the free thermal strains in a lamina. Both the thermal expansion vector, $\{\alpha_\ell\}\Delta\mathrm{T}$, and the thermal stress vector, $\{\Gamma_\ell\}\Delta\mathrm{T}$, can be transformed to arbitrary coordinates using the relations developed for stress and strain transformations, Equations 4.3.1(k) - (n).

With the transformed thermal expansion and stress vectors, the thermal elastic laminate relations can be developed. Following directly from the development of Equations 4.3.2(g) - (l), the membrane relations are:

$$\{\mathrm{N}\} = [\mathrm{A}]\{\varepsilon^\circ\} + [\mathrm{B}]\{\kappa\} + \{\mathrm{N}^{\mathrm{T}}\} \qquad 4.3.3.3(f)$$

where

$$\{N^T\} = -\int_{-h}^{h} \{\Gamma_x\}\Delta T dz \qquad 4.3.3.3(g)$$

Similarly, the bending relations are

$$\{M\} = [B]\{\varepsilon^\circ\} + [D]\{\kappa\} + \{M^T\} \qquad 4.3.3.3(h)$$

where

$$\{M^T\} = -\int_{-h}^{h} \{\Gamma_x\}\Delta T z dz \qquad 4.3.3.3(i)$$

The integral relations for the thermal stress resultant vector $\{N^T\}$ and thermal moment resultant vector $\{M^T\}$ can be evaluated only when the change in temperature through the thickness is known. For the case of uniform temperature change through the thickness of a laminate, the term ΔT is constant and can be factored out of the integral, yielding:

$$\{N^T\} = -\Delta T \sum_{i=1}^{N} \{\Gamma_x\}^i (z_i - z_{i-1}) \qquad 4.3.3.3(j)$$

$$\{M^T\} = -\frac{1}{2}\Delta T \sum_{i=1}^{N} \{\Gamma_x\}^i \left(z_i^2 - z_{i-1}^2\right) \qquad 4.3.3.3(k)$$

With Equations 4.3.3.3(f) - (i), it is possible to determine effective laminate coefficients of thermal expansion and thermal curvature. These quantities are the extension and curvature changes resulting from a uniform temperature distribution.

Noting that for free thermal effects {N} = {M} = 0, and defining a free thermal expansion vector as

$$\{\alpha_x\} = \{\varepsilon^\circ\}\frac{1}{\Delta T} \qquad 4.3.3.3(l)$$

and a free curvature vector as

$$\{\delta_x\} = \{\kappa\}\frac{1}{\Delta T} \qquad 4.3.3.3(m)$$

Equations 4.3.3.3(f) - (i) can be solved. After suitable matrix manipulations, the following expressions for thermal expansion and thermal curvature for symmetric laminates are found:

$$\{\alpha_x\} = -\frac{1}{\Delta T}[A]^{-1}\{N^T\} \qquad 4.3.3.3(n)$$

$$\{\delta_x\} = -\frac{1}{\Delta T}[D]^{-1}\{N^T\} \qquad 4.3.3.3(o)$$

If the relation for $\{M^T\}$ in Equation 4.3.3.3(i) is examined, symmetry eliminates the $\{M^T\}$ vector. Therefore $\{\delta_x\} = 0$ and no curvatures occur due to uniform temperature changes in symmetric laminates.

The variation of the longitudinal thermal expansion coefficient for a symmetric angle-ply laminate is shown in Figure 4.3.3.3 to illustrate the effect of lamina orientation. At 0° the term α_x is simply the axial lamina coefficient of thermal expansion, and at 90°, α_x equals the lamina transverse thermal expansion coefficient. An interesting feature of the curve is the large negative value of α_x in the region of 30°. Referring to Figure 4.3.3.1, the value of Poisson's ratio also behaves peculiarly in the region of 30°. The odd variation of both the coefficient and Poisson's ratio stems from the magnitude and sign of the shear-extensional coupling present in the individual laminae.

Previously, classes of laminates were shown to have isotropic stiffnesses in the plane of the laminate. Similarly, laminates can be specified which are isotropic in thermal expansion within the plane of the laminate. The requirements for thermal expansion isotropy are considerably less restrictive than those for elastic constants. In fact, any laminate which has two identical, orthogonal thermal expansion coefficients and a zero shear thermal expansion coefficient is isotropic in thermal expansion. Therefore, $[0/90]_s$ and $[\pm 45]_s$ laminates are isotropic in thermal expansion even though they are not quasi-isotropic for elastic stiffnesses.

Laminates which are isotropic in thermal expansion have thermal expansions of the form:

$$\alpha_x = \begin{Bmatrix} \alpha_x \\ \alpha_y \\ \alpha_{xy} \end{Bmatrix} = \begin{Bmatrix} \alpha^* \\ \alpha^* \\ 0 \end{Bmatrix} \qquad 4.3.3.3(p)$$

where the term α^* can be shown to be a function of lamina properties only, as follows:

$$\alpha^* = \alpha_1 + \frac{(\alpha_2 - \alpha_1)(1+\nu_{12})}{1+2\nu_{12}+\frac{E_1}{E_2}} \qquad 4.3.3.3(q)$$

Thus, all laminates of a given ply material, which are isotropic in thermal expansion, have identical thermal expansion coefficients.

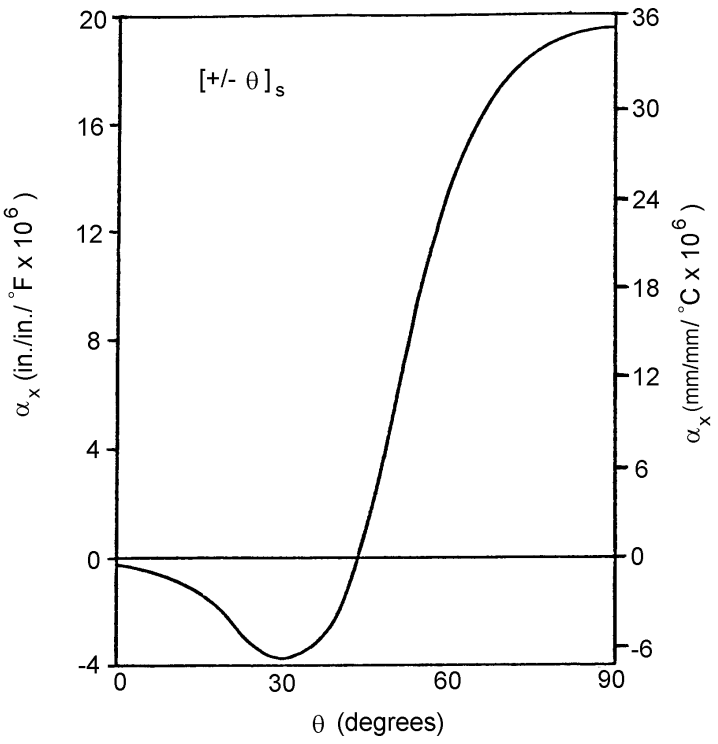

FIGURE 4.3.3.3 *Thermal expansion coefficients for high modulus carbon/epoxy.*

4.3.3.4 Moisture expansion

The term hygroelastic refers to the phenomenon in resin matrix composites when the matrix absorbs and desorbs moisture from and to the environment. The primary effect of moisture is a volumetric change in the laminae. When a lamina absorbs moisture, it expands, and when moisture is lost, the lamina contracts. Thus, the effect is very similar to thermal expansion.

In a lamina, a free moisture expansion vector can be defined as

$$\{\varepsilon_\ell\} = \{\beta_\ell\}\Delta c \qquad 4.3.3.4(a)$$

where

$$\{\beta_\ell\} = \begin{pmatrix} \beta_1 \\ \beta_2 \\ 0 \end{pmatrix} \qquad 4.3.3.4(b)$$

and Δc is the change in specific moisture. Noting that the relations 4.3.3.4(a) and (b) are identical to thermal expansion with $\{\beta_\ell\}$ substituted for $\{\alpha_\ell\}$ and Δc for ΔT, it can easily be seen that all the relations developed for thermal effects can be used for moisture effects.

4.3.3.5 Conductivity

The conductivity (thermal or moisture) of a laminate in the direction normal to the surface is equal to the transverse conductivity of a unidirectional fiber composite. This follows from the fact that normal conductivity for all plies is identical and unaffected by ply orientation.

In-plane conductivities will be required for certain problems involving spatial variations of temperature and moisture. For a given uniform state of moisture in a laminate, the effective thermal conductivities in the x and y directions can be obtained by methods entirely analogous to those used for stiffnesses in Section 4.3.2:

$$\mu_x = \frac{1}{2h}\sum_{i=1}^{N}(\mu_1 m^2 + \mu_2 n^2)t_\ell^i \qquad 4.3.3.5$$

where

μ_1 = conductivity in the fiber direction
μ_2 = conductivity transverse to the fibers
m = $\cos\theta^i$
n = $\sin\theta^i$
θ^i = orientation of ply i
t_ℓ^i = thickness of ply i
N = the number of plies
$2h$ = laminate thickness

The results apply to both symmetric and unsymmetric laminates. The results for moisture conductivity are identical.

4.3.4 Thermal and hygroscopic analysis

The distribution of temperature and moisture through the thickness of a laminate influences the behavior of that laminate. The mathematical descriptions of these two phenomena are identical and the physical effects are similar. Some of these aspects have already been discussed in Sections 4.2.2.3 - 4.2.2.4 and 4.3.3.3 - 4.3.3.5.

A free lamina undergoes stress-free deformation due to temperature change or moisture swelling. In a laminate, stress-free deformation is constrained by adjacent layers producing internal stresses. In addition to these stresses, temperature and moisture content also affect the properties of the material. These effects are primarily related to matrix-dominated strength properties.

The principal strength-degrading effect is related to a change in the glass transition temperature of the matrix material. As moisture is absorbed, the temperature at which the matrix changes from a glassy state to a viscous state decreases. Thus, the elevated-temperature strength properties decrease with increasing moisture content. Limited data suggest that this process is reversible. When the moisture content of the composite is decreased, the glass transition temperature increases and the original strength properties return.

The same considerations also apply for a temperature rise. The matrix, and therefore the lamina, lose strength and stiffness when the temperature rises. Again, this effect is primarily important for the matrix-dominated properties such as $E_2, G_{12}, F_2^{tu}, F_2^{cu}$, and F_{12}^{su}.

The differential equation governing time-dependent moisture sorption of an orthotropic homogeneous material is given by

$$D_1 \frac{\partial^2 c}{\partial x_1^2} + D_2 \frac{\partial^2 c}{\partial x_2^2} + D_3 \frac{\partial^2 c}{\partial x_3^2} = \frac{\partial c}{\partial t} \qquad 4.3.4(a)$$

where

t	= time
x_1, x_2, x_3	= coordinates in principal material directions
c	= specific moisture concentration
D_1, D_2, D_3	= moisture diffusivity coefficients

Equation 4.3.4(a) is based on Fick's law of moisture diffusion. The equation is analogous to the equation governing time dependent heat conduction with temperature ϕ replacing concentration c and thermal conductivities μ_1, μ_2, and μ_3 replacing the moisture diffusivities. For a transversely isotropic lamina with x_1 in the fiber direction, x_2 in the transverse direction, and $x_3 = z$ in the direction normal to the lamina,

$$D_2 = D_3 \qquad 4.3.4(b)$$

These quantities are analogous to the thermal conductivities of a unidirectional fiber composite and have been discussed in Section 4.2.2.4.

An important special case is one-dimensional diffusion or conduction through the thickness of a lamina. In this case, Equation 4.3.4(a) reduces to

$$D_3 \frac{\partial^2 c}{\partial z^2} = \frac{\partial c}{\partial t} \qquad 4.3.4(c)$$

This equation also applies to moisture diffusion or thermal conduction through a laminate, in the direction normal to its laminae planes, since all laminae are homogeneous in the z direction with equal diffusion coefficients, $D_3 = D_z$.

Equation 4.3.4(c) is applicable to the important problem of time-dependent moisture diffusion through a laminate where the two faces are in different moisture environments. After a sufficiently long time has elapsed, the concentration reaches a time-independent state. In this state, since c is no longer time-dependent, Equation 4.3.4(c) simplifies to

$$\frac{d^2 c}{dz^2} = 0 \qquad 4.3.4(d)$$

The specific moisture concentration is a linear function of z and, if the laminate faces are in environments with constant saturation concentrations, c_1 and c_2, then

$$c = \frac{1}{2}[(c_2 - c_1) z/h + c_2 + c_1] \qquad 4.3.4(e)$$

where the laminate thickness is $2h$ and z originates at the mid-surface. In the case where $c_1 = c_2$, Equation 4.3.4(e) reduces to $c = c_1$ = constant as would be expected.

The above discussion of moisture conduction also applies to heat conduction.

Solutions to the time-dependent problem are readily available and considerable work has been performed in the area of moisture sorption (Reference 4.3.4). The most interesting feature of the solutions relates to the magnitude of the coefficient D_z. This coefficient is a measure of how fast moisture diffusion can occur. In typical epoxy matrix systems, D_z is of the order of 10^{-8} (in^2/s, cm^2/s) to 10^{-10} (in^2/s, cm^2/s). The diffusion coefficient is sufficiently small that full saturation of a resin matrix composite may require months or years even when subjected to 100% relative humidity.

The approach typically taken for design purposes is to assume a worst case. If the material is assumed to be fully saturated, it is possible to compute reduced allowable strengths. This is a conservative approach, since typical service environments do not generate full saturation. This approach is used since it allows for inclusion of moisture effects in a relatively simple fashion. It is to be expected that as the design data base and analytical methodologies mature, more physically realistic methods will be developed.

For heat conduction, the time required to achieve the stationary, or time-independent, state is extremely small. Therefore, the transient time-dependent state is generally of little practical importance for laminates.

4.3.4.1 Symmetric laminates

The laminate stacking sequence (LSS) can be chosen to control the effects of environment on stiffness and dimensional stability. When considering the special case of constant temperature and moisture content distributions in symmetric laminates, the effect of environment on in-plane stiffness relates to the relative percentages of chosen ply orientations. For example, LSS dominated by 0° plies will have longitudinal moduli that are nearly independent of environment. Note that increasing the environmental resistance of one laminate in-plane modulus may decrease another.

Bending and torsional stiffnesses depend on both LSS and environment. Preferential stacking of outer ply groups having relatively high extensional or shear moduli will also promote high bending or torsional stiffness, respectively. As with in-plane moduli, the higher the bending or torsional stiffness the better the corresponding environmental resistance. When optimizing environmental resistance, compromises between longitudinal bending, transverse bending and torsion need to be made due to competing relationships with LSS.

Unsymmetric temperature and moisture content distributions will affect the components of the stiffness matrix [ABD] differently, depending on LSS. In general, coupling components which were zero for symmetric laminates having symmetric temperature and moisture content distributions become nonzero for an unsymmetric environmental state. This effect can be minor or significant depending on LSS, material type, panel thickness and the severity of temperature/moisture content gradients.

Environmentally-induced panel warpage will occur in symmetric laminates when conditions yield an unsymmetric residual stress distribution about the laminate midplane. This may occur during the cure process due to uneven heating or crystallization through the laminate thickness. Unsymmetric temperature and moisture content distributions can also lead to panel warpage in symmetric laminates. This is due to the unsymmetric shrinkage or swelling through the laminate thickness.

4.3.4.2 Unsymmetric laminates

The in-plane thermal and moisture expansion of unsymmetric laminated plates subjected to any environmental condition (i.e., constant, symmetric and unsymmetric temperature and moisture content distributions) is dependent on LSS (e.g., Reference 4.3.4.2(a)). In general, environmentally induced panel warpage occurs with unsymmetric laminates.

Panel warpage in unsymmetric laminates depends on LSS and changes as a function of temperature and moisture content. Zero warpage will occur in unsymmetric laminates only when temperature and moisture content distributions result in either zero or symmetric residual stress distributions. Equilibrium environmental states that result in zero residual stresses are referred to as stress-free conditions (see Reference 4.3.2(e).

Since unsymmetric LSS warp as a function of temperature and moisture content, their use in engineering structures has generally been avoided. The warped shape of a given unsymmetric laminate has been found to depend on LSS and ratios of thickness to in-plane dimensions (e.g., References 4.3.4.2(b) and (c)). Relatively thin laminates tend to take a cylindrical shape rather than the saddle shape predicted

by classical lamination theory. This effect has been accurately modeled using a geometrically nonlinear theory.

Additional information on laminate stacking sequence effects is found in Section 4.6.5.

4.3.5 Laminate stress analysis

The physical properties defined in Section 4.3.3 enable any laminate to be represented by an equivalent homogeneous anisotropic plate or shell element for structural analysis. The results of such analyses will be the definition of stress resultants, bending moments, temperature, and moisture content at any point on the surface which defines the plate. With this definition of the local values of state variables, a laminate analysis can be performed to determine the state of stress in each lamina to assess margins for each critical design condition.

4.3.5.1 Stresses due to mechanical loads

To determine stresses in the individual plies, the laminate mid-plane strain and curvature vectors are used. Writing the laminate constitutive relations

$$\left\{\begin{array}{c} N \\ \hline M \end{array}\right\} = \left[\begin{array}{c|c} A & B \\ \hline B & D \end{array}\right]\left\{\begin{array}{c} \varepsilon^{\circ} \\ \hline \kappa \end{array}\right\} \qquad 4.3.5.1(a)$$

a simple inversion will yield the required relations for $\{\varepsilon^{\circ}\}$ and $\{\kappa\}$. Thus

$$\left\{\begin{array}{c} \varepsilon^{\circ} \\ \hline \kappa \end{array}\right\} = \left[\begin{array}{c|c} A & B \\ \hline B & D \end{array}\right]^{-1}\left\{\begin{array}{c} N \\ \hline M \end{array}\right\} \qquad 4.3.5.1(b)$$

Given the strain and curvature vectors, the total strain in the laminate can be written as

$$\{\varepsilon_x\} = \{\varepsilon^{\circ}\} + z\{\kappa\} \qquad 4.3.2(d)$$

The strains at any point through the laminate thickness are now given as the superposition of the mid-plane strains and the curvatures multiplied by the distance from the mid-plane. The strain field at the center of ply i in a laminate is

$$\{\varepsilon_x\}^i = \{\varepsilon^{\circ}\} + \frac{1}{2}\{\kappa\}(z^i + z^{i-1}) \qquad 4.3.5.1(c)$$

where the term

$$\frac{1}{2}(z^i + z^{i-1})$$

corresponds to the distance from the mid-plane to the center of ply i. It is possible to define curvature induced strains at a point through the laminate thickness simply by specifying the distance from the mid-plane to the point in question.

The strains defined in Equation 4.3.5.1(c) correspond to the arbitrary laminate coordinate system. These strains can be transformed into the principal material coordinates for this ply using the transformations developed previously (Equation 4.3.1(m)). Thus

$$\{\varepsilon_\ell\}^i = \left[\theta^i\right]^{-1}\{\varepsilon_x\}^i \qquad 4.3.5.1(d)$$

where the superscript i indicates which layer and, therefore, which angle of orientation to use.

With the strains in the principal material coordinates defined, stresses in the same coordinates are written by using the lamina reduced stiffness matrix (Equation 4.3.1(h)).

$$\{\sigma_\ell\}^i = \left[Q^i\right]\{\varepsilon_\ell\}^i \qquad 4.3.5.1(e)$$

Again, the stiffness matrix used must correspond to the correct ply, as each ply may be a different material.

The stresses in the principal material coordinates can be determined without the use of principal material strains. Using the strains defined in the laminate coordinates (Equation 4.3.5.1(c)) and the transformed lamina stiffness matrix (Equations 4.3.1(o,q,r)), stresses in the laminate coordinate system can be written as

$$\{\sigma_x\}^i = \left[\overline{Q}^i\right]\{\varepsilon_x\}^i \qquad 4.3.5.1(f)$$

and these stresses are then transformed to the principal material coordinates using the relations 4.3.1(m). Thus

$$\{\sigma_\ell\}^i = \left[\theta^i\right]^{-1}\{\sigma_x\}^i \qquad 4.3.5.1(g)$$

By reviewing these relations, it can be seen that, for the case of symmetric laminates and membrane loading, the curvature vector is zero. This implies that the laminate coordinate strains are identical in each ply and equal to the mid-plane strains. The differing angular orientation of the various plies will promote different stress and strain fields in the principal material coordinates of each ply.

4.3.5.2 Stresses due to temperature and moisture

In Section 4.3.3.3, equations for the thermoelastic response of composite laminates were developed. It was indicated that thermal loading in laminates can cause stresses even when the laminate is allowed to expand freely. The stresses are induced because of a mismatch in thermal expansion coefficients between plies oriented in different directions. Either the mechanical stresses of the preceding section or the thermomechanical stresses can be used to evaluate laminate strength.

To determine the magnitude of thermally induced stresses, the thermoelastic constitutive relations (Equations 4.3.3.3(f) - (i)) are required. Noting that free thermal stress effects require that $\{N\} = \{M\} = 0$, these relations are written as

$$\begin{Bmatrix} 0 \\ --- \\ 0 \end{Bmatrix} = \begin{bmatrix} A & | & B \\ --- & | & --- \\ B & | & D \end{bmatrix} \begin{Bmatrix} \varepsilon^\circ \\ --- \\ \kappa \end{Bmatrix} + \begin{Bmatrix} N^T \\ --- \\ M^T \end{Bmatrix} \qquad 4.3.5.2(a)$$

Inverting these relations yields the free thermal strain and curvature vectors for the laminate. Proceeding as before, the strain field in any ply is written as

$$\{\varepsilon_x\}^i = \{\varepsilon^\circ\} + \tfrac{1}{2}(z^+ \quad z^{i-1})\{\kappa\} \qquad 4.3.5.2(b)$$

Stresses in the laminate coordinates are

$$\{\sigma_x\}^i = \left[\overline{Q}^i\right]\{\varepsilon_x\}^i - \{\Gamma_x\}^i \Delta T^i \qquad 4.3.5.2(c)$$

which can then be transformed to the principal material coordinates. Thus

$$\{\sigma_\ell\} = \left[\theta^i\right]^{-1}\{\sigma_x\}^i \qquad 4.3.5.2(d)$$

The stresses can also be found by transforming the strains directly to principal material coordinates and then finding the principal material coordinate stresses.

For uniform temperature fields in symmetric laminates, the coupling matrix, $[B]$, and the thermal moment resultant vector, $\{M^T\}$, vanish and:

$$\{\varepsilon^\circ\} = \{\alpha_x\}\Delta T \qquad 4.3.5.2(e)$$

and

$$\{\kappa\} = 0 \qquad 4.3.5.2(f)$$

In this case, the strains in the laminate coordinates are identical in each ply with the value

$$\{\varepsilon_x\}^i = \{\varepsilon^\circ\} = \{\alpha_x\}\Delta T \qquad 4.3.5.2(g)$$

and the stresses in the principal material coordinates are

$$\{\sigma_x\}^i = \left[\overline{Q}^i\right](\{\alpha\} - \{\alpha_x\}^i)\Delta T \qquad 4.3.5.2(h)$$

These relations indicate that the stresses induced by the free thermal expansion of a laminate are related to the differences between the laminate and ply thermal expansion vectors. Therefore, the stresses are

proportional to the difference between the amount the ply would freely expand and the amount the laminate will allow it to expand.

A further simplification can be found if the laminate under investigation is isotropic in thermal expansion. It can be shown that, for this class of laminates subjected to a uniform temperature change, the stresses in the principal material coordinates are identical in every ply. The stress vector is

$$\{\sigma_\ell\} = \frac{E_{11}(\alpha_{22} - \alpha_{11})\Delta T}{1 + 2\nu_{12} + \frac{E_{11}}{E_{22}}} \begin{Bmatrix} 1 \\ -1 \\ 0 \end{Bmatrix} \qquad 4.3.5.2(i)$$

where it can be seen that the transverse direction stress is equal and opposite to the fiber direction stress.

Similar developments can be generated for moisture-induced stresses. All of the results of this section apply when moisture swelling coefficients, $\{\beta_\ell\}$, are substituted for thermal expansion coefficients, $\{\alpha_\ell\}$.

4.3.5.3 Netting analysis

Another approach to the calculation of ply stresses is sometimes used for membrane loading of laminates. This procedure is netting analysis and, as the name implies, treats the laminate as a net. All loads are carried in the fibers while the matrix material serves only to hold the geometric position of the fibers.

Since only fibers are assumed to load in this model, stress-strain relations in the principal material directions can be written as

$$\sigma_{11} = E_1 \varepsilon_{11} \qquad 4.3.5.3(a)$$

or

$$\varepsilon_{11} = \frac{1}{E_1}\sigma_{11} \qquad 4.3.5.3(b)$$

and

$$E_2 = G_{12} = \sigma_{22} = \sigma_{12} = 0 \qquad 4.3.5.3(c)$$

The laminate stiffnesses predicted with a netting analysis will be smaller than those predicted using lamination theory, due to the exclusion of the transverse and shear stiffnesses. This effect is demonstrated in Table 4.3.5.3 for a quasi-isotropic laminate comprised of high-modulus graphite/epoxy. The stiffness properties predicted using a netting analysis are approximately 10% smaller than lamination theory predictions. Experimental work has consistently shown that lamination theory predictions are more realistic than netting analysis predictions.

Although the stiffness predictions using netting analysis are of limited value, the analysis can be used as an approximation of the response of a composite with matrix damage. It may be considered as a worst case analysis and is frequently used to predict ultimate strengths of composite laminates

TABLE 4.3.5.3 *Laminate elastic constants.*

Analysis	E_x Msi (GPa)	E_y Msi (GPa)	G_{xy} Msi (GPa)	γ_{xy}
Lamination Theory	9.42 (64.9)	9.42 (64.9)	3.55 (24.5)	0.325
Netting Analysis	8.33 (57.4)	8.33 (57.4)	3.13 (21.6)	0.333

4.3.5.3.1 Netting analysis for design of filament wound pressure vessels

Netting analysis is a simple tool for approximating hoop and axial stresses in filament wound pressure vessels. The technique assumes that the stresses induced to the structure are carried entirely by the reinforcing fiber, and that all fibers are uniformly stressed in tension. The load carrying contribution of the matrix is neglected, and its only function is to hold the geometric position of the fibers. Netting analysis cannot be used to determine bending, shear or discontinuity stresses or resistance to buckling.

To illustrate the netting analysis principles, consider a filament wound pressure vessel of radius R with an internal pressure P. Assume the vessel is wound with only helical fibers at a wrap angle of $\pm\alpha$, an allowable fiber stress of σ_f, and thickness t_f. Figure 4.3.5.3.1(a) illustrates the forces acting on the $\pm\alpha$ helical layer in the axial direction. The running load, N_X, is the force per unit length in the axial direction.

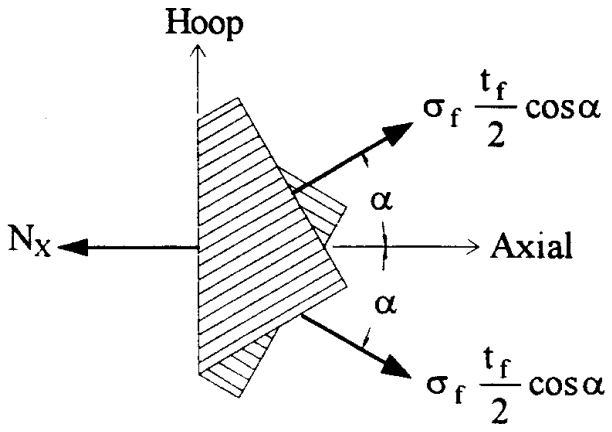

FIGURE 4.3.5.3.1(a) *Helical layer element - axial direction.*

Summing forces in the axial direction:

$$N_x = \frac{PR}{2} = \sigma_f \, t_f \cos^2 \alpha \qquad 4.3.5.3.1(a)$$

Solving for t_f provides the helical fiber thickness required to carry the internal pressure:

$$t_f = \frac{PR}{2\sigma_f \cos^2 \alpha} \qquad 4.3.5.3.1(b)$$

Figure 4.3.5.3.1(b) shows the forces acting in the $\pm\alpha$ helical layer in the hoop direction. The running load, N_H, is the force per unit length in the hoop direction.

Summing forces in the hoop direction:

$$N_h = PR = \sigma_f \, t_f \sin^2 \alpha \qquad 4.3.5.3.1(c)$$

Solving for t_f,

$$t_f = \frac{PR}{\sigma_f \sin^2 \alpha} \qquad 4.3.5.3.1(d)$$

Substituting t_f for Equation 4.3.5.3.1(b) in Equation 4.3.5.3.1(c), yields $\tan^2 \alpha = 2$, solving for wrap angle, $\alpha = \pm 54.7$ degrees. This is the wrap angle required for a pressure vessel utilizing only helical layers.

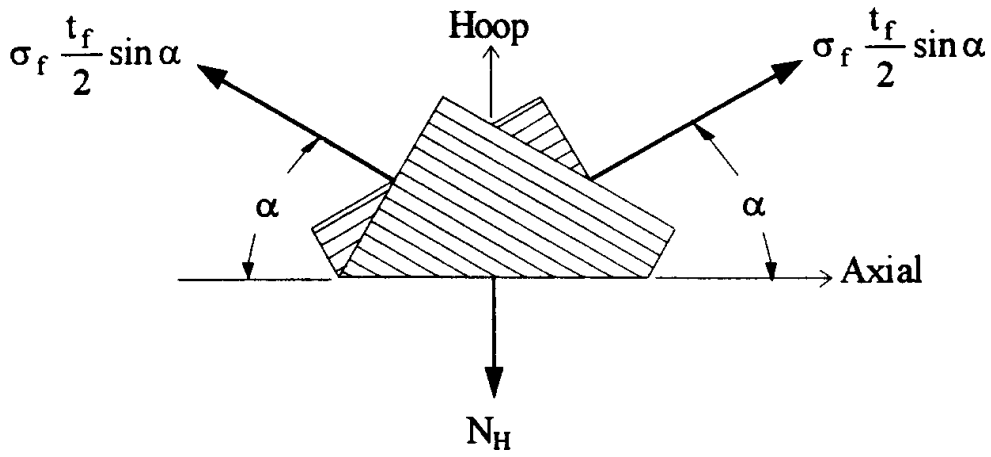

FIGURE 4.3.5.3.1(b) *Helical layer element - hoop direction.*

Now consider a filament wound pressure vessel with both helical and hoop layers. Where the helical layers have a wrap angle of $\pm\alpha$ and the hoop layers have a wrap angle of 90 degrees. Again, Figure 4.3.5.3.1(a) illustrates the forces acting on the $\pm\alpha$ helical layer in the axial direction. Summing forces in the axial direction and solving for t_f, yields Equation 4.3.5.3.1(b), which is the helical fiber thickness required to carry the internal pressure. Figure 4.3.5.3.1(c) shows the forces acting on the $\pm\alpha$ helical layer and the hoop layer in the hoop direction. Summing forces in the hoop direction and substituting t_f from Equation 4.3.5.3.1(b) yields:

$$t_f = \frac{PR}{2\sigma_f}\left(2 - \tan^2\alpha\right) \qquad 4.3.5.3.1(e)$$

where t_f is the hoop layer thickness required to carry the internal pressure.

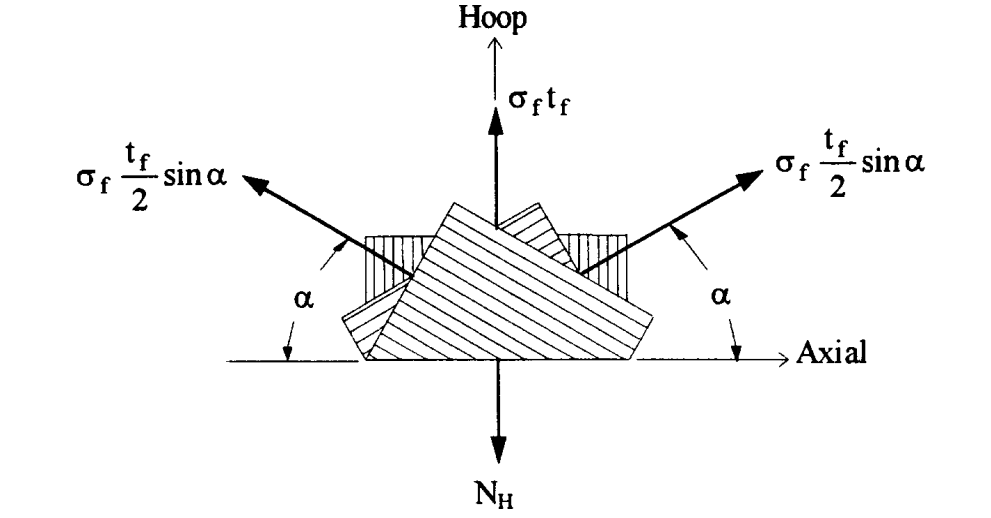

FIGURE 4.3.5.3.1(c) *Helical and hoop layer element - hoop direction.*

The fiber thickness (t_f) and allowable fiber stress (σ_f) can also be expressed in the following standard filament winding terms. Band density (A), which is the quantity of fiber reinforcement per inch of band width, where the band width (W) is the width of fiber reinforcement as it is applied to the mandrel. Tow tensile capacity (f), which is the load carrying capability of one tow of reinforcement fiber, and layers (L), which is the number of layers required to carry the internal pressure. Substituting these terms into Equation 4.3.5.3.1(b) and solving for L:

$$L = \frac{PR}{2Af_{HELIX}\cos^2\alpha} \qquad 4.3.5.3.1(f)$$

Where L is the number of helical layers required to carry the internal pressure. Substituting these terms into Equation 4.3.5.3.1(e) and solving for L:

$$L = \frac{PR}{2Af_{HOOP}}\left(2 - \tan^2\alpha\right) \qquad 4.3.5.3.1(g)$$

Where L is the number of hoop layers required to carry the internal pressure.

The tow tensile capacities (f_{HELIX} and f_{HOOP}) can be determined experimentally. Standard practice is to design and fabricate pressure vessels that will fail in either helix or hoop during hydroburst testing. Substituting the design parameters and hydroburst results into Equations 4.3.5.3.1(f) and 4.3.5.3.1(g), and solving for f provides the tow tensile capacity for the given fiber in both the helix and hoop directions.

Netting analysis is a useful tool for approximating hoop and axial stresses in filament wound pressure vessels. It is a conservative analysis technique that considers only the strength of the reinforcing fiber. However, when utilizing experimentally determined tow tensile capacities, netting analysis is an excellent preliminary design tool that is still used throughout the filament winding industry.

4.3.5.4 Interlaminar stresses

The analytical procedures which have been developed can be used to predict stresses within each lamina of a laminate. The stresses predicted are planar due to the assumed state of plane stress. There are cases where the assumption of plane stress is not valid and a three-dimensional stress analysis is required.

An example of such a case exists at certain free edges in laminates where stress free boundary conditions must be imposed.

4.3.5.5 Nonlinear stress analysis

All the preceding material in this chapter has related to laminae which behave in a linear elastic fashion. Composites can behave in a nonlinear manner due to internal damage or nonlinear behavior of the matrix material. Matrix nonlinearity or micro-cracking can result in laminae which have nonlinear stress-strain curves for transverse stress or axial shear stress. When this situation exists, the elastic laminate stress analysis of Section 4.3.5.1 must be replaced by a nonlinear analysis. A convenient procedure for the nonlinear analysis is presented in Reference 4.3.5.5.

4.3.6 Summary

- When laminae are at an angle to the laminate reference axes, the lamina stiffness relations described in Section 4.2 must be transformed into the laminate coordinate system to perform laminate stress-strain analysis.

- Stresses and strains are related in the principal lamina material directions by 6 x 6 symmetric compliance [S] and stiffness [Q] matrices.

- The transformation of stresses and strains from the principal lamina material direction to the laminate coordinate system is accomplished by following the rules for transformation of tensor components (equations 4.3.1(k) and 4.3.1(m)).

- Lamination theory makes the same simplifications as classical thin plate theory for isotropic materials. Therefore, the procedures used to calculate stresses and deformations are dependent on the fact that laminate thickness is considerably smaller than the laminate's in-plane dimensions.

- The strain at a y point in a laminate is defined as the sum of the mid-surface strain (ε), and the product of the curvature (κ) and the distance from the mid surface (z).

- Laminate load (N) and moment (M) resultants are related to mid-plane strains and curvatures as described by the [A], [B], and [D] 3 x 3 stiffness matrices (Equations 4.3.2 (k) - (m)).

- Two-dimensional lamination theory can generally be used to predict stresses within each lamina of a laminate. The planar stresses are predicted based on an assumption of plane stress. In cases where interlaminar stresses exist, three-dimensional stress analysis is required.

- In symmetric laminates, bending-extensional coupling is eliminated by a symmetric stacking sequence whereby $[B] = 0$.

- Since they are susceptible to warping as a result of processing and usage conditions, use of unsymmetric laminates in composite structures should generally be avoided for both design and manufacture.

4.4 LAMINATE STRENGTH AND FAILURE

Methods of stress analysis of laminates subjected to mechanical loads, temperature changes, and moisture absorption were presented in Section 4.3.5. The results of such a stress analysis can be used to assess the strength of a laminate. As a result of the complexity of the structure of a composite laminate, several modes of failure are possible, and it is desirable for the failure mode as well as the failure stress or strain to be predicted. The analytical problem is to define the failure surface for the laminate in either stress or strain space.

Laminate failure may be calculated by applying stress or strain limits at the laminate level or, alternatively, at the ply level. Ply level stresses or strains are the more frequently used approach to laminate strength. The average stresses in a given ply may be used to calculate either an onset of damage, which is frequently called "first ply failure", or a critical failure which is regarded as ultimate strength. In the former case, subsequent damages leading to laminate failure are then calculated. This calculation of subsequent damage is sometimes performed using the "sequential ply failure" methodology, and sometimes performed using "netting" analysis. These approaches are discussed subsequently. Four factors should be considered in assessing the validity of using ply level stresses for failure calculation. The first is the question of which tests (or analyses) should be used to define the ply strength values. In particular, it must be recognized that a crack parallel to the fibers may result in failure of a transverse tensile test specimen of a unidirectional composite, while the same crack may have an insignificant effect in a laminate test. The second factor is the assumption that local failures within a ply are contained within the ply and are determined solely by the stress/strain state in that ply. There is evidence that the former assumption is not valid under fatigue loading, during which a crack within one ply may well propagate into adjacent plies. In this case, the ply-by-ply model may not be the best analytical approach. Furthermore, matrix cracking within one ply is not determined uniquely by the stresses and strains within that ply but is influenced by the orientation of adjacent layers as well as by the ply thickness (Reference 4.4). The third factor is the existence of residual thermal stresses, usually of unknown magnitude, resulting from the fabrication process. The fourth factor is that it does not cover the possibility of delaminations which can occur, particularly at free edges. Thus, the analysis is limited to in-plane failures.

4.4.1 Sequential ply failure approach

4.4.1.1 Initial ply

To predict the onset of damage, consider stresses remote from the edges in a laminate which is loaded by in-plane forces and/or bending moments. If there is no external bending, if the membrane forces are constant along the edges, and if the laminate is balanced and symmetric, the stresses in the ith layers are constant and planar. With reference to the material axes of the laminae, fiber direction x_1 and transverse direction x_2, the stresses in the ith ply are written σ_{11}^{i}, σ_{22}^{i}, and σ_{12}^{i}. Failure is assumed to occur when the selected semi-empirical failure criteria involving these calculated stresses or the associated strains are satisfied. Numerous criteria have been proposed for calculation of onset of damage. These may be grouped into two broad categories - mode-based and purely empirical. Mode based criteria treat each identifiable physical failure mode, such as fiber-direction tensile failure and matrix-dominated transverse failure, separately. A purely empirical criterion generally consists of a polynomial combination of the three stress or strain components in a ply. Such criteria attempt to combine the effects of several different failure mechanisms into one function and may, therefore, be less representative than physically based criteria. All criteria rely on test data at the ply level to set parameters and are therefore at least partially empirical in nature.

The selection of appropriate criteria can be a controversial issue and the validity of any criterion is best determined by comparison with test data. As a consequence, different criteria may be best for different materials. Two mode-based failure criteria are presented here as examples: the maximum strain criteria and the failure criteria proposed by Hashin. It is important, however, for the engineer to consider the material, the application, and the test data in choosing and utilizing a failure criterion.

The maximum strain criteria may be written as

$$\begin{aligned} \varepsilon_{11}^{cu} \;\le\; \varepsilon_{11}^{i} \;\le\; \varepsilon_{11}^{tu} \\ \varepsilon_{22}^{cu} \;\le\; \varepsilon_{22}^{i} \;\le\; \varepsilon_{22}^{tu} \\ |\, \varepsilon_{12}^{i} \,| \;\le\; \varepsilon_{12}^{su} \end{aligned} \qquad \text{4.4..1.1(a)}$$

For given loading conditions, the strains in each ply are compared to these criteria. Whichever strain reaches its limiting value first indicates the failure mode and first ply to fail for those loading conditions. The limiting strains, ε_{11}^{tu}, ε_{11}^{cu}, etc., are the specified maximum strains to be permitted in any ply. Generally, these quantities are specified as some statistical measure of experimental data obtained by uniaxial loading of a unidirectional laminate. For example, in the case of axial strain, ε_{11}, a B-basis strain allowable from unidirectional tests can be used. Other limits may also be imposed. For example, in the case of shear strain, something equivalent to a "yield" strain may be used in place of the ultimate shear strain.

The failure criteria proposed by Hashin (Reference 4.4.1.1(a)) may be written as:

Fiber modes

Tensile

$$\left(\frac{\sigma_{11}}{F_1^{tu}}\right)^2 + \left(\frac{\sigma_{12}}{F_{12}^{su}}\right)^2 = 1 \qquad \text{4.2.4(f)}$$

Compressive

$$\left(\frac{\sigma_{11}}{F_1^{cu}}\right)^2 = 1 \qquad \text{4.2.4(g)}$$

Matrix modes

Tensile

$$\left(\frac{\sigma_{22}}{F_2^{tu}}\right)^2+\left(\frac{\sigma_{12}}{F_{12}^{su}}\right)^2=1 \qquad 4.2.4(h)$$

Compressive

$$\left(\frac{\sigma_{22}}{2F_{23}^{su}}\right)^2+\left[\left(\frac{F_2^{cu}}{2F_{23}^{su}}\right)^2-1\right]\left(\frac{\sigma_{22}}{F_2^{cu}}\right)+\left(\frac{\sigma_{12}}{F_{12}^{su}}\right)^2=1 \qquad 4.2.4(i)$$

It should be noted that some users of these criteria add a shear term to equation 4.2.4(g) to reflect the case in which shear mode instability contributes to the compressive failure mechanism (Reference 4.4.1.1(b)). In that case, equation 4.2.4(g) is replaced by:

$$\left(\frac{\sigma_{11}}{F_1^{cu}}\right)^2+\left(\frac{\sigma_{12}}{F_{12}^{su}}\right)^2=1 \qquad 4.4..1.1(b)$$

The limiting stresses in the criteria, F_1^{cu}, F_{12}^{su}, etc., are the specified maximum stresses to be permitted in any ply. As with the case of strains, statistical data from unidirectional tests are generally used to define these quantities. However, as an example of the care required, it should be noted that the stress which produces failure of a 90° coupon in tension is not necessarily a critical stress level for a ply in a multi-directional laminate. One may wish to use, instead, the stress level at which crack density in a ply reduces the effective stiffness by a specified amount. Such a stress level could be determined by either a fracture mechanics analysis or testing of a crossply laminate (Reference 4.4).

In an onset of damage approach, the selected failure criteria are used for each layer of the laminate. The layer for which the criteria are satisfied for the lowest external load set will define the loading which produces the initial laminate damage. The layer which fails and the nature of the failure (i.e., fiber failure or cracking along the fibers) are identified. This is generally called first-ply failure. When the first ply failure is the result of fiber breakage, the resulting ply crack will introduce stress concentrations into the adjacent plies. In this case, it is reasonable to consider that first ply failure is equivalent to laminate failure. A different criterion exists when the first ply failure results from matrix cracking and/or fiber/matrix interface separations. Here it is reasonable to consider that the load-carrying capacity of the ply will be changed significantly when there is a substantial amount of matrix mode damage. Treatment of this case is discussed in the following section.

Additional concerns to be addressed in considering the initial failure or onset of damage include bending, edge stresses, and residual thermal stresses. Bending occurs when there are external bending and/or twisting moments or when the laminate is not symmetric. In these cases the stresses σ_{11}^i, σ_{22}^i, and σ_{12}^i in a layer are symmetric in x_3. Consequently, the stresses assume their maximum and minimum values at the layer interfaces. The failure criteria must be examined at these locations for each layer. Different approaches utilize the maximum value or the average value in such cases.

The evaluation of onset of failure as a result of the edge stresses is much more complicated as a result of the sharp gradients (indicated by analytical singularities) in these stresses. Numerical methods cannot uncover the nature of such stress singularity, but there are analytical treatments (e.g. Reference 4.4.1) which can. The implication of such edge stress fields for failure of the laminate is difficult to assess. This situation is reminiscent of fracture mechanics in the sense that stresses at a crack tip are theoretically infinite. Fracture mechanics copes with this difficulty with a criterion for crack propagation based on the amount of energy required to open a crack, or equivalently, the value of the stress intensity factor. Similar considerations may apply for laminate edge singularities. This situation in composite materials is more complicated since a crack initiating at the edge will propagate between anisotropic layers. It appears, therefore, that at the present time the problem of edge failure must be relegated to experimentation, or approximate analysis.

In the calculation of first-ply failure, consideration must also be given to residual thermal stresses. The rationale for including residual thermal stresses in the analysis is obvious. The stresses exist after processing. Therefore, they can be expected to influence the occurrence of first-ply failure. However, matrix materials exhibit viscoelastic, or time-dependent, effects, and it may be that the magnitude of the residual stresses will be reduced through a process of stress relaxation. Additionally, the processing stresses may be reduced through the formation of transverse matrix microcracks. The question of whether to include residual stresses in the analysis is complicated by difficulties in measuring these stresses in a laminate and by difficulties in observing first-ply failure during a laminate test. It is common practice to neglect the residual thermal stresses in the calculation of ply failure. Data to support this approach do not appear to be available. However, at the present time, damage tolerance requirements limit allowable strain levels in polymeric matrix laminates to 3000 to 4000 $\mu\varepsilon$. This criterion becomes the dominant design restriction and obviates, temporarily, the need to resolve the effects of residual thermal stresses.

4.4.1.2 Subsequent failures

Often laminates have substantial strength remaining after the first ply has experienced a failure, particularly if that first failure is a matrix-dominated failure. A conservative approach for analyzing subsequent failure is to assume that the contribution of that first failed ply is reduced to zero. If failure occurs in the fiber-dominated mode, this may be regarded, as discussed earlier, as ultimate laminate failure. If not, then the stiffness in the fiber direction E_L is reduced to zero. If failure occurs in the matrix-dominated mode, the elastic properties E_T and G_L are reduced to zero. The analysis is then repeated until all plies have failed. Generally, the progressive failures of interest are initial and subsequent failures in the matrix mode. In that case, the basic assumptions for netting analysis result where the ultimate load is defined by E_T and G_L vanishing in all laminae. The basic issues involved in modeling post-first-ply behavior are described in Reference 4.4.2. For some materials and/or for some properties, matrix mode failures may not have an important effect. However, for some properties, such as thermal expansion coefficients, ply cracking may have a significant effect.

4.4.2 Fiber failure approach (laminate level failure)

In composites laminates, there are two characteristic stress or strain levels which can be considered in the evaluation of strength. One is the stress or strain state at which a non-catastrophic first-ply failure can occur and the other is the maximum static stress or strain state which the laminate can carry. In those cases where the material exhibits minimal micro-cracking, or where the application is such that effects of micro-cracking need not be considered, a failure criterion based only upon fiber failure may be used. A common practice in the aerospace industry is to use a failure criterion based only upon fiber strain allowables, for which fiber failure in any lamina is considered laminate ultimate failure. Hence, failure is a single event rather than the result of a process.

Perhaps the most common example of this laminate level failure criterion is a modification of the maximum strain criterion. The same assumptions of no external bending, membrane forces constant along the edges, and a balanced and symmetric laminate, are initially used. The basic lamina failure envelope is the same as the conventional maximum-strain envelope for tension- and compression-dominated loads, but introduces truncations in the tension-compression (shear) quadrants as shown in Figure 4.4.2. A critical assumption in this criterion is that the laminate behavior is fiber-dominated meaning that there are fibers in sufficient multiple directions such that strains are limited by the presence of the fibers to inhibit matrix cracking. In many practical applications, this typically translates into having fibers in (at least) each of four directions relative to the primary loads: 0°, 90°, and ±45°. Furthermore, plies are not "clustered" (that is, several plies of the same orientation are not layed together) in order to inhibit matrix macrocracking. With these assumptions, the first translation of the maximum strain criterion to the laminate level is a limiting of the strain in the transverse direction, θ_{90}, to the fiber direction limiting strain to reflect the fact that such "well-designed" laminates with fibers in multiple directions restrict strains in any in-plane direction. Alternatively, if there is reason to believe that matrix cracking will be structurally

significant, the 90° strain cutoff based on fiber direction strain could be replaced by an empirically established tensile limit reflecting a matrix-dominated mode. This limit was originally expressed as a constant strain limit. However, if such a limit is based upon the case of a constant 90° stress in a ply, this would result in a sloped line in the strain plane with the slope related to the Poisson's ratio of the unidirectional lamina:

$$\alpha = \tan^{-1}\left(\nu_{LT}^{lamina}\right) \qquad 4.4.2(a)$$

Such a cutoff is parallel to the uniaxial load line shown in Figure 4.4.2. It should be further noted that possible limitations due to lamina level shear strains are inoperative due to the assumption that the fibers in multiple directions restrict such strains to values below their failure values.

Many users recognize a need to truncate the maximum strain predictions in the tension-compression quadrants. While the particular truncations vary, perhaps the most widely used version is that shown in Figure 4.4.2. These truncations were originally based on data obtained for shear loading of such fiber-dominated laminates. These data lie in the second and fourth quadrants. The 45° cutoffs represent the locus of constant shear strain. These two symmetric truncations are located by finding the intersections of the limiting uniaxial strain lines with the lines representing pure uniaxial stress conditions in fiber directions in 0° and 90° unidirectional plies. At this point, the axial strain now becomes more critical than the shear. The endpoints of the truncations are therefore found by drawing lines through the origin with angles from the relative axes of a which account for the unidirectional ply Poisson's ratio:

$$\alpha = \tan^{-1}\left(\nu_{LT}^{lamina}\right) \qquad 4.4.2(b)$$

thereby yielding the desired pure uniaxial state of stress in the fiber direction. The intersection of these two lines with the greater of the two pure uniaxial stress conditions in the unidirectional plies locates the endpoint of each cutoff. It is always necessary that the cutoff be located by the higher of the uniaxial strengths since, otherwise, the cutoff would undercut the measured uniaxial strain to failure at the other end. This procedure results in the same failure diagram for all fiber-dominated laminates. It should be emphasized that this procedure requires the use of the Poisson's ratio of the unidirectional ply even when the laminate contains fabric plies.

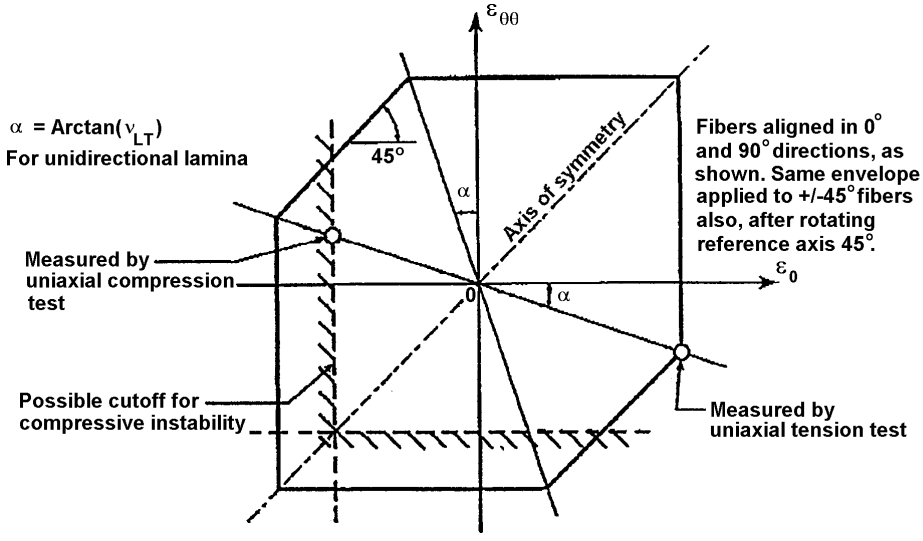

FIGURE 4.4.2 *Illustration of laminate level failure approach.*

This failure model, as represented in Figure 4.4.2, has been developed from experience with fiber-reinforced polymer matrix composites used on subsonic aircraft, particularly with carbon/epoxy mate-

rials, for which the lamina n_{TL} is approximately 0. It should not be applied to other composites, such as whisker-reinforced metal-matrix materials. Figure 4.4.2 addresses only fiber-dominated failures because, for the fiber polymer composites used on subsonic aircraft, the microcracking in the matrix has not been found to cause reductions in the static strength of laminates, particularly if the operating strain level has been restricted by the presence of bolt holes or provision for damage tolerance and repairs. However, with the advent of new composite materials, cured at much higher temperature to withstand operation at supersonic speeds, this approach may no longer be appropriate. The residual stresses developed during cool-down after cure will be far higher, because of the greater difference between the cure temperature and the minimum operating temperature.

This set of truncations together at the laminate level with the original maximum strain criterion results in the following operative set of equations applied *at the laminate level* with respect to axes oriented along and normal to each fiber direction in the laminate

$$\begin{aligned} \varepsilon_{11}^{cu} \;&\le\; \varepsilon_{11}^{i} \;\le\; \varepsilon_{11}^{tu} \\ \varepsilon_{11}^{cu} \;&\le\; \varepsilon_{22}^{i} \;\le\; \varepsilon_{11}^{tu} \\ |\varepsilon_{11}^{i} - \varepsilon_{22}^{i}| \;&\le\; \left(1+\nu_{LT}^{lamina}\right)|\varepsilon_{11}^{tu} \text{ or } \varepsilon_{11}^{cu}|^{*} \end{aligned} \qquad 4.4.2(c)$$

* whichever is greater

However, it is important to note that these equations can only be applied in the context of a fiber-dominated laminate as previously described. It should further be noted that the limits on the transverse strain in each ply, ε_{22}^{i}, are set by the fibers in plies transverse to the ply under consideration and thus cannot characterize matrix cracking. This must be carefully taken into account if hybrid laminates are utilized. Furthermore, as previously discussed, if matrix cracking is considered to be structurally significant, a stress or strain cutoff must be added based on empirical observation. In this case, an assessment of the effects of the matrix cracks on subsequent properties of the laminate must be made.

As noted in Section 4.4.1, bending occurs when there are external bending and/or twisting moments or when the laminate is not symmetric. In these cases, as with other failure criteria, it is necessary to take into account the fact that the laminate level strains vary through the thickness.

4.4.3 Laminate design

Design charts in the form of "carpet plots" are valuable for selection of the appropriate laminate. Figure 4.4.3 presents a representative carpet plot for the axial tensile strength of laminates having various proportions of plies oriented at 0°, ±45°, and 90°. Appropriate strength data suitable for preliminary design can be found for various materials in References 4.4.3(a) and (b).

The development of laminate stacking sequence (LSS) optimization routines for strength-critical designs is a difficult task. Such a scheme must account for competing failure mechanisms that depend on material, load type (e.g., tension versus compression), environment (e.g., temperature and moisture content) and history (e.g., fatigue and creep). In addition, the load transfer must be adequately modeled to account for component geometry and edge effects. Even for a simple uniaxial load condition, the relationship between LSS and strength can be complex. Some qualitative rules currently exist for optimizing LSS for strength but they have been developed for a limited number of materials and load cases.

Relationships between LSS and laminate strength depend on several considerations. The initiation and growth of local matrix failures are known to depend on LSS. As these failures occur, internal stress distributions also depend on LSS strength through local stiffness and dimensional stability considerations. For example, delamination divides a base laminate into sublaminates having LSS that are generally unsymmetric. Reduced stiffness due to edge delaminations, causes load redistribution and can decrease the effective tensile strength of laminates. Likewise, local instability of sublaminates also causes load redistri-

bution which can lower the effective compressive strength of laminates. As a result, both laminate and sublaminate LSS affect laminate strength.

Shear stress distributions play a significant role in determining the mechanical behavior and response of multi-directional laminates. As was the case for ply transverse tensile strength, ply shear strength depends on LSS. Laminates with homogeneous LSS have been found to yield higher in-situ ply shear strengths than those with ply orientations clumped in groups (Reference 4.4.3(b)). An inherent flaw density and interlaminar stresses appear to be major factors affecting the distribution of ply shear strengths in a LSS.

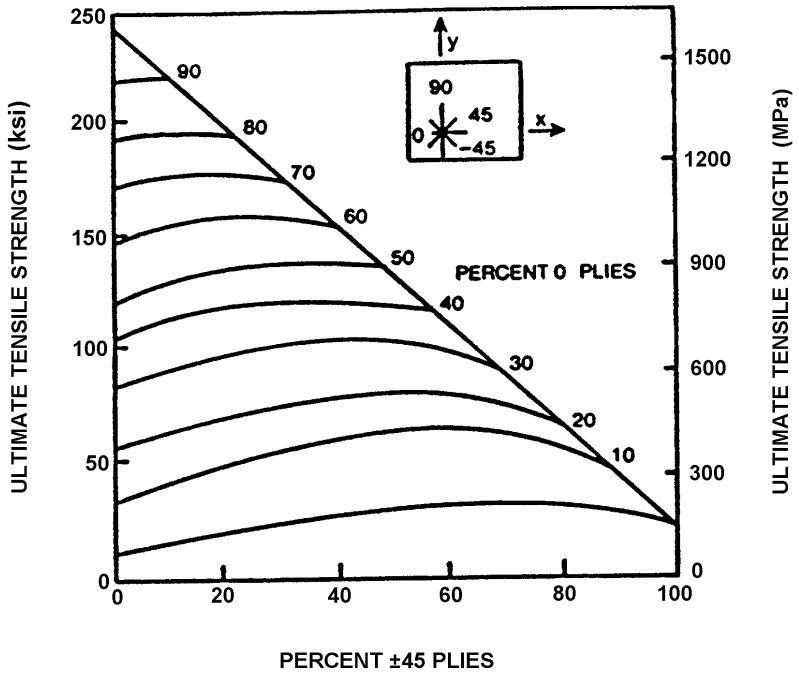

FIGURE 4.4.3 *Tensile strength of $[0_i/\pm45_j/90_k]_s$ family of high strength carbon/epoxy laminates (reference 4.4.3).*

As was the case for bending stiffness, bending strength in composite laminates is strongly dependent on LSS. Failure mechanisms characteristic of tension, shear, and compression load conditions may all combine to affect bending strength. Table 4.3.3.2(b) showed that preferential stacking of plies in outer layers of the LSS increased bending stiffness. The bending strength performance of undamaged laminates may show similar trends; however, surface damage due to impact or other in-service phenomena would cause severe degradation to such laminates.

Additional information on laminate stacking sequence effects is found in Section 4.6.5.

4.4.4 Stress concentrations

The presence of a hole or other discontinuity in a structure introduces local stress concentrations. These high local stresses can result in initial localized failure. The analysis of failure due to cracking, or fracture, which can result in this situation is complicated for composite materials because of material het-

erogeneity at the microscale and in a layer-to-layer basis. Effective in-plane laminate stiffnesses, E_x, E_y, and G_{xy}, may be calculated for any laminate by using the methods presented in Section 4.3.3. With these properties specified, a balanced symmetric laminate may be regarded as a homogeneous orthotropic plate, for structural analysis. Orthotropic elasticity theory may be used for the evaluation of stresses around a hole in such a plate (Reference 4.4.4(a)). Examples of the resulting stress concentrations are shown in Figure 4.4.4(a) for carbon/epoxy laminates. The laminae orientation combinations influence both the magnitude and the shape of the stress variation near the hole. The high stresses at the edge of the hole may initiate fracture.

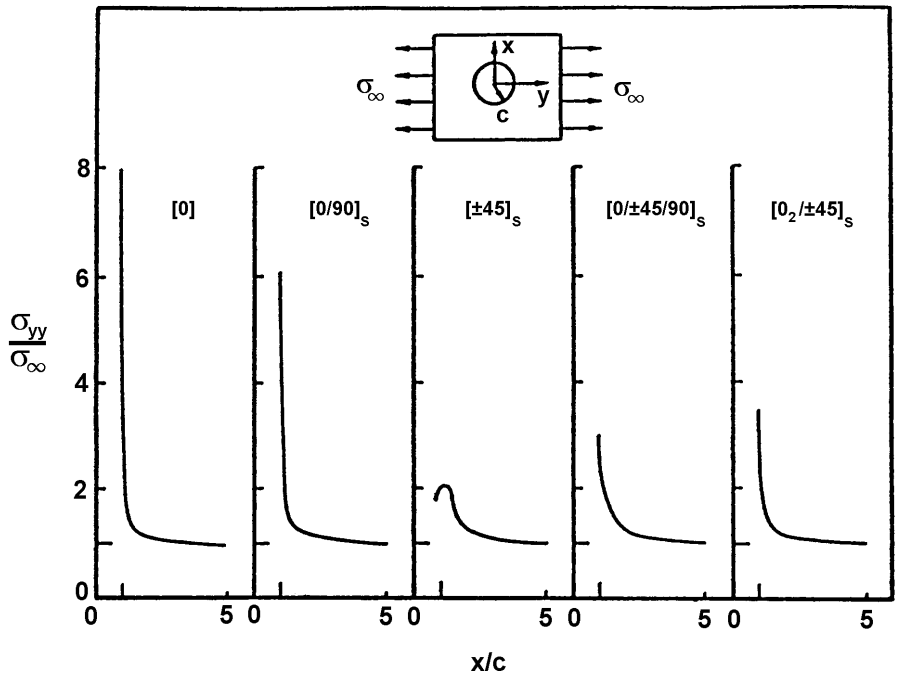

FIGURE 4.4.4(a) *Stress concentration factors for a circular hole in a homogeneous, orthotropic, infinite plate.*

If the laminate fails as a brittle material, fracture will be initiated when the maximum tensile stress at the edge of the hole equals the strength of the unnotched material. In a tensile coupon with a hole, as shown in Figure 4.4.4(a), failure will occur at the minimum cross-section. The failure will initiate at the edge of the hole, where the stress concentration is a maximum.

Consider the stress concentration factor in a finite width isotropic plate with a central circular hole. Stress distribution for this configuration are shown in Figure 4.4.4(b) for various ratios of hole diameter, a, to plate width, W. The basic stress concentration factor for this problem is the ratio of the axial stress at the edge of the hole ($x = a/2$, $y = 0$) to the applied axial stress, σ_∞. For small holes in an isotropic plate, this factor is three. The average stress at the minimum section, σ_n, is higher than the applied stress, σ_∞, and is given by the following relationship:

$$\sigma_n = \frac{\sigma\infty}{(1 - \frac{a}{W})} \qquad 4.4.4(a)$$

The net section stress concentration factor, k_n, is the ratio of the maximum stress to this average stress.

$$k_n = \frac{\dfrac{\sigma(\frac{a}{2},0)}{\sigma\infty}}{(1-\frac{a}{W})} \qquad 4.4.4(b)$$

Laminate fracture for the elastic-brittle case will occur at stress σ_{fr}:

$$\sigma_{fr} = F^{tu} / k_n \qquad 4.4.4(c)$$

A material which fails in this fashion is denoted a notch-sensitive material. In contrast, a ductile, or notch-insensitive, material will yield locally to alleviate the stress concentration effect.

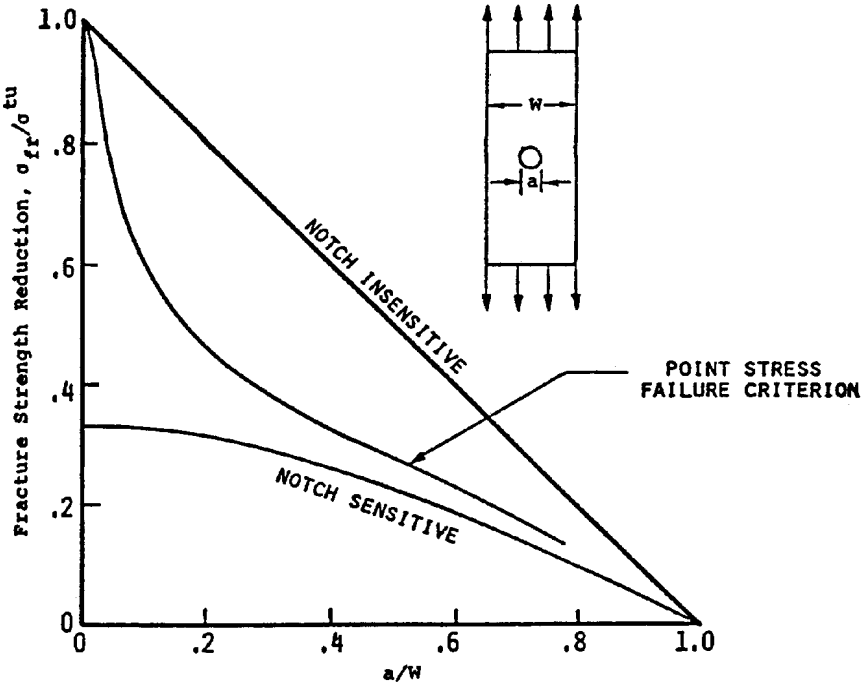

FIGURE 4.4.4(b) *Approximate failure theories.*

Various matrix damage effects are expected to occur at the maximum stress locations. This localized damage reduces the material stiffness and diminishes and spreads the stress concentration effects. Semi-empirical methods have been proposed to account for this reduction in the stress concentration.

The "point stress theory" (Reference 4.4.4(b)) proposes that the elastic stress distribution curve, e.g., Figure 4.4.4(a), be used, but that the stress concentration be evaluated at a distance, d_o, from the edge of the hole. The numerator of Equation 4.4.4(b) is evaluated at $x = a/2 + d_o$. The characteristic length, d_o, must be evaluated experimentally. The "average stress theory" (Reference 4.4.4(b)) takes a similar approach by proposing that the elastic stress distribution be averaged over a distance, a_o, to obtain the stress concentration.

$$k_n = \frac{\int_{a/2}^{(a/2)+a_o} \sigma_y \, dx}{\int_{a/2}^{W/2} \sigma_y \, dx} \qquad 4.4.4(d)$$

Again, the characteristic dimension, a, must be found experimentally. For both methods, the resulting stress concentration is used in Equation 4.4.4(c) to define the fracture stress. Representative results are plotted in Figure 4.4.4(b) to illustrate the differences associated with different types of material behavior.

The relationship between tensile strength and laminate stacking sequence (LSS) for laminates with holes, cutouts, and through-penetrations (i.e., a damage tolerance consideration) is complex (see References 4.4.4(c) - (g)). Certain combinations of ply splitting and delamination that occur at the tip of a notch can enhance residual strength by effectively reducing the stress concentration. Delaminations which uncouple plies, allowing individual plies to fail without fiber breaks, reduce the residual strength. Most existing analysis methods for predicting notched tensile strength are based on parameters determined by some notched laminate tests (e.g., characteristic dimension, fracture energy parameter). The effects of LSS on failure is included in the test parameter. Future analysis development that simulates progressive damage accumulation will provide a more efficient approach for studying the effects of LSS. Additional information on laminate stacking sequence effects is found in Section 4.6.5.

4.4.5 Delamination

The formation and growth of delaminations is generally related to LSS. Delaminations can have varying effects on tensile strength performance, depending on delamination location and the specific property of interest. Most studies performed to date have considered specimens with significant free edge surface area where interlaminar stresses are known to concentrate. Although all structures have some free edges, it is important to realize the limits of analysis and tests performed with specimen geometries. For example, the magnitude of interlaminar tensile stresses, which are crucial to edge delamination, approach zero for plate width to thickness ratios of 30 and greater (Ref. 4.4.5(a)).

As shown in Figure 4.4.5, laminated specimens prone to edge delamination have been shown to exhibit generally lower strength (ultimate stress level) when loaded in uniaxial tension (e.g., References 4.6.5.5.1.1(b), 4.4.5(b) - (f)). The reduction in strength has been directly tied to a drop in stiffness with increased edge delamination area for laminates exhibiting stable delamination growth (References 4.6.5.5.1(b), 4.4.5 (b) - (e)). The onset of edge delamination has been shown to relate to tensile strength for laminates exhibiting unstable delamination growth coupled with matrix cracks (Reference 4.4.5(f)).

The reduced laminate stiffness due to edge delamination can affect the measured tensile strength in two distinct ways (e.g., Reference 4.4.5(e)). If all plies remain loaded after delamination, the ultimate laminate strain has been found to equal the critical strain of primary load bearing plies. In these cases laminate strength drops in proportion to the apparent axial modulus. However, if off-axis plies cease to carry loads because they have been isolated by an interconnected network of matrix cracks and delamination, a local strain concentration can form. When this occurs, the global laminate strain for failure can be less than the critical strain of primary load bearing plies.

Free edge delaminations split a laminate into sublaminates, each of which continue to carry tensile loads. The apparent modulus of this laminate depends on delamination length and the sublaminate moduli which may be calculated using lamination theory. These moduli will depend on LSS if unsymmetric sublaminates with strong extension/bending couplings are involved (References 4.4.5(g) and (h)). A simple rule-of-mixtures approach has been used to accurately calculate apparent moduli for edge delamination (References 4.4.5(e), (g) and (h)).

Local coupling between intralaminar matrix cracks and delaminations can cause complete or partial ply isolation. Note that complete ply isolation cannot occur unless associated damage extends the full laminate width. When this occurs, the apparent laminate stiffness and strain concentration can be calculated in a modified rule-of-mixtures approach which discounts isolated ply groups (References 4.6.5.5.1.1(c) and 4.4.5(e)). A local area of reduced stiffness also causes strain concentration (Reference 4.4.5(i)). The strain concentration depends on both the local reduced stiffness and global laminate stiffness. For example, hard laminates with strong anisotropy, such as lay-ups dominated by 0° plies and loaded uniaxially, will have large strain concentration factors. Consequently, hard laminates will be less tolerant of local damage than relatively soft laminates (e.g., quasi-isotropic).

When high interlaminar shear stresses are present, coupled edge delamination and matrix crack growth are possible and may lead to catastrophic failure. Edge delamination behavior of laminates commonly used in design (e.g., quasi-isotropic laminates) become dominated by interlaminar shear stresses when subjected to off-axis loading. Note that for this problem the laminate lay-up is generally unbalanced relative to the loading axis. The measured tensile strength coincides with the onset of edge delamination for such laminates (Reference 4.4.5(f)). As a result, failure criteria that account for interlaminar stresses are needed to predict the tensile strength.

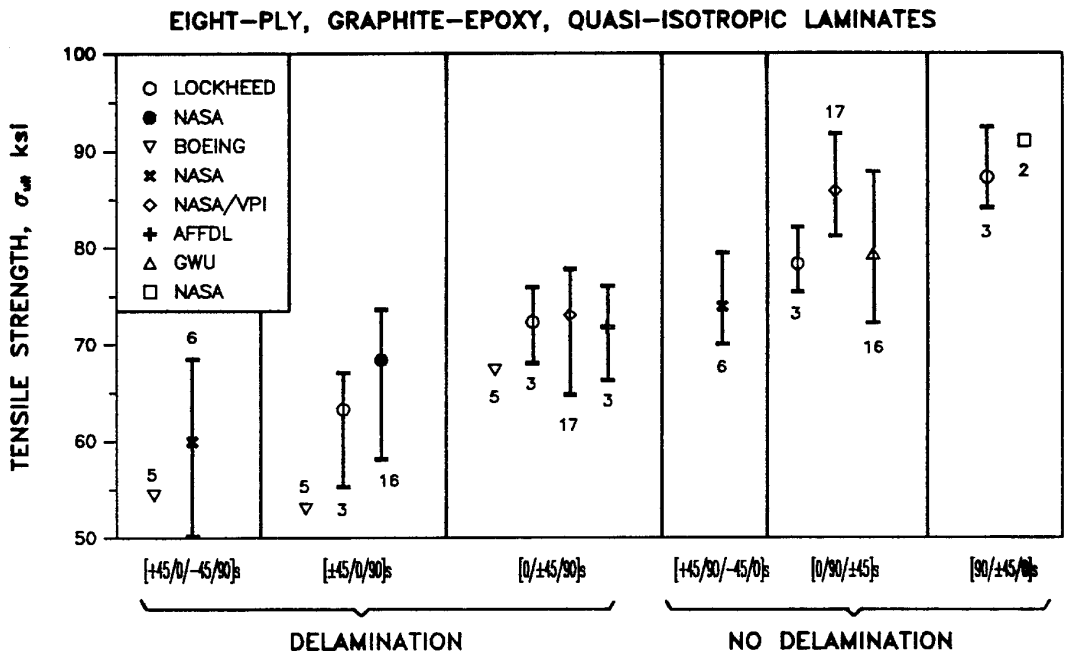

FIGURE 4.4.5 *Unnotched tensile strength variation with LSS (from Reference 4.4.5(d)).*

The use of a suitable analysis method is recommended to evaluate edge effects in composite materials (e.g., References 4.4.6.1.1(f), 4.4.5(d), (g), (h), (j) - (l)). Applied mechanical loads and environmental effects should be included in the free edge analysis. Two approaches have been successfully applied to quantify free edge stresses and predict edge delamination: (1) a fracture mechanics based method using strain energy release rates (References 4.6.5.5.1.1(f), 4.4.5(d), (g), (h), (j)), and (2) a strength of materials based approach using an average stress failure criterion (References 4.4.5(k) and (l)).

The combined use of resin interlayers between the plies in a laminate and specimen edge polishing have been found to be effective methods for suppressing edge delamination (Reference 4.4.5(f)). Materials with high interlaminar toughness have an inherent resistance to delamination. Other methods that have been used to suppress edge delamination include resin interlayer strips at critical interfaces along the edge of laminates (Reference 4.4.5(m)), termination of critical plies offset from the edge (Reference 4.4.5(n)), hybridization (References 4.4.5(o) and (p)), and serrated edges (Reference 4.4.5(p)).

Most of the above discussion on the effects of delamination suggest a decrease in tensile properties. This is generally true for unnotched specimen geometries prone to edge delamination. Isolated delaminations that occur away from the edge of a laminate (e.g., manufacturing defects) and are not coupled with matrix cracks have been shown to have little effects on tensile strength (Reference 4.4.5(r)). Theoreti-

cally, such delaminations do not result in local reduced laminate stiffness when loaded in tension due to compatibility considerations. Multiple delaminations located away from the edge of a laminate have been shown to cause a small reduction in tensile strength (Reference 4.4.5(r)). This was explained by coupling between delaminations and other matrix damage (e.g., ply splits) that occurred during loading, resulting in partial ply isolation and local reduced stiffness. Most of the discussion in this section is related to free edge effects (Section 4.6.3) and laminate stacking sequence effects (Section 4.6.5).

4.4.5.1 Compression

Delaminations generally have a stronger affect on compressive strength than on tensile strength. As a result, the potential for delamination should always be considered when selecting a suitable LSS. The effect of delamination occurring due to manufacturing defects and/or in-service events such as impact needs to be included in this evaluation. For example, the best LSS for avoiding edge delamination in specimen geometries may not be best for suppressing the effects of delaminations occurring in structures due to impact.

Delamination breaks the laminate into sublaminates, each having associated stiffness, stability, and strength characteristics. Sublaminates are usually unsymmetric and, therefore, all of the sublaminate stiffnesses will depend on LSS. As shown in Figure 4.4.6.2, stability and local compressive performance of sublaminate ply groups ultimately determines catastrophic failure.

Compressive failure in composite laminates having delaminations is strongly tied to the stability of sublaminate plates. Since delaminations may occur at many different interfaces in a laminate, sublaminates LSS will generally not be balanced and symmetric. As discussed earlier, the bending/extension couplings characteristic of such LSS reduce buckling loads. The sublaminate boundary conditions and shape are also crucial to the relationship between LSS and stability.

Several methods exist for predicting sublaminate stability in composite laminates (e.g., References 4.4.5.1(a) - (e)). These models differ in assumed bending stiffness, boundary conditions, and sublaminate shape. Experimental data bases are needed to determine which assumption is appropriate for a given problem. The in-plane and out-of-plane stress redistribution due to a buckled sublaminate is crucial to compressive strength.

Environment can play a significant role in delamination growth and load redistribution if the environmental resistance of combined sublaminate stiffnesses are significantly different than those of the base laminate. The combined effects of environment and LSS on laminate dimensional stability were covered in earlier sections. The stability of unsymmetric sublaminates is expected to relate to warpage. The warp depends on both LSS and environmental conditions. Warp may be treated as an imperfection in stability analysis.

The initiation of free edge delamination in compressively loaded laminates can be predicted using methods similar to those used for tension (e.g., Reference 4.4.5.1(a)). Once initiated, delamination growth depends on sublaminate stability. An adequate sublaminate stability analysis model must, therefore, be coupled with the growth model (e.g., References 4.4.5.1(b) and (c)). Delamination growth can be stable or unstable, depending on sublaminate LSS, delamination geometry, structural geometry, and boundary conditions. Growth of multiple delaminations, characteristic of impact damage, is currently not well understood.

4.4.6 Damage and failure modes

4.4.6.1 Tension

Tensile rupture of laminates with multidirectional plies normally involves a series of pre-catastrophic failure events, including both matrix damage and localized fiber breaks. Catastrophic failure is expected whenever the longitudinal tensile strength of any ply in a laminate is exceeded; however, laminates can

separate without fiber failure by coupling various forms of matrix damage. Example laminates that can fail due to matrix damage include those with less than three distinct ply orientations (angle-ply laminates loaded in the 0° direction). Recommendation 2 in Section 4.6.5.2.1 is intended to avoid the low strengths associated with catastrophic failures occurring without fiber breaks.

Figure 4.4.6.1 shows the various failure mechanisms that can occur at micro and lamina dimensional scales for a multidirectional laminate loaded in tension. Depending on load conditions and material properties, matrix failure (e.g., transverse matrix cracks, delamination) or isolated fiber breaks occur at stress levels less than the static strength. Load redistributes around local failures until a critical level of damage is reached, upon which catastrophic fiber failure occurs. Resin is of secondary importance through its effect on resistance to matrix damage accumulation and local load transfer (i.e., near matrix damage and isolated fiber breaks). The LSS also plays a secondary role by affecting damage accumulation and load transfer.

Critical micro failure mechanisms shown in Figure 4.4.6.1 include localized fiber failure and fiber/matrix interfacial cracking. These mechanisms occur mostly in plies aligned with a major axis of tensile stress. The laminate stress levels at which these failures occur depend on load redistribution due to the characteristic damage state in adjacent plies. A limited number of fiber breaks are tolerated within a lamina before the entire ply fails, which can trigger catastrophic laminate failure.

Matrix failure mechanisms at the lamina scale for laminates with multidirectional plies are also shown in Figure 4.4.6.1. Intralaminar matrix cracks align parallel to the fiber direction and span the thickness of a ply or group of plies stacked with the same orientation. These have also been referred to as transply cracks or ply splits depending on whether a crack orients at an angle or parallel to the tensile load axis, respectively.

Interlaminar matrix failure, often referred to as delamination, can form near free edges or at intersections between intralaminar cracks. Delaminations form due to excessive interlaminar normal and shear stresses. The accumulation of intralaminar and interlaminar matrix failures depends strongly on LSS.

4.4.6.1.1 Matrix cracks

Matrix cracks occur in plies of laminated composites due to combined mechanical and environmental stresses. These transverse cracks align with fibers and, when fully formed, span the thickness of individual plies or ply groups stacked together in the same orientation. Matrix cracks redistribute local stress in multidirectional laminates, allowing a crack density to develop in the ply of ply group as a function of load and environmental history. These cracks can also form prior to service exposure due to processing.

Studies with coupons loaded in uniaxial tension have shown that initial fiber failures found in 0° plies occur near intralaminar matrix cracks in neighboring off-axis plies (Ref. 4.4.6.1.1(a)). When matrix cracks span a single off-axis ply, the stress concentration in a neighboring 0° ply is generally small and localized over a small portion of the neighboring ply thickness. This has been found to influence the location of laminate failure, but has little effect on tensile strength (Refs. 4.4.6.1.1(b) and 4.4.6.1.1(c)).

Intralaminar matrix cracks normally span the full thickness of multiple off-axis plies that have been stacked together. The associated stress concentration in a neighboring ply increases with the thickness of a cracked group of stacked plies. The stress concentration in a 0° ply due to matrix cracks in a large group of stacked 90° plies was found to significantly decrease laminate tensile strength (Refs. 4.4.6.1.1(c) and 4.4.6.1.1(d)). This is one of the reasons for Recommendation 3, Section 4.6.5.2.1.

Even when strength is not altered by the presence of matrix cracks, it is important to understand the mechanics of matrix cracking for composite materials used in aerospace applications. For example, matrix cracks can play a fundamental role in the generation of delaminations. The increased surface area due to a network of matrix cracks can also alter physical properties such as composite thermal expansion, liquid permeability, and oxidative stability.

Residual stresses, that develop due to differences in thermal and moisture expansion properties of constituents, affect the formation of matrix cracks. In general, tensile residual stress develops in the transverse-fiber directions of lamina when multidirectional polymer matrix composites are exposed to temperatures below the residual stress free temperature. This occurs during a temperature drop because unconstrained shrinkage of tape lamina is much greater in transverse-fiber directions than in fiber directions. As moisture is absorbed into a laminate, matrix swelling counteracts thermal shrinkage, decreasing the transverse-fiber tensile stress.

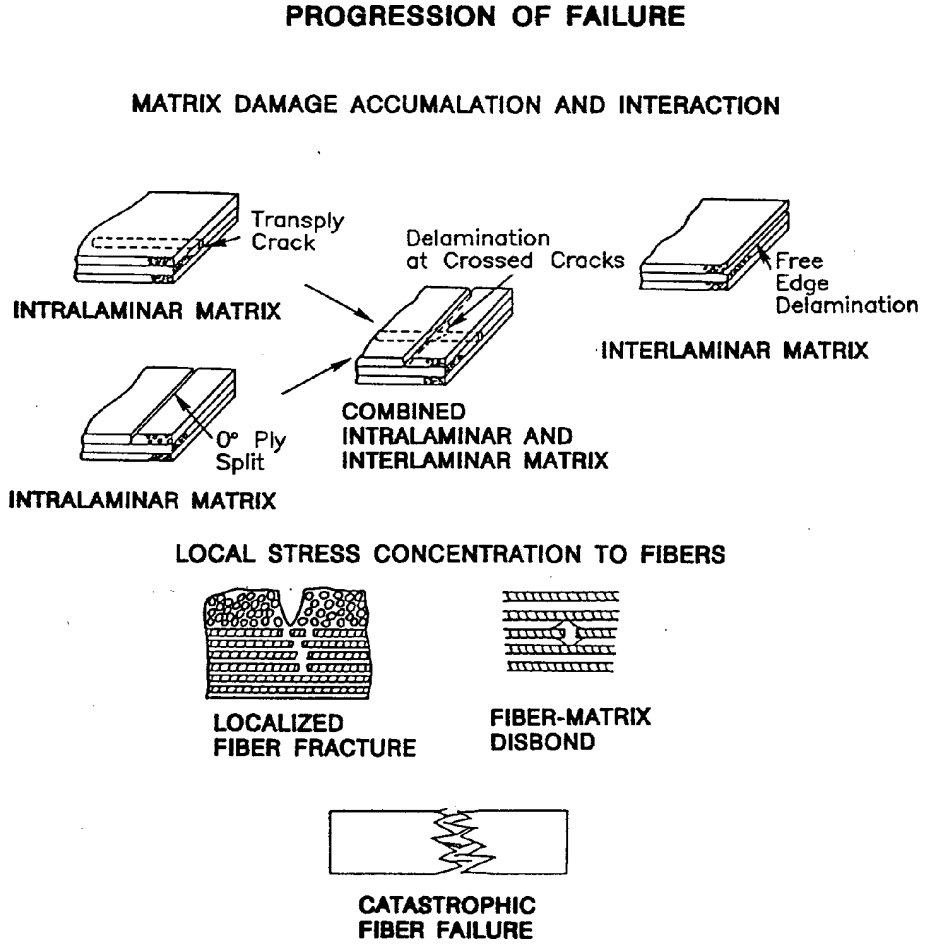

FIGURE 4.4.6.1 *Failure mechanisms for laminates loaded in tension.*

The critical stress or strain causing the onset of matrix cracking in plies of a laminate has been referred to as in situ transverse lamina strength. This strength is not a material constant since it depends on LSS. Experiments and analysis have shown that in situ strength increases as the thickness of plies grouped together with the same orientation decreases (e.g., Refs. 4.4.6.1.1(e) - (i)). These studies have also shown that neighboring plies can impose differing constraints on matrix crack formation, depending on fiber orientation. Many materials currently used in the aerospace industry have resin-rich interlaminar layers (RIL). The magnitude of the in situ strengthening effect decreases if a RIL with significant thickness exists between plies (Ref. 4.4.6.1.1(j)). Relatively soft RIL eliminate some of the constraint imposed by neighboring plies.

4.4.6.2 Compression

Compressive strength is ultimately related to the local response of individual ply groups. Assuming no matrix damage exists due to impact or previous load history, the local stability and strength of plies aligned with the axis of loading will determine final failure. The location of load-carrying plies relative to the laminate surface can play a role in this instance. The short wavelength buckling load is reduced when critical plies are located in outer layers of the laminate stacking sequence. When matrix damage does exist, the combined local response of individual ply groups affects the compression strength. The stability and load redistribution within individual ply groups or sublaminates is crucial to the local response.

Figure 4.4.6.2 shows three different types of local compressive failure mechanisms. These mechanisms were observed to occur as a function of θ for $(\pm\theta)_s$ type laminates (References 4.4.6.2(a) and (b)). When delamination occurs, all three of the local failure modes may combine to determine the compressive strength of a laminate stacking sequence. (Additional information on the effects of the laminate stacking sequence is found in Section 4.6.5.) In-plane matrix shearing and matrix compression failures were observed for $(\pm\theta)_s$ type laminates with $15° \le \theta \le 90°$ and $60° \le \theta \le 90°$, respectively. The shear mode of fiber microbuckling is most commonly observed for composites. This mode was shown to initiate compressive failure for $(\pm\theta)_s$ type laminates with $0° \le \theta \le 10°$. Depending on matrix and fiber combination, final local failures for such laminates involved some combination of fiber failure (shear, kinking, or bending) and matrix splitting or yielding (References 4.4.6.2(c) and (d)).

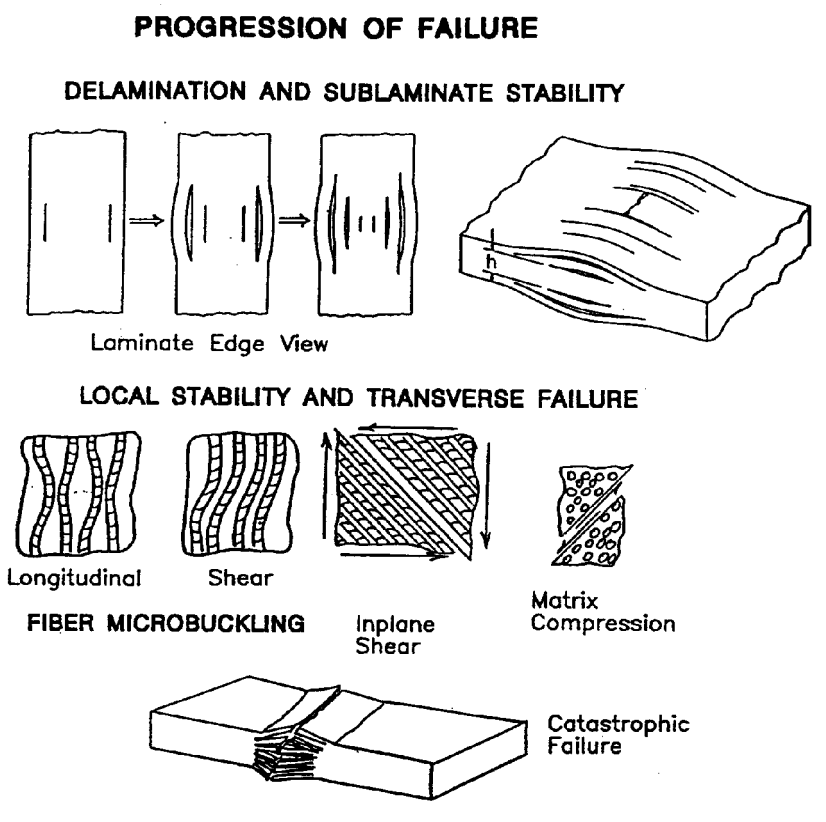

FIGURE 4.4.6.2 *Failure mechanisms for laminates loaded in compression.*

4.4.7 Summary

- Ply level stresses are commonly used to predict first ply and subsequent ply failures leading up to laminate failure. Once a ply has failed, its contribution to laminate strength and stress is conservatively reduced. Typically, in-plane failure criteria are applied only to lamina fiber loading conditions; in-plane matrix-dominated static failure criteria should not be used since it will generally lead to overly conservative failure predictions.

- Under static loading conditions, composites are particularly notch-sensitive as a function of layup and more specifically stacking sequence.

4.5 COMPLEX LOADS

4.5.1 Biaxial in-plane loads

4.5.2 Out-of-plane loads

4.6 LAMINA TO LAMINATE CONSIDERATIONS

4.6.1 Residual stresses and strains

Residual curing stresses and strains have virtually no effect on fiber-dominated laminate properties. However, residual stresses in the resin can be greater than the mechanical stresses needed to cause failure. Neglecting these residual stresses therefore may be nonconservative. The residual stresses may be high enough that resin microcracking may occur before any mechanical load is applied. Consequently, the principle of superposition may not be applicable as the mechanical loading may result in nonlinear behavior. As an example, typical epoxy matrix residual strains at the microlevel, resulting from cool down after curing at 350°F (180°C), may be approximately 25 to 100% of the laminate failure strain.

4.6.2 Thickness effects

Much of the difference in properties found when comparing laminates with different thicknesses can be explained by the residual stresses developed during processing. Internal stresses developed during processing may produce voids, delaminations, and microcracks or cause residual stresses in the laminate that may affect material properties. Excessive porosity, generally caused by poor processing, or environmental effects due to temperature and moisture conditions may also degrade the material and affect its behavior.

Variations in material properties between thick laminate test data from different sources, for laminates having the same thickness, can generally be attributed to differences in processing. Such variations can be minimized by optimizing the cure cycle and by proper process control.

The residual stresses may be caused by non-isothermal conditions present during the solidification phase. Different layers of the laminate will undergo different degrees of volume contraction at any given time during the process cycle. This gives rise to a self-equilibrating force system producing tension stresses in the center and compression stresses in the surface layers of the laminate as reported by Manson and Seferis (Reference 4.6.2(a)). Thickness effects observed in composite laminates are primarily due to this phenomena.

In thermosetting materials, these through-the-thickness stress gradients can be virtually eliminated by modeling the total process, including cool-down, so isothermal conditions are present near the resin gelation point and are maintained for a sufficient period of time. In some high-temperature processing materials where rapid cooling is required, significant thermal stresses may build up in the laminate.

In their work, the authors in Reference 4.6.2(a) present a method to experimentally determine and analyze the internal stresses developed during processing of a composite laminate. This method consists of laying up a certain number of plies, separated by a release ply that can be removed after processing. The internal stresses in the laminate can then be analyzed by considering the deformations of the individual sublaminates.

In summary, variations in material properties in laminated composites are mostly the result of thermally induced residual stresses, although environmental effects and process parameters other than temperature may affect test data. True thickness effects are caused by temperature gradients across the thickness of the laminate. These effects may be minimized by mathematical modeling of the total process and can be virtually eliminated in thermosetting materials. Advance process models such as ROAST, described in Reference 4.6.2(b), may be used to optimize the process parameters.

4.6.3 Edge effects

Consideration of edge effects in laminated composites is necessary due to behavior not observed in homogeneous solids. A complex stress state exists between the layers of different orientation at the free edge of a laminate, such as along a straight edge or around the perimeter of a hole. Where a fiber in a laminate has been subjected to thermal or mechanical strain, the end of the cut fibers must transfer the load to adjacent fibers. If these adjacent fibers have a different orientation, they will present a locally stiffer path and accept the load. The matrix is the only mechanism for this load transfer. The stresses due to this load, namely interlaminar stresses, can be sufficient to cause local microcracking and edge delamination. These interlaminar stresses, in general, include normal (peel stress σ_z) and shear components (τ_{yz}, τ_{xz}) and are only present in a small region near the free edge. A typical interlaminar stress distribution is shown in Figure 4.6.3. The high gradients of these stresses depend on differences in Poisson's ratio and in-plane shear stiffness that exist between the laminae groups in a laminate. The same kinds of stresses are induced by residual thermal stresses due to cool-down after cure at elevated temperatures.

Failure often occurs as a result of delamination at the locations of high interlaminar stresses because of low interlaminar strength. The effects of free edge stress are sufficient to reduce the strength of certain coupons in both static and fatigue tests significantly. This premature failure makes coupon data difficult to apply to large components because of the local effects of the free edge failure mode. Classical laminate theory which assumes a state of plane stress is incapable of predicting the edge stresses. However, determination of such stresses by higher order plate theory or finite element analysis is practical. Therefore, consideration of edge interlaminar stresses in a laminate design is feasible. The gradients of this stress can be reduced by such measures as 1) changing the laminate stacking order, 2) minimizing the mismatch of the Poisson's ratio, the coefficient of mutual influence, and coefficients of thermal and moisture expansion between adjacent laminae, and 3) by inserting an inner layer which has a lower shear modulus and a finite thickness between laminae, thus allowing greater local strain to occur (Reference 4.6.3(a)).

Edge effects may be analyzed by fracture mechanics, strength of materials, or other methods (References 4.6.3(a) - (d)). These methods can be used to provide a guideline for designers to select the laminate configuration and material system best suited for a particular application.

Very little work has been performed to date on free edge effects for load conditions other than uniaxial tension or compression. Some analysis results indicate that in-plane shear, out-of-plane shear/bending, in-plane bending, twisting moments, and combined loading yield a higher magnitude of interlaminar stress relative to those associated with axial load conditions (Reference 4.6.3(f)). For example, out-of-plane shear due to bending causes free edge interlaminar stresses that are an order of magnitude higher than that caused by axial tension. For more information on delaminations and free edge effects, see Section 4.4.5. Information on the laminate stacking sequence effects is found in Section 4.6.5.

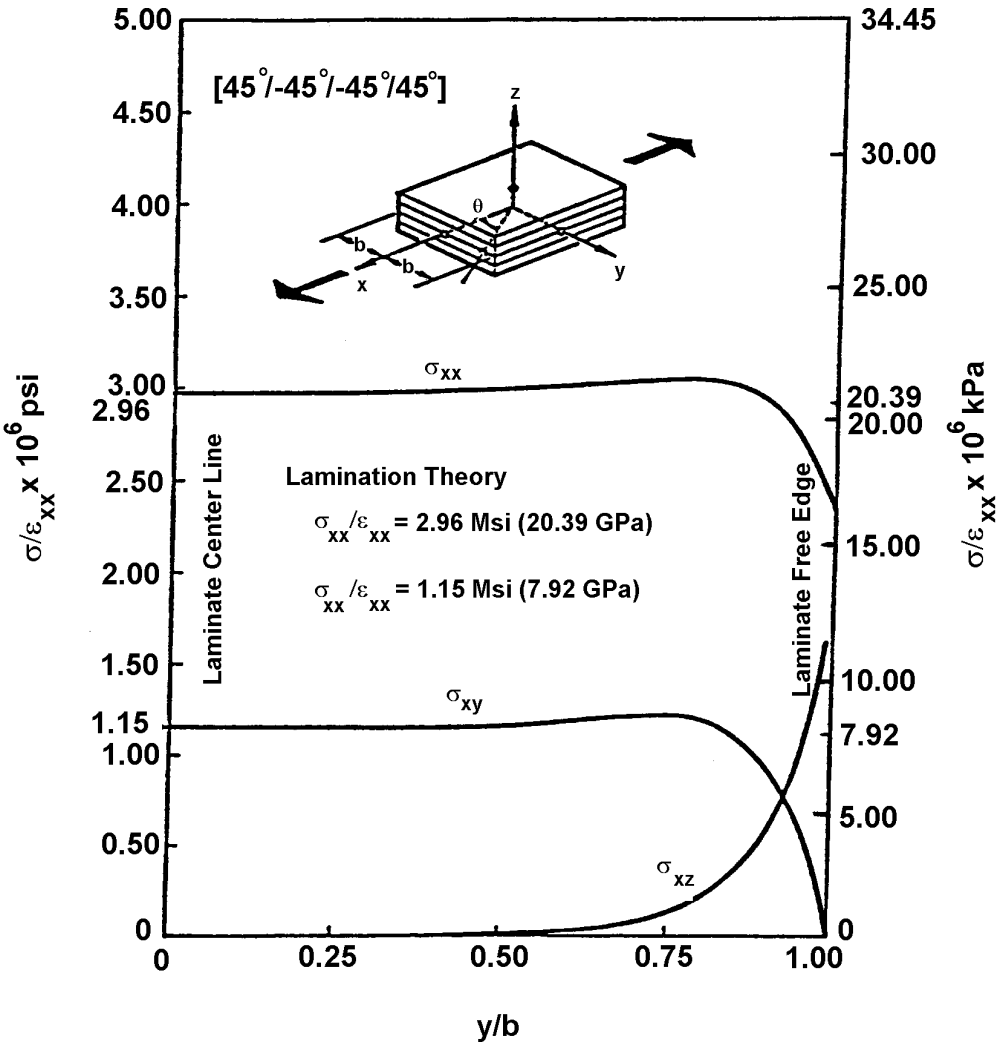

FIGURE 4.6.3 *Interlaminar stresses normalized with respect to the applied strain (reproduced by permission from Reference 4.6.3(e)).*

4.6.4 Effects of transverse tensile properties in unidirectional tape

The transverse strength properties play only a minor role in establishing cross-plied laminate strengths. It is, however, well-known that the effective "in-situ" transverse strength of transverse plies is much greater than the strength measured on the lamina. This effect has been handled by post-first ply failure analysis methods.

In-plane shear tests on laminae exhibit relatively high strains to failure (4 -5%). The much lower transverse tensile strains to failure (1/2%) indicate a marked notch sensitivity that is suppressed in cross-plied laminates. The initial cracks that fail laminae are arrested by fibers in other directions; thus laminae with microcracks are still effective. Most laminae develop cracks due to residual thermal stresses and continue to function.

4.6.5 Laminate stacking sequence effects

4.6.5.1 Introduction

Stacking sequence describes the distribution of ply orientations through the laminate thickness. As the number of plies with chosen orientations increase, more stacking sequences are possible. For example, a symmetric 8-ply laminate with four different ply orientations has 24 different stacking sequences. This presents a predicament when attempting to optimize composite performance as a function of stacking sequence.

Laminated composite structural properties such as stiffness, dimensional stability, and strength have all been found to depend on laminate stacking sequence (LSS). Generally, each property has a different relationship with LSS. Therefore, the choice of LSS for a particular design application may involve a compromise. Design optimization requires verified analysis methods and an existing materials database. The development of verified analysis methods for predicting stiffness and stability of laminated composites is more mature than that for predicting strength.

Some simplified design guidelines for LSS are provided in Section 4.6.5.2. These guidelines are generally conservative; however, they limit design optimization, and may even be misleading for some special cases. As a result, a comment on the reason for each guideline is included in the discussion. Verified analysis methods should be used to help judge the effects of LSS whenever possible.

Additional discussion of stacking sequence effects on particular topics are provided in the sections noted in Table 4.6.5.1.

TABLE 4.6.5.1 *Additional discussions on stacking sequence effects.*

Topic	Section	Page
Bending	4.3.3.2, 4.4.3	4-42, 4-62
Buckling	4.7.1.8	4-88
Compression after impact	4.11.1.4	4-107
Delamination	4.4.5	4-69
Free edge effects	4.6.3	4-77
Hygroscopic analysis	4.3.4	4-50
Lamination theory	4.3.2	4-33
Notched strength	4.4.4	4-63
Ply shear strength	4.4.3	4-62
Thermal analysis	4.3.4	4-50
Vibration	4.12.2	4-118

4.6.5.2 Design guidelines

Laminate design starts by selecting the number of plies and ply angles required for a given application. Once the number of plies and ply angles are selected, a LSS is chosen. A LSS is considered heterogeneous when there is preferential stacking of specific ply orientations in different locations through the thickness of the laminate. Thick laminates with heterogeneous LSS are created by clumping plies of similar orientation. A LSS is said to be homogeneous if ply angles are evenly distributed through the laminate thickness. The ability to generate homogeneous LSS depends on the number of plies and ply angles. For example, it is impossible to create a homogeneous LSS for a four-ply laminate consisting of four different ply angles.

The following LSS guidelines are based on past experience from test and analysis. Guidelines are lumped under two categories; (1) strong recommendation, and (2) recommendation. Despite this classification, exceptions to the guidelines should be considered based on an engineering evaluation of the specific application.

4.6.5.2.1 Strong recommendations

1. Homogeneous LSS are recommended for strength controlled designs (In other words, thoroughly intersperse ply orientations throughout the LSS).

   Comment: *Heterogeneous laminates should be avoided for strength-critical designs unless analysis and test data is available that indicates a clear advantage. In cases where heterogeneous laminates cannot be avoided (e.g., minimum gage laminates), it is generally best to stack primary load-carrying plies toward the laminate core. The best way to view possible strength problems with heterogeneous LSS is to consider the behavior of individual sublaminates (i.e., groups of plies separated by delaminations) that may be created during manufacturing or service exposure. This will be discussed later in greater detail.*

   Heterogeneous LSS can yield optimum stiffness or stability performance; however, the effects on all other aspects of the design (e.g., strength, damage tolerance, and durability) should be considered before ignoring Recommendation 1. For example, interlaminar stress distributions are affected by variations in the in-plane stress field around the periphery of holes and cutouts and the "effective" LSS (i.e., ply orientations relative to a tangent to the edge). Since it is difficult to optimize for a single lay-up in this case, the best solution is to make the LSS as homogeneous as possible.

2. A LSS should have at least four distinct ply angles (e.g., 0°, $\pm\theta$°, 90°) with a minimum of 10% of the plies oriented at each angle. Ply angles should be selected such that fibers are oriented with principal load axes.

   Comment: *This rule is intended to avoid the matrix-dominated behavior (e.g., nonlinear effects and creep) of laminates not having fibers aligned with principal load axes. Such behavior can lead to low strengths and dimensional stability problems.*

3. Minimize groupings of plies with the same orientation. For tape plies, stack no more than four plies of the same orientation together (i.e., limit stacked ply group thicknesses $\leq$0.03 in. (0.8 mm)). In addition, stacked ply group thicknesses with orientations perpendicular to a free edge should be limited to $\leq$0.015 in.(0.38 mm).

   Comment: *This guideline is used for laminate strength-critical designs. For example, it will help avoid the shear-out failure mode in bolted joints. It also considers relationships between stacked ply group thickness, matrix cracking (i.e., transverse tension and shear ply failures) and delamination.*

In general, ply group thickness should be limited based on details of the design problem (e.g., loads, free edges, etc.) and material properties (e.g., interlaminar toughness). Note that the absolute level of ply group thickness identified in this guideline is based on past experience. It should be confirmed with tests for specific materials and design considerations.

4. If possible, LSS should be balanced and symmetric about the midplane. If this is not possible due to other requirements, locate the asymmetry or imbalance as near to the laminate midplane as possible. A LSS is considered symmetric if plies positioned at an equal distance above and below the midplane are identical (i.e., material, thickness, and orientation). Balanced is defined as having equal numbers of $+\theta$ and $-\theta$ plies, where θ is measured from the primary load direction.

   Comment: *This guideline is used to avoid shear/extension couplings and dimensional stability problems (e.g., warpage which affects component manufacturing tolerances). The extension/bending coupling of unsymmetric laminates can reduce buckling loads. Note that some coupling may be desired for certain applications (e.g., shear/extension coupling has been used for aeroelastic tailoring).*

4.6.5.2.2 Recommendations

5. Alternate $+\theta$ and $-\theta$ plies through the LSS except for the closest ply either side of the symmetry plane. A $+\theta/-\theta$ pair of plies should be located as closely as possible while still meeting the other guidelines.

   Comment: *This guideline minimizes the effect of bending/twisting coupling, which is strongest when angle plies are separated near the surface of a laminate. Modifications to this rule may promote more efficient stiffness and stability controlled designs.*

6. Shield primary load carrying plies from exposed surfaces.

   Comment: *The LSS for laminates primarily loaded in tension or compression in the 0° direction should start with angle and transverse plies. Tensile strength, microbuckling resistance, impact damage tolerance and crippling strength can all increase by shielding the main load bearing plies from the laminate surface. With primary load fibers buried, exterior scratches or surface ply delamination will not have a critical effect on strength. For laminates loaded primarily in shear, consideration should be given to locating +45° and -45° plies away from the surface. For cases in which an element is shielded by other structures (e.g., shear webs), it may not be necessary to stack primary load carrying plies away from the surface.*

7. Avoid LSS that create high interlaminar tension stresses (σ_z) at free edges. Analyses to predict free edge stresses and delamination strain levels are recommended to help select LSS.

   Comment: *Composite materials tend to have a relatively low resistance to mode I delamination growth. Edge delamination, followed by sublaminate buckling can cause premature failure under compressive loads. Edge delamination occurring under tensile loads can also effectively reduce stiffness and lower the load carrying capability. Since delaminations occurring at the core of the laminate can have the strongest effect on strength, avoid locating tape plies with fibers oriented perpendicular to a free edge at the laminate midplane.*

8. Minimize the Poisson's ratio mismatch between adjacent laminates that are cocured or bonded.

   Comment: *Excessive property mismatches between cobonded elements (e.g., skin and stringer flange) can result in delamination problems. In the absence of more sophisticated analysis tools, a general rule of thumb is*

$$\left|\nu_{xy}(\text{laminate 1}) - \nu_{xy}(\text{laminate 2})\right| < 0.1 \qquad 4.6.5.2.2$$

As opposed to static strength, composites are not particularly notch-sensitive in fatigue; hole wear is often used as the governing criterion constituting fatigue failure of composites loaded in bearing.

4.6.6 Lamina-to-laminate statistics

4.6.7 Summary

- Laminate properties such as strength, stiffness, stability, and damage resistance and damage tolerance have been found to have some dependency upon laminate stacking sequence (LSS). Each property can have a different relationship with LSS. Thus, each given design application may involve a compromise relative to LSS determination.

- Homogeneous LSS are recommended for strength controlled designs (in other words, thoroughly intersperse ply orientations throughout the LSS).

- A LSS should have at least four distinct ply angles (e.g., 0°, ±θ°, 90°) with a minimum of 10% of the plies oriented at each angle. Ply angles should be selected such that fibers are oriented with principal load axes.

- Minimize groupings of plies with the same orientation. For tape plies, stack no more than four plies of the same orientation together (i.e., limit stacked ply group thicknesses <0.03 in. (0.8 mm)). In addition, stacked ply group thicknesses with orientations perpendicular to a free edge should be limited to ≤ 0.015 in. (0.38 mm).

- If possible, LSS should be balanced and symmetric about the midplane. If this is not possible due to other requirements, locate the asymmetry or imbalance as near to the laminate midplane as possible. A LSS is considered symmetric if plies positioned at an equal distance above and below the midplane are identical (i.e., material, thickness, and orientation). Balanced is defined as having equal numbers of $+\theta$ and $-\theta$ plies, where θ is measured from the primary load direction.

4.7 COMPRESSIVE BUCKLING AND CRIPPLING

4.7.1 Plate buckling and crippling

4.7.1.1 Introduction

Rectangular flat plates are readily found in numerous aerospace structures in the form of unstiffened panels and panels between stiffeners of a stiffened panel, and as elements of a stiffener. Closed form classical buckling solutions available in the literature are limited to orthotropic plates with certain assumed boundary conditions. These boundary conditions may be fixed, simply supported, or free. For expediency, the engineer may wish to assume the most appropriate boundary conditions and obtain a quick solution rather than resort to using a buckling computer program such as Reference 4.7.1.1(a). However, the closed form solutions of laminated orthotropic plates are appropriate only when the lay-ups are symmetrical and balanced. Symmetrical implies identical corresponding plies about the plate mid-surface. Balanced refers to having a minus θ ply for every plus θ ply on each side of the mid-surface. Symmetrical and balanced laminated plates have B_{ij} terms vanish and the D_{16} and D_{26} terms virtually vanish. However, the balanced plies ($\pm\theta$) should be adjacent; otherwise the D_{16} and D_{26} terms could become significant and invalidate the use of the orthotropic analysis. The buckling solutions could be significantly nonconservative for thin unbalanced or unsymmetric plates (see Reference 4.7.1.1(b)). Note that not all closed form solutions give direct answers; sometimes the equations must be minimized with respect to certain parameters as will be shown later.

The behavior of flat plates in compression involves initial buckling, postbuckling out-of-plane displacements, and crippling (ultimate postbuckling failure). Only at crippling does permanent damage occur, usually some form of delamination due to interlaminar tensile or shear stresses.

Nomenclature used to describe the buckling behavior of composite plates in Section 4.7.1 is given in Table 4.7.1.1.

TABLE 4.7.1.1 *Buckling and crippling symbols.*

SYMBOL	DEFINITION
a	length
b	width
B_{ij}	stiffness coupling terms of laminated plate
D_{ij}	flexural/twisting stiffness terms of laminated plate
$F^{cr}_{x,cl}$	classical orthotropic longitudinal compressive buckling stress
$F^{cr}_{x,i}$	initial longitudinal compressive buckling stress from test
F^{cc}_{x}	longitudinal crippling stress from test
F^{cu}_{x}	longitudinal ultimate compressive stress of laminate
$N^{cr}_{x,cl}, N^{cr}_{y,cl}$	classical orthotropic longitudinal and transverse compressive uniform buckling loads, respectively
$N^{cr}_{x,i}$	initial longitudinal uniform buckling load from test
$N^{cr}_{x,w}$	longitudinal compressive uniform buckling load based on anisotropic theory, including transverse shear effects
N_x, N_y	longitudinal and transverse applied uniform loads, respectively, on a plate
$P^{cr}_{x,i}$	total longitudinal initial buckling load form test
$P^{cc}_{x,i}$	total longitudinal crippling load from test
t	thickness

4.7.1.2 Initial buckling

Initial buckling is defined to occur at a load that results in incipient out-of-plane displacements. The classical equations are elastic, and finite transverse shear stiffness effects are neglected. (Reference 4.7.1.2). The buckling of certain plate geometries, however, can be influenced by the finite shear stiffness effects as shown in Section 4.7.1.8.

4.7.1.3 Uniaxial loading - long plate with all sides simply supported

The case of a long plate ($a/b > 4$) with all sides simply supported (SS) and loaded uniaxially is shown in Figure 4.7.1.3(a) and described by Equation 4.7.1.3.

$$N^{cr}_{x,cl} = \frac{2\Pi^2}{b^2}\left[(D_{11}D_{22})^{1/2} + D_{12} + 2D_{66}\right] \qquad 4.7.1.3$$

Equation 4.7.1.3 is the most frequently used plate buckling equation. It can be shown by the use of the STAGS computer program (Reference 4.7.1.1(a)) that this equation is also valid for fixed boundary conditions (FF) on the loaded edges, which is important since all testing is performed with fixed boundary conditions on the loaded edges to prevent local brooming. Comprehensive testing has shown these equation to be valid except for very narrow plates. Figure 4.7.1.3(b) shows the comparisons between experiment

and classical theory from References 4.7.1.3(a) and (b), where the test results are plotted as $N^{cr}_{x,i} / N^{cr}_{x,cl}$ versus the b/t ratios. Notice the discrepancy becomes worse at the low b/t ratios (narrow plates). Thus the equation should be used with caution at b/t ratios less than 35. In Figure 4.7.1.3(c) the same experimental data has been normalized by the buckling load prediction which includes the effects of transverse shear ($N^{cr}_{x,w}$) from References 4.7.1.3(c) and (d)). Note that most available computer buckling programs will not account for this transverse shear effect.

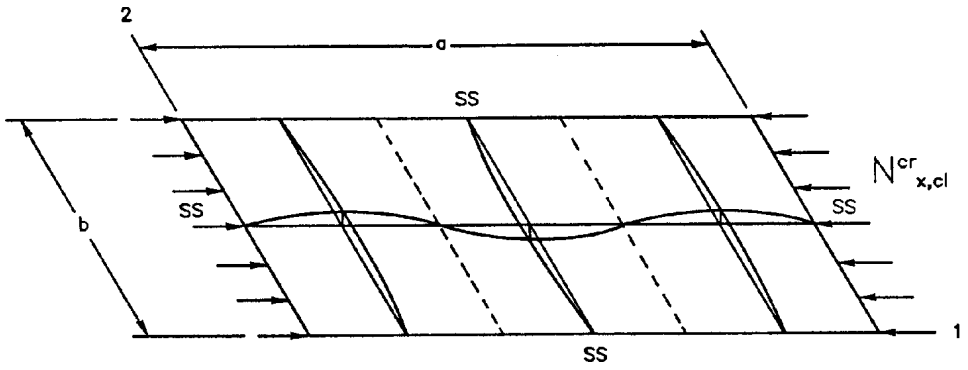

FIGURE 4.7.1.3(a) *Uniaxial loading - long plate ($a/b > 4$) with all sides simply supported (SS).*

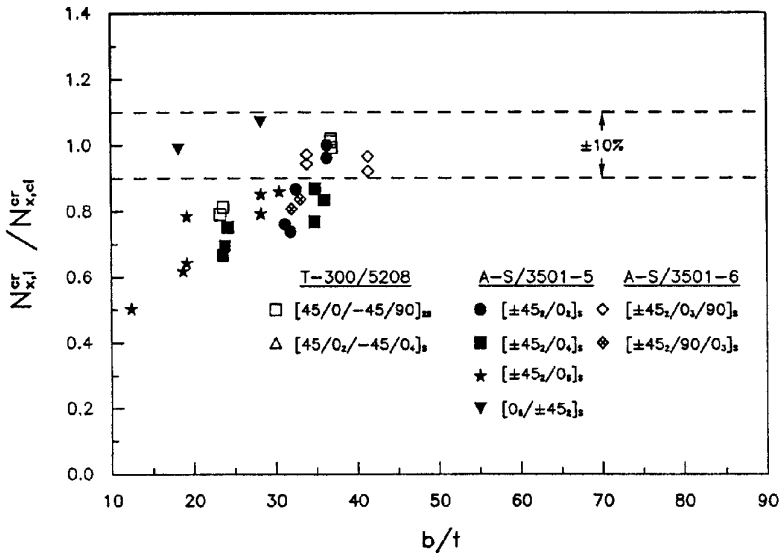

FIGURE 4.7.1.3(b) *Predicted classical buckling loads compared to experimental data (Reference 4.7.1.3(b)).*

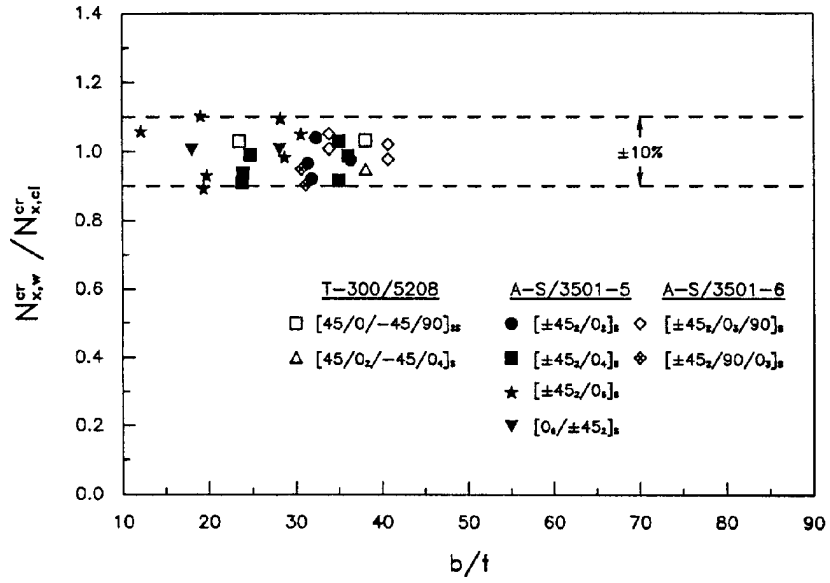

FIGURE 4.7.1.3(c) *Predicted buckling loads of the current theory compared to experimental data (Reference 4.7.1.3(b)).*

4.7.1.4 Uniaxial loading - long plate with all sides fixed

The case of a long plate ($a/b > 4$) with all sides fixed (FF) and loaded uniaxially is shown in Figure 4.7.1.4 and described by Equation 4.7.1.4.

$$N^{cr}_{x,cl} = \frac{\Pi^2}{b^2}\left[4.6(D_{11}D_{22})^{1/2} + 2.67D_{12} + 5.33D_{66}\right] \qquad 4.7.1.4$$

This equation has not had the comprehensive experimental study as has Equation 4.7.1.3. However, by conjecture the effect of transverse shear for narrow plates would be quite similar to that found for plates with all edges simply supported.

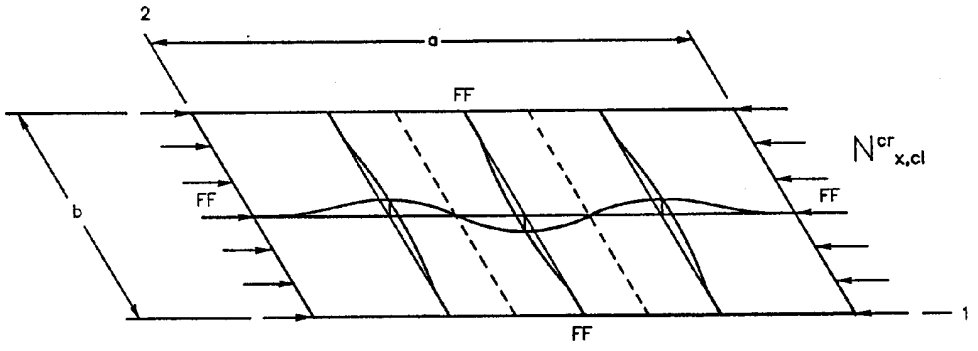

FIGURE 4.7.1.4 *Uniaxial loading - long plate ($a/b > 4$) with all sides fixed.*

4.7.1.5 Uniaxial loading - long plate with three sides simply supported and one unloaded edge free

Figure 4.7.1.5 shows the case of a long plate ($a/b > 4$) with three sides simply supported and the remaining unloaded edge free. This plate is uniaxially loaded. This loading situation is described by Equation 4.7.1.5.

$$N^{cr}_{x,cl} = \frac{12\,D_{66}}{b^2} + \frac{\Pi^2 D_{11}}{a^2} \qquad 4.7.1.5$$

where b/t must be greater than 20 because of transverse shear effects in narrow plates as discussed in Section 4.7.1.3.

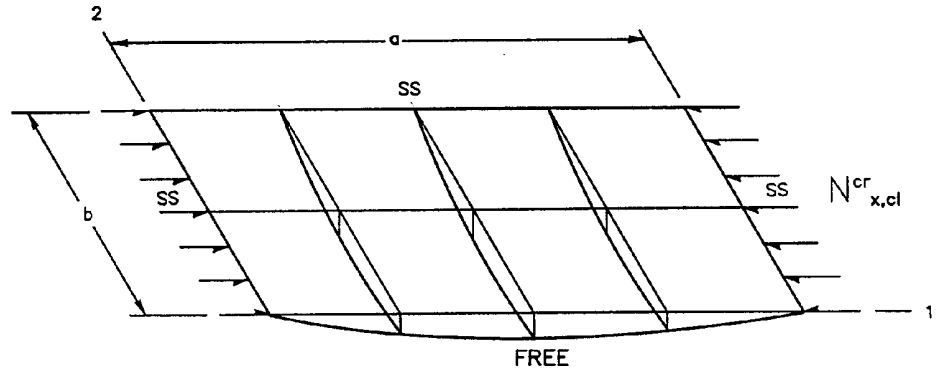

FIGURE 4.7.1.5 *Uniaxial loading - long plate with three sides simply supported and one unloaded edge free.*

4.7.1.6 Uniaxial and biaxial loading - plate with all sides simply supported

Biaxial and uniaxial loading of a simply supported plate is shown in Figure 4.7.1.6, where $1 < a/b < \infty$. The following classical orthotropic buckling equation must be minimized with respect to the longitudinal and transverse half-waves numbers, m and n:

$$N^{cr}_{x,cl} = \frac{\Pi^2}{b^2} \frac{D_{11} m^4 (b/a)^4 + 2(D_{12} + 2D_{66}) m^2 n^2 (b/a)^4 + D_{22} n^4}{m^2 (b/a)^2 + \phi n^2}, \min \qquad 4.7.1.6(a)$$

where

$$\phi = N_y / N_x \qquad 4.7.1.6(b)$$

which is the ratio of applied transverse to longitudinal loading. Accordingly, the corresponding transverse buckling load is

$$N^{cr}_{y,cl} = \phi\, N^{cr}_{x,cl} \qquad 4.7.1.6(c)$$

For uniaxial loading, let $\phi = 0$.

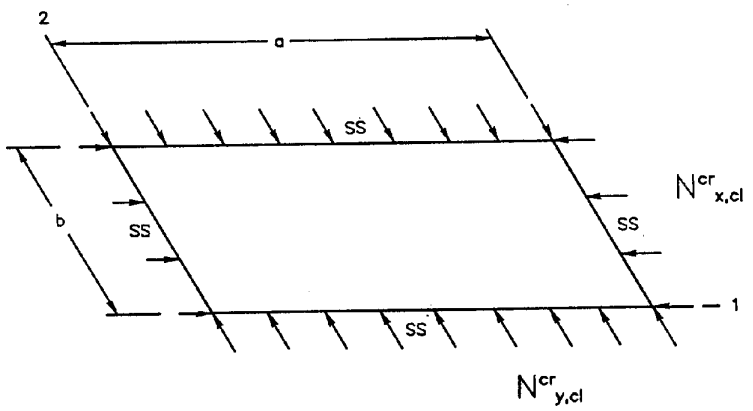

FIGURE 4.7.1.6 *Uniaxial and biaxial loading - plate with all sides simply supported.*

4.7.1.7 Uniaxial loading - plate with loaded edges simply supported and unloaded edges fixed

The case of a uniaxially loaded plate ($1 < a/b < \infty$) with the loaded sides simply supported (SS) and the unloaded sides fixed (FF) can also be considered. For this case, the following classical orthotropic buckling equation must be minimized with respect to the longitudinal half-wave number, m:

$$N^{cr}_{x,cl} = \frac{\Pi^2}{b^2}\left\{D_{11}m^2(b/a)^2 + 2.67D_{12} + 5.33\left[D_{22}(a/b)^2 + (1/m)^2 + D_{66}\right]\right\} \qquad 4.7.1.7$$

4.7.1.8 Stacking sequence effects in buckling

Methods to accurately predict the stability of laminated plates have been documented (e.g., References 4.7.1.8(a)-(c)). Laminated plate stability can be strongly affected by LSS. However, factors such as plate geometry, boundary conditions and load type each contribute to the relationship between LSS and plate stability. As a result, general rules that define the best LSS for plate stability do not exist. Instead, such relationships must be established for specific structure and loading types. Three examples that illustrate this point will be shown in this section. Two different analysis methods were used in these examples. The first, utilized design equations from Reference 4.7.1.8(c) and bending stiffnesses as calculated using lamination theory. This method assumed the plate bending behavior to be "specially orthotropic" (D_{16} and D_{26} terms were set equal to zero). The second method was a Boeing computer program called LEOTHA (an enhanced version of OTHA, Reference 4.7.1.8(a) which uses the Galerkin method to solve equations for buckling. This method allowed nonzero D_{16} and D_{26} terms.

Figures 4.7.1.8(a), (b), and (c) show plate buckling predictions for the seven LSS used in an earlier example (see Table 4.3.3.2(b)).[1] All plates were assumed to have simply-supported boundary conditions on the four edges. Figures 4.7.1.8(a) and (b) are rectangular plates loaded by uniaxial compression in long and short directions, respectively. Figure 4.7.1.8(c) shows shear buckling predictions for a square plate. Horizontal dashed lines on Figures 4.7.1.8(a) - (c) represent the results obtained when using the DOD/NASA design equations and assuming no LSS effect (i.e., a homogeneous orthotropic plate). The homogeneous plate assumption results in a buckling load that is roughly an average of the predictions for all LSS shown in the figures.

[1] The LSS used in Figures 4.7.1.9(a), (b), and (c) were chosen for illustrative purposes only and do not represent optimal LSS for a given application.

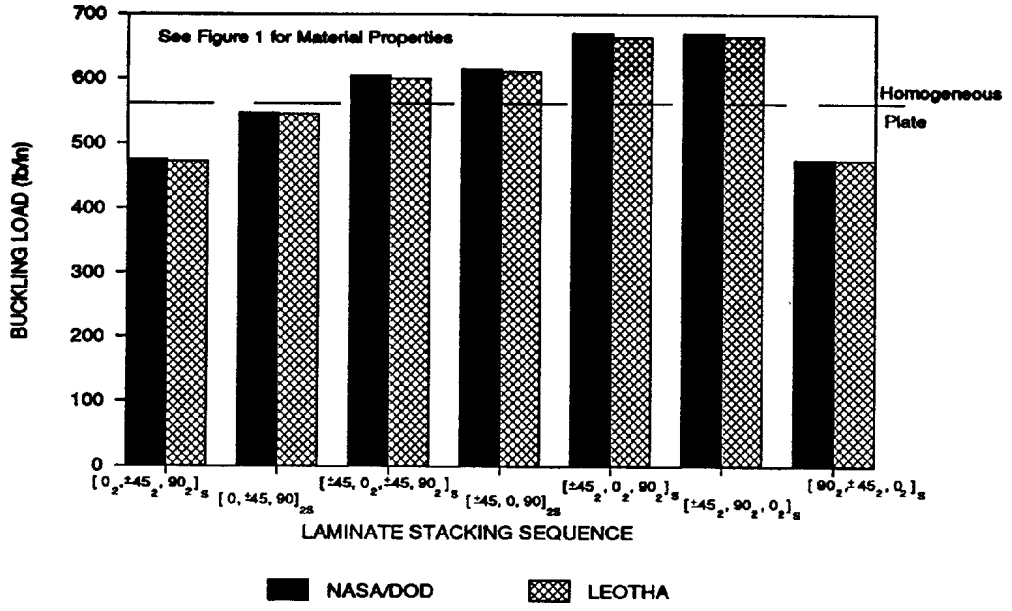

FIGURE 4.7.1.8(a) *Buckling analysis of 4 sides simply-supported, 24 in. by 6 in., laminated plates loaded in the long direction.*

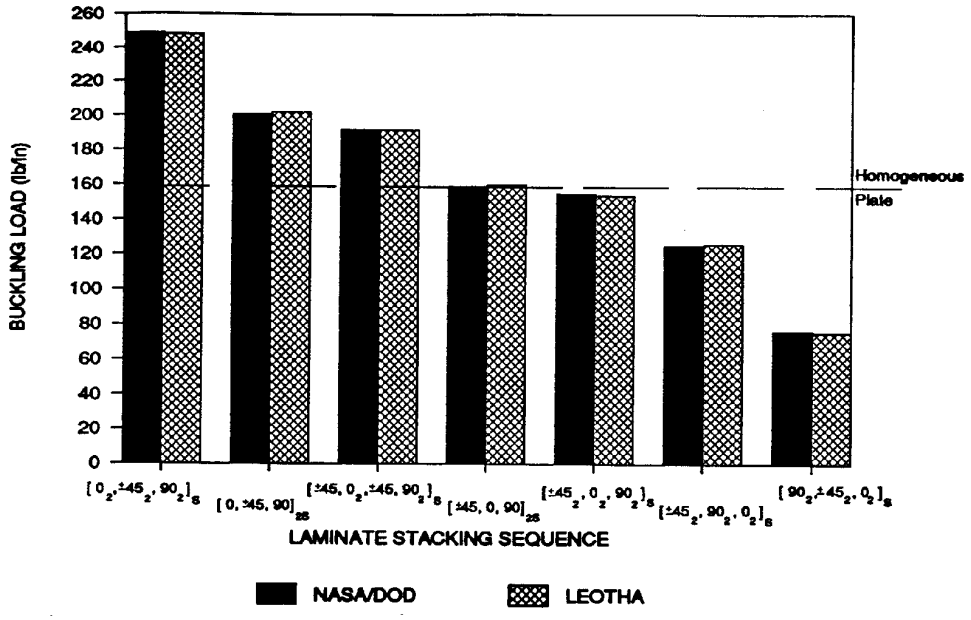

FIGURE 4.7.1.8(b) *Buckling analysis of 4 sides simply-supported, 6 in. by 24 in., laminated plates loaded in the short direction.*

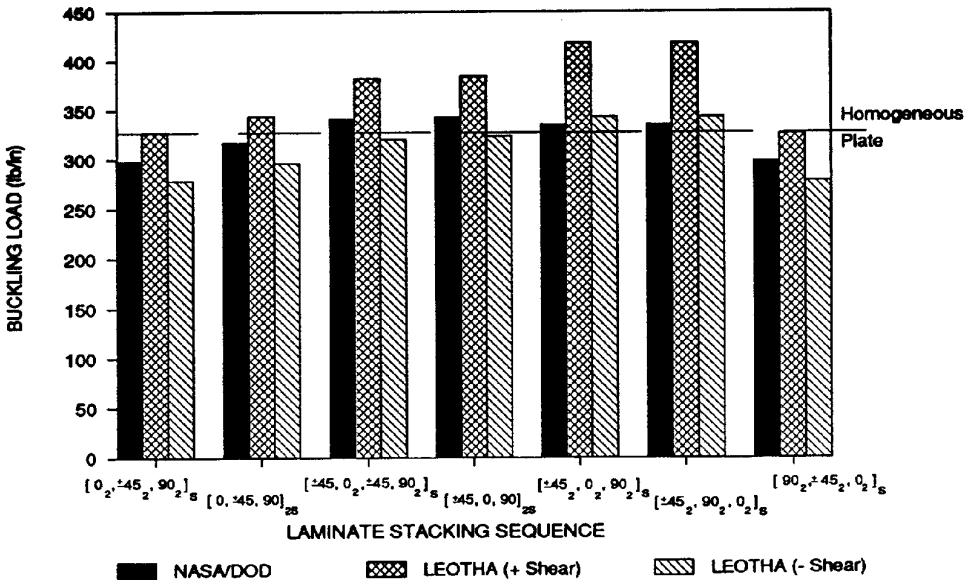

FIGURE 4.7.1.8(c) *Buckling analysis of 4 sides simply-supported, 12 in. by 12 in., laminated plates loaded in shear.*

The highest buckling loads for rectangular plates loaded in the long direction occur with preferential clumping of ±45° plies toward the surface layers (Figure 4.7.1.8(a)). Such is not the case for rectangular plates loaded in the short direction, where preferential stacking of 0° plies yield the highest buckling loads (Reference 4.7.1.8(b)). Note that predictions using the homogeneous plate assumption can be conservative or nonconservative depending on LSS. The DOD/NASA equations compare well with LEOTHA for conditions shown in Figures 4.7.1.8(a) and (b).

The highest buckling loads for square plates loaded in shear occur with preferential clumping of ±45° plies toward the surface layers (Reference 4.7.1.8(d)). Predictions using LEOTHA are different for positive and negative shear due to the relative positions of +45° and -45° plies. Predictions from DOD/NASA equations were generally lower than those of LEOTHA for positive shear loads. The opposite was true for negative shear loads. Differences may be attributed to the influence of D_{16} and D_{26} terms which were not included in the DOD/NASA design equations.

As with bending, structural geometry can overshadow the effects of LSS on stability (see the discussion pertaining to Figure 4.3.3.2). For example, the Euler buckling load of a laminated I-section used as a column is more strongly dependent on geometrical dimensions than on LSS of web and flanges. In fact, the effects of LSS on Euler buckling load diminishes sharply with increasing web height.

Design for local buckling and crippling of composite plates has typically relied on empirical data (e.g., Reference 4.7.1.8(e)). Local buckling and crippling have been found to relate to LSS. The lowest values for local buckling and crippling under uniaxial compression occurred with preferential stacking of 0° plies towards the outside surface of a laminate. Hence, when considering an I-section, Euler buckling loads may be independent of LSS while local buckling and crippling can relate to LSS.

The effects of LSS on the stability of a stiffened panel is more complex. Assuming no local buckling and crippling, stiffener stability will not depend directly on LSS. However, post-buckling behavior of the

skin and load redistribution to the stringer is strongly affected by the skin's LSS. As a result, overall stiffened panel stability can be influenced by the skin's LSS.

Basic information on laminate stacking sequence effects is found in Section 4.6.5.

4.7.2 Compression postbuckling and crippling

Wide exploitation of advanced composites in stability critical structural designs depends to a large degree on the ability of composites to support loads well beyond the initial buckling level. Unquestionably, the high stiffness-to-weight ratio of composites renders them potentially attractive up to initial buckling. However, since postbuckling design has been established over several decades for certain types of conventional metallic alloy construction, it should be anticipated that composites demonstrate a similar capability. Hence, this section addresses this vitally important issue as it pertains to the design of structural compression members.

Postbuckling. Postbuckling is the ability of a compression member or stiffened panel to carry loads well in excess of the initial buckling load. The "postbuckling range" may be considered to exist between the initial buckling load and some higher load representing failure, e.g., delamination at the free edge of a compression member or the disbonding of a stiffener from the panel in a stiffened panel. When stiffened panels are loaded in compression, load is shared between skin and stiffeners in proportion to their respective stiffnesses. At initial buckling, the tangent stiffness of the skin is reduced sharply and as a result, a greater portion of the total load will be carried by the stiffeners. For an isotropic material with linear elastic behavior prior to initial buckling, the tangent stiffness at buckling is reduced to one half of its initial value. For composite panels, tangent stiffnesses are a function of material properties and lay-up. Local buckling of one or more of the plate elements comprising a stiffener will similarly reduce the in-plane stiffnesses of the affected elements and will cause the load to shift to the unbuckled portions of the stiffener. The upper limit of the postbuckling range is sometimes referred to as "local crippling" or simply "crippling".

Crippling. Compression crippling is a failure in which the cross section of a stiffener is loaded in compression and becomes distorted in its own plane without translation or rotation of the entire column taking place. Typical deflected shapes seen in crippling tests of angles and channel section stiffeners are shown in Figure 4.7.2(a). Angles or cruciforms loaded in compression are commonly used as crippling specimens for the "one-edge-free" case. Channels or simply supported compression panels are normally used for the "no-edge-free" case, in which the center channel segment is approximately simply supported with "no-edge-free".

The postbuckling behavior of composite plates presented here is derived from the empirical graphite tape data obtained from References 4.7.2(a) through (h). Relatively narrow plates, with simply supported unloaded edges or one-edge-free and fixed loading edges were tested and analyzed. The simply supported unloaded edges were simulated by the use of steel V-blocks mounted on the compression test fixture. Specifically, the plates with both unloaded edges simply supported are defined as "no-edge-free". Plates with one unloaded edge simply supported and the other free are defined as "one-edge-free". A typical no-edge-free test in progress with the specimen in the postbuckling range is shown in Figure 4.7.2(b). In addition, a typical one-edge-free test where crippling of the specimen has occurred is shown in Figure 4.7.2(c). Typical load-displacement curves of no-edge-free and one-edge-free tests are shown in Figures 4.7.2(d) and 4.7.2(e), respectively. Figure 4.7.2(d) clearly shows the reduction in stiffness at initial buckling as indicated by the change in slope of the load deflection curve at that point. A convenient plot that exemplifies the postbuckling strength of the no-edge-free composite plates is shown in Figure 4.7.2(f). The value for F_{11}^{cu} is the ultimate compressive strength of the particular laminate. A typical failed test specimen is shown in Figure 4.7.2(g). Figure 4.7.2(h) illustrates the postbuckling strengths of one-edge-free plates. Note that all the empirical data presented involved the testing of high strength carbon/epoxy tape. Other material systems or other forms of carbon/epoxy composites may yield different results.

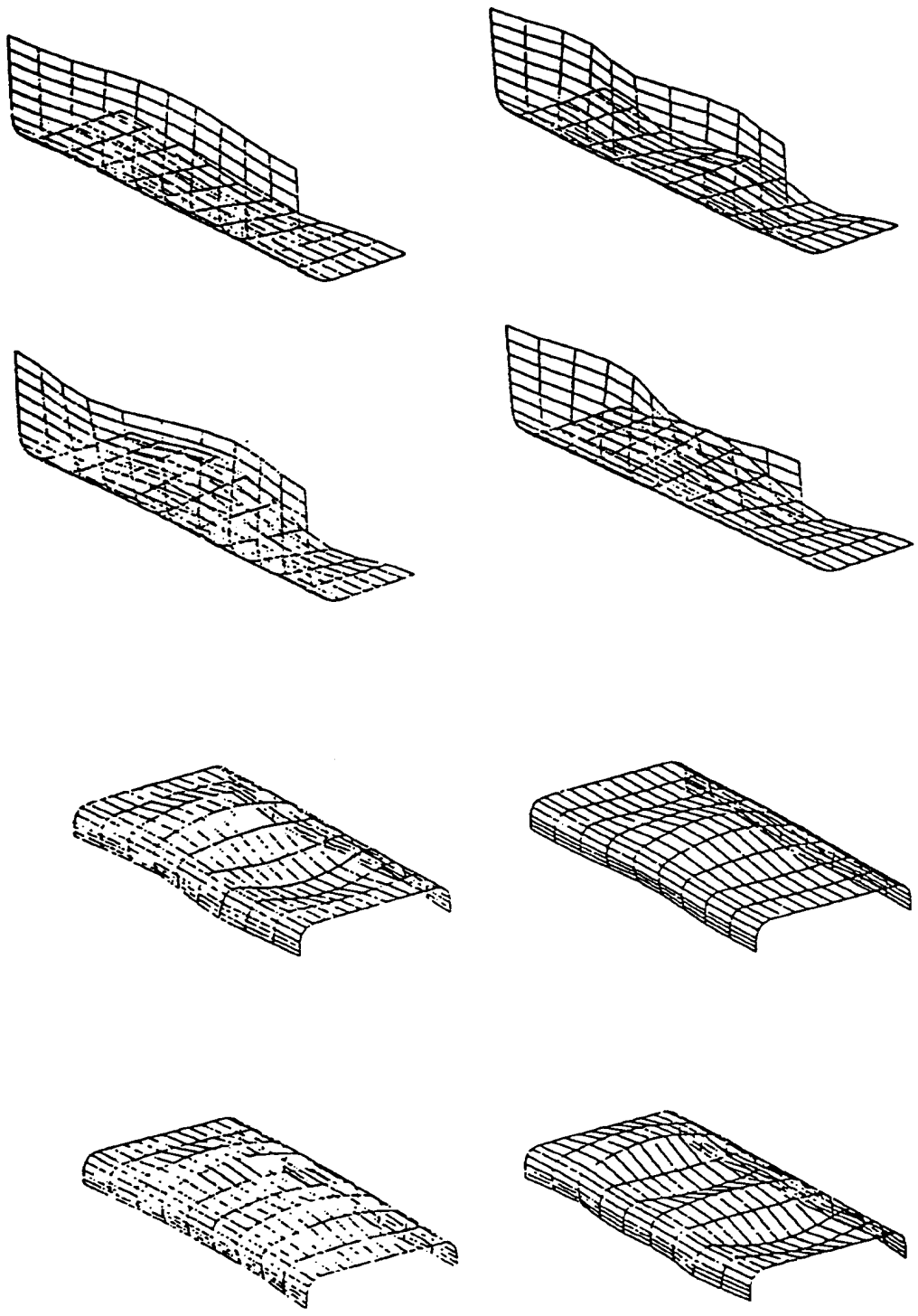

FIGURE 4.7.2(a) *Typical crippling shapes.*

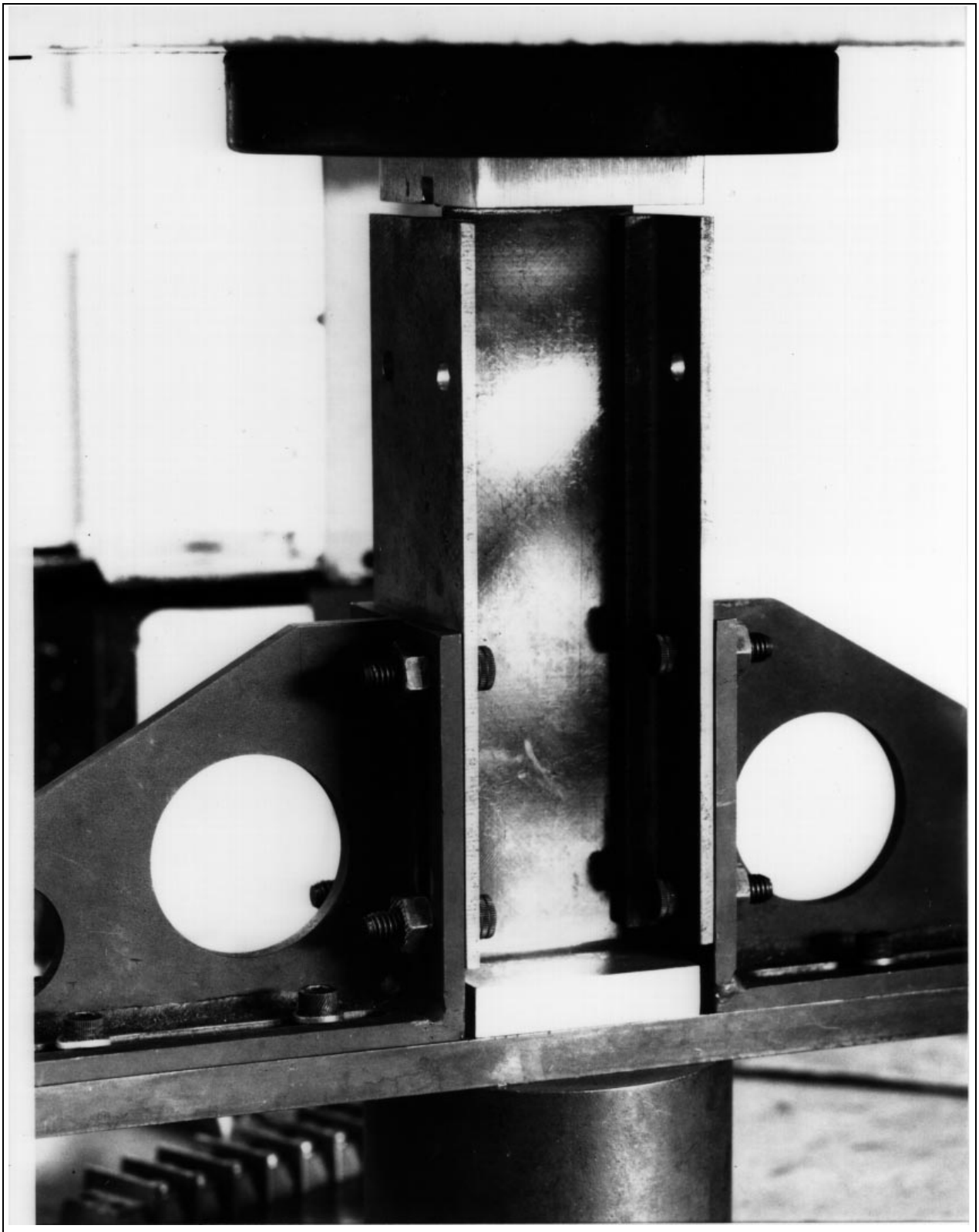

FIGURE 4.7.2(b) *No-edge-free carbon/epoxy test.*

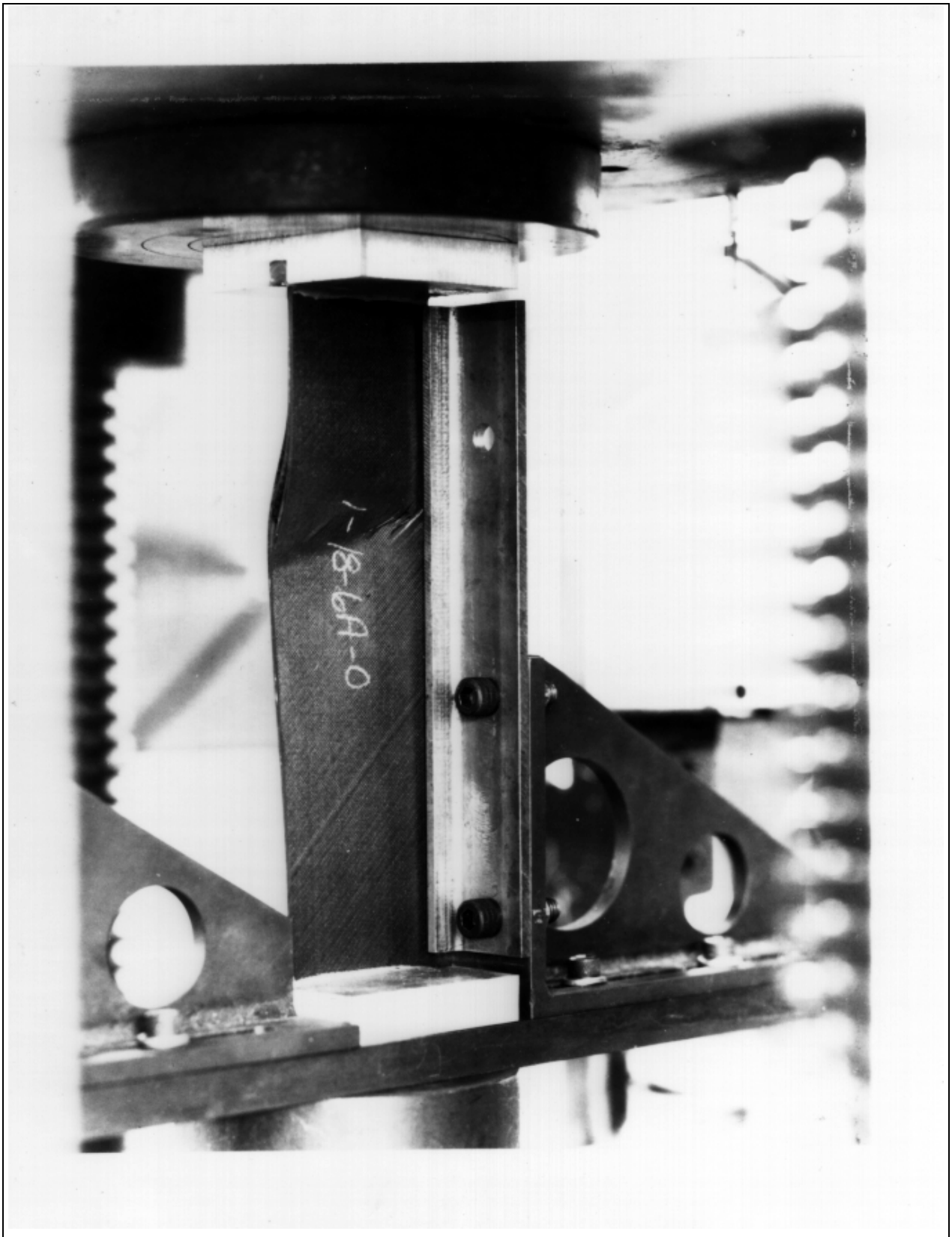

FIGURE 4.7.2(c) *One-edge-free carbon/epoxy postbuckling test at crippling.*

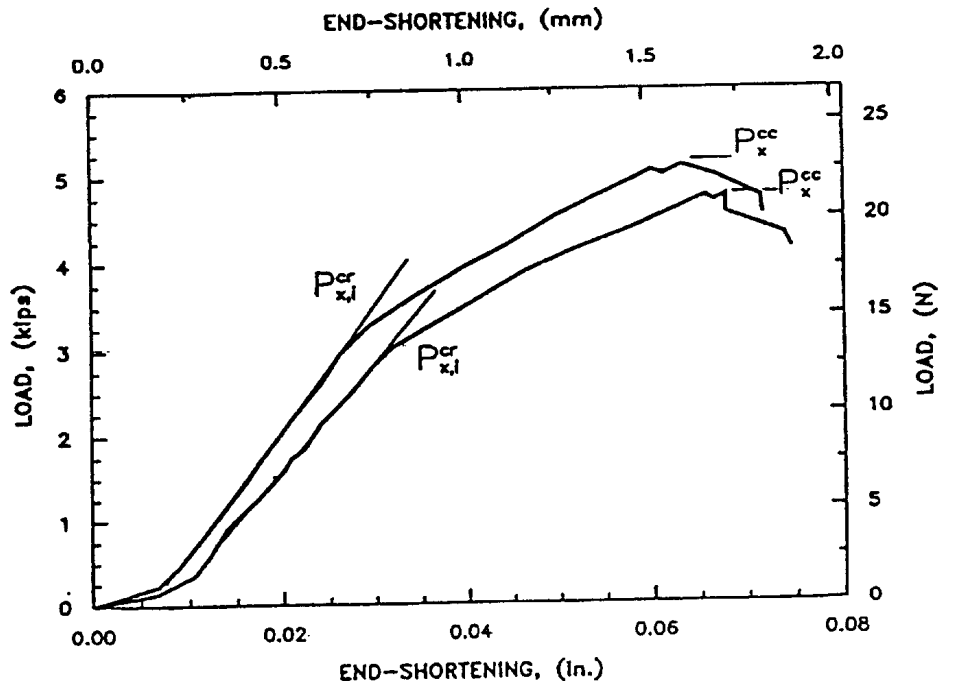

FIGURE 4.7.2(d) *No-edge-free plate. Crippling tests - AS/3501-6 $[\pm 45/90/0_3]_s$ - $b/t \approx 32$.*

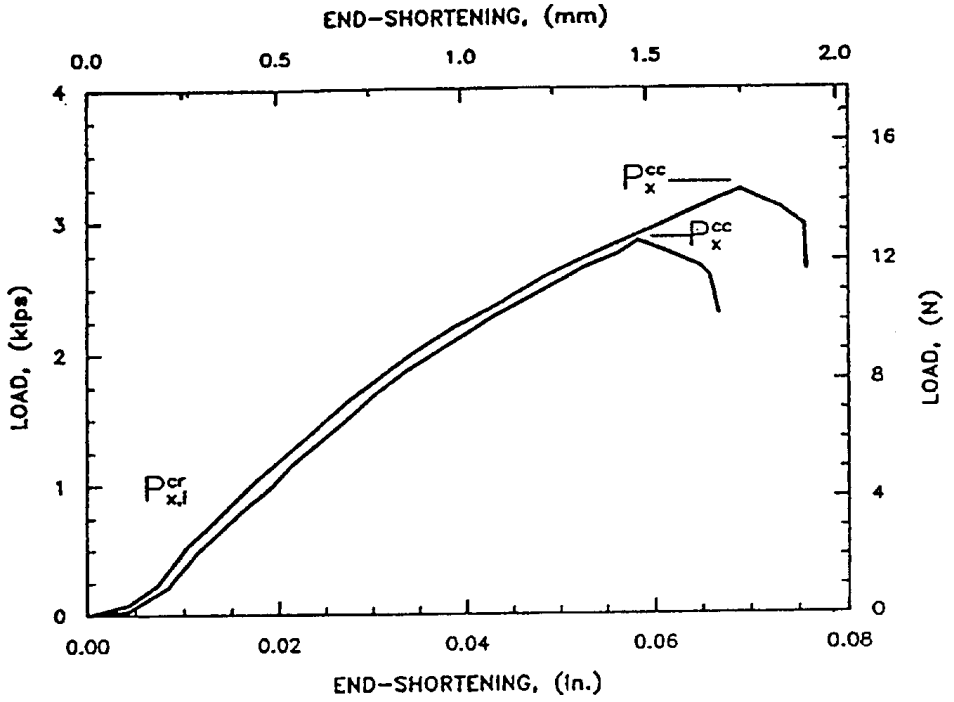

FIGURE 4.7.2(e) One-*edge-free plate. Crippling tests - AS/3501-6 $[\pm 45/90/0_3]_s$ - $b/t \approx 30$.*

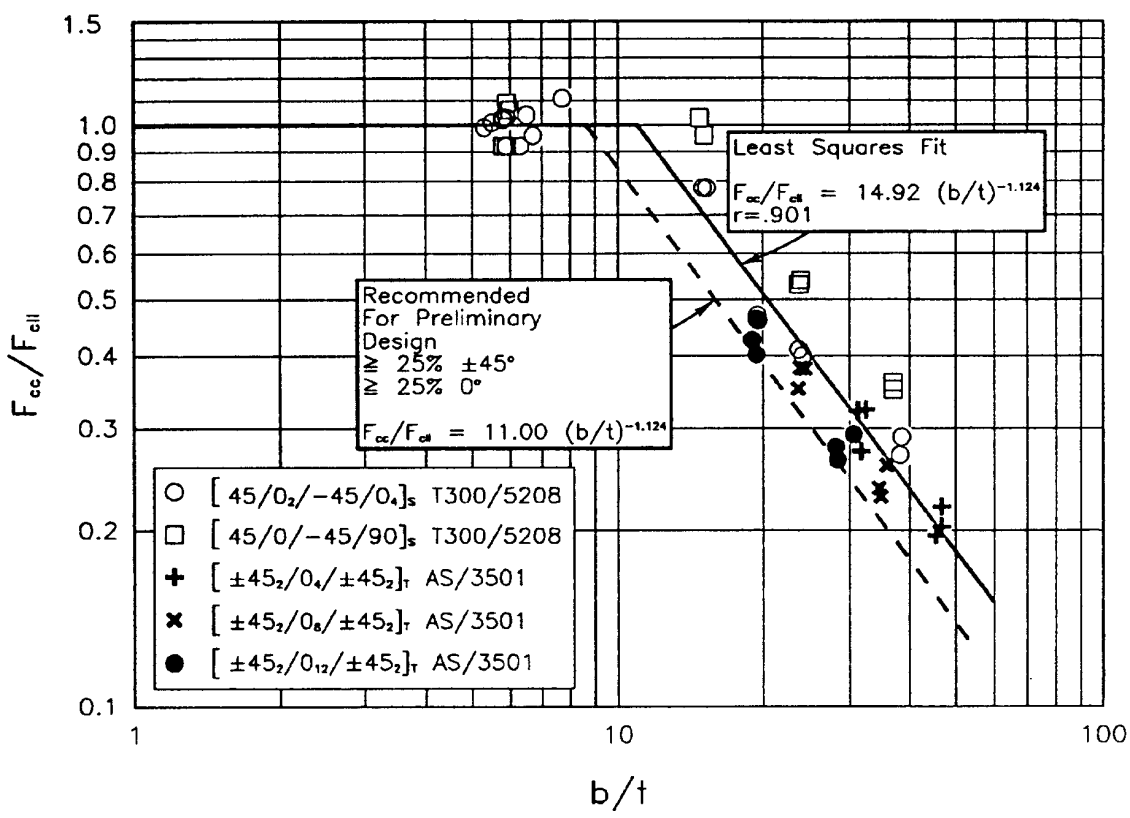

FIGURE 4.7.2(f) *Normalized crippling data - no-edge-free.*

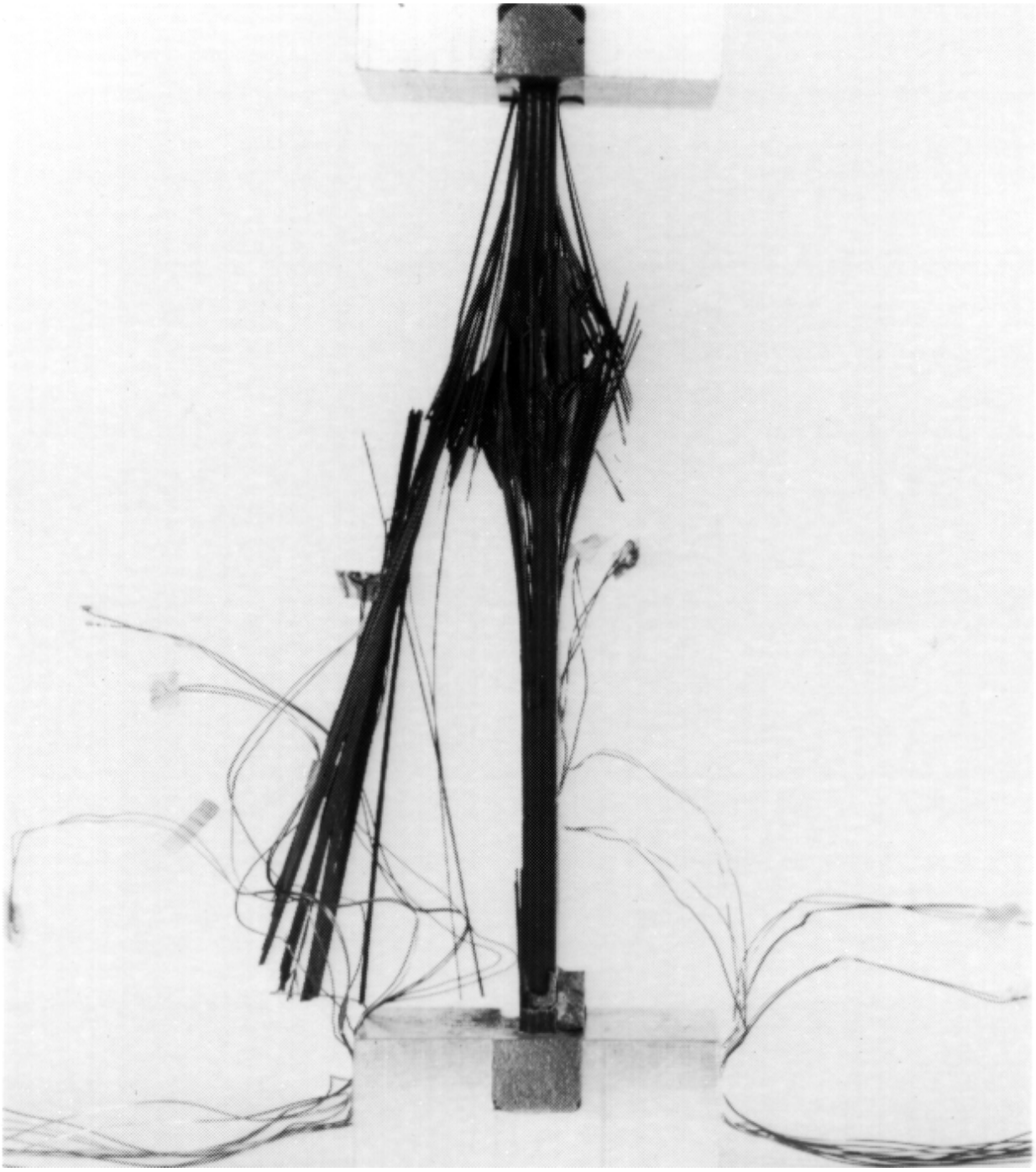

FIGURE 4.7.2(g) *Typical carbon/epoxy failed ultimate compression specimen.*

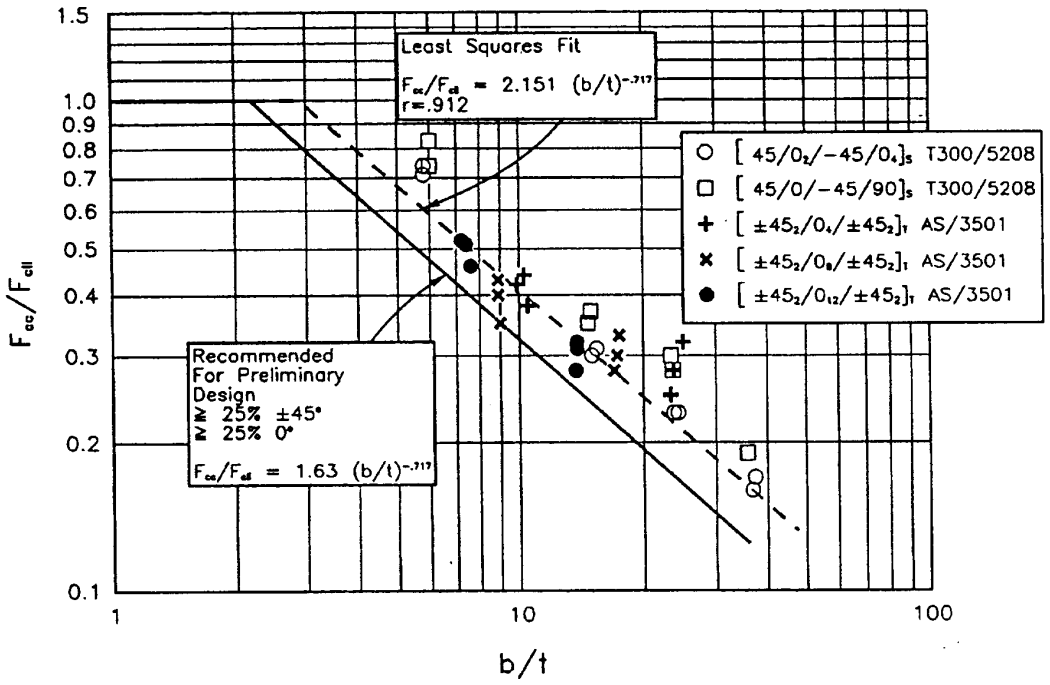

FIGURE 4.7.2(h) *Normalized crippling data - one-edge free.*

4.7.2.1 Analytical models

As stated in Section 4.7.1.2, initial buckling is more accurately determined by including the effects of transverse shear and material nonlinearity as is done in References 4.7.1.3(c) and (d). Transverse shear effects become especially important for thick laminates ($b/t < 20$). Stress-strain curves for laminates with a high percentage of ±45° plies may show significant material nonlinearity prior to initial buckling. These effects are equally important, of course, for plates loaded in the postbuckling range. Some examples of test results vs. the theory of these references are shown in Figures 4.7.2.1(a) and (b). Unfortunately, most of the computer programs available today are based on linear elastic theory and do not include transverse shear effects. Consequently, experimental data must be obtained to correct for these and other deficiencies in the analytical models.

The theoretical buckling loads for orthotropic one-edge-free and no-edge-free plates are given by:

$$N_x^{cr}\ (OEF) = \frac{12\,D_{66}}{b^2} + \frac{\pi^2 D_{11}}{L^2}$$

$$N_x^{cr}\ (NEF) = \frac{2\pi^2}{b^2}\left[\sqrt{D_{11}D_{22}} + D_{12} + 2D_{66}\right] \qquad 4.7.2.1(a)$$

These expressions do not include the bending-twisting terms D_{16} and D_{26}. These terms are present in all laminates that contain angle plies but, except in laminates having very few plies, their effect on the initial buckling load is generally not significant. Hence, the above equations are accurate for most practical laminates that are balanced and symmetrical about their mid-surface. The reader is referred to studies performed by Nemeth (Reference 4.7.2.1(a)) for additional information on the buckling of anisotropic plates and the effect of the various parameters on the buckling loads.

The Euler term in the first of the above equations is generally found to be negligible and, therefore, initial buckling of a one-edge-free plate is largely resisted by the torsional stiffness (D_{66}) of the laminate. This explains why higher initial buckling loads may be obtained for a given lay-up when the ±45° plies are on the outside surfaces of the plate.

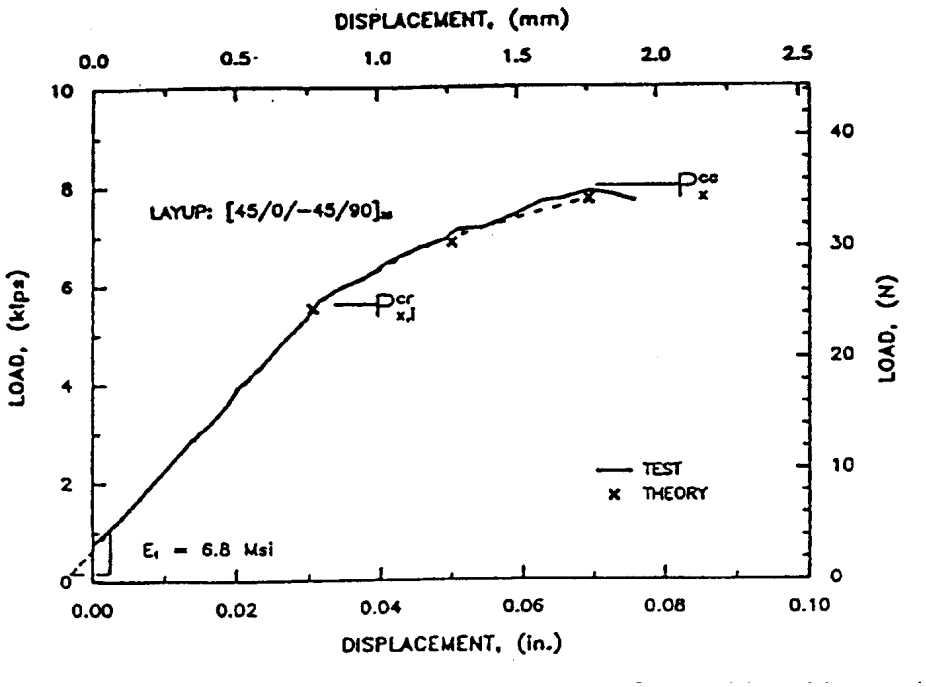

FIGURE 4.7.2.1(a) *Comparison of theory in References 4.7.1.3(b) and (c) with experiments for postbuckling curves and crippling strengths.*

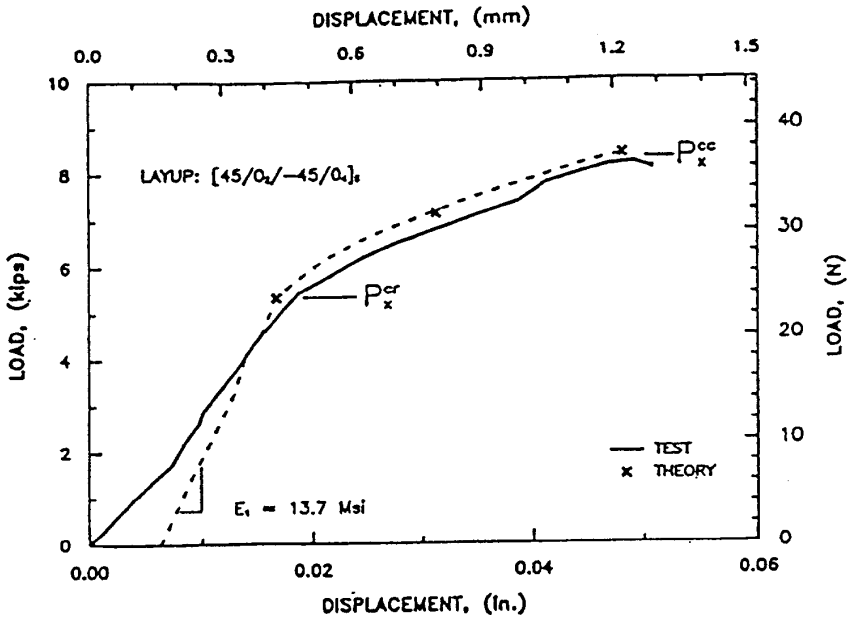

FIGURE 4.7.2.1(b) *Comparison of theory in References 4.7.1.3(b) and (c) with experiments for postbuckling curves and crippling strengths.*

For laminates that are only slightly unbalanced or unsymmetrical, approximate values for the initial buckling load may be obtained by substituting "equivalent" bending stiffnesses $\overline{D}_{ij}$ in place of D_{ij} in the buckling equations, where

$$[\overline{D}] = [D] - [B][A]^{-1}[B] \qquad 4.7.2.1(b)$$

The analysis of panels loaded in the postbuckling range becomes a geometrically nonlinear problem and, therefore, "conventional" plate buckling programs or other linear analysis codes cannot be used to accurately predict the crippling strength of composite plates. One example is shown in Figure 4.7.2.1(c), which shows experimental crippling curves and theoretical buckling curves for a quasi-isotropic T300/5208 laminate. (The AS/3501 and T300/5208 carbon/epoxy crippling data was taken from References 4.7.2(b) - (e)). The theoretical buckling curves shown in Figure 4.7.2.1(c) are very conservative at high b/t values and very unconservative at low b/t values. This may be explained by the fact that thin plates buckle at low strain levels and may thus be loaded well into the postbuckling range. On the other hand, neglecting transverse shear effects will cause strength predictions at low b/t ratios to be unconservative. The analysis of laminated plates is further complicated by the fact that high interlaminar stresses in the corners or at the free edge of the plate may trigger a premature failure.

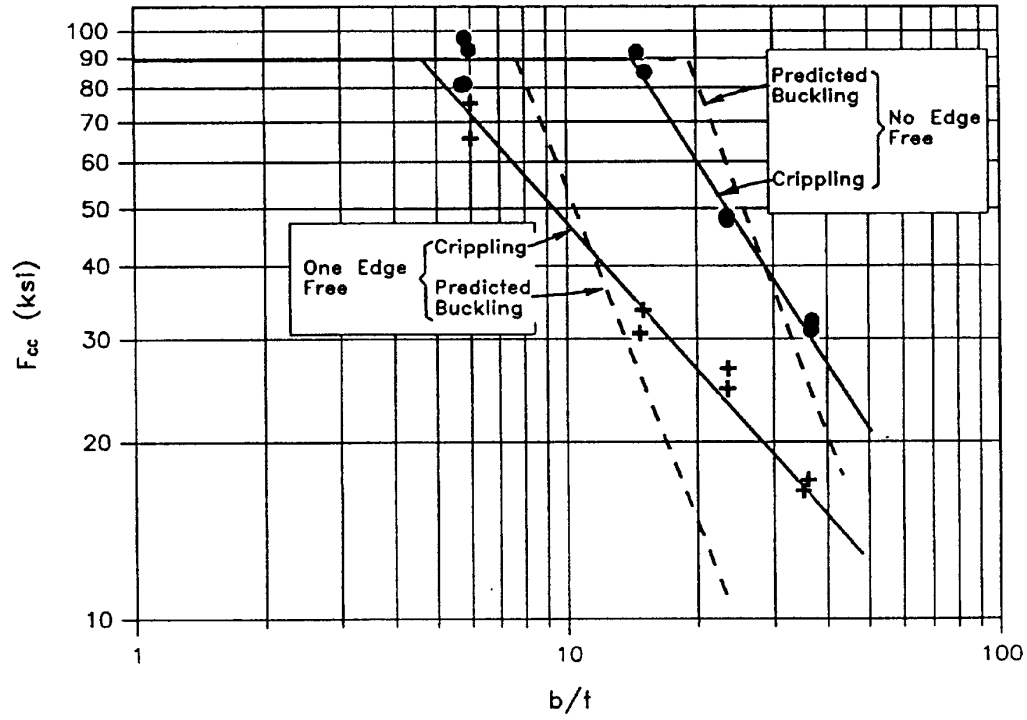

FIGURE 4.7.2.1(c) *Comparison of predicted buckling and crippling curves.*

As it would not be practical during preliminary design to conduct nonlinear analyses for a large number of lay-ups and b/t ratios, a better approach may be to use semi-empirical data to correct initial buckling predictions.

4.7.2.2 Fatigue effects

Postbuckling fatigue may be permitted under certain circumstances without jeopardizing the structural integrity of the plate (References 4.7.2(b), 4.7.2(g), and 4.7.2(h)). Significant conclusions identified in Reference 4.7.2(h) stated: "Composite panels demonstrated a high fatigue threshold relative to the initial

skin buckling loads. Composite panels showed a greater sensitivity to shear dominated fatigue loading as compared with compression dominated fatigue loading. The fatigue failure mode in composite panels was separation between the cocured stiffener and skin."

4.7.2.3 Crippling curve determination

Non-dimensional crippling curves are used to determine the crippling strength of the one-edge and no-edge-free composite elements. Different normalization techniques have been suggested for composites, most of which are modifications of those currently used in the aircraft industry for metallic structures. Perhaps, the most obvious change in the analysis and presentation of crippling data is the proposed use of the ultimate compression strength, F^{cu} to normalize the crippling strength, F^{cc}, for composites, instead of the material yield stress, F^{cy} commonly used for metallic elements.

Crippling curves for carbon/epoxy one- and no-edge-free plates are presented in Reference 4.7.2(e) in terms of the non-dimensional parameters F^{cc}/F^{cu} and $(b/t) * [F^{cu}/(E_x * E_y)^{1/2}]^{1/2}$. The latter parameter was chosen to reflect the orthotropic nature of composites. Test data for the one-edge-free plate elements were found to be in excellent agreement with the expected behavior, when the data were presented in terms of these non-dimensional parameters, but test results for the no-edge-free elements fell below the expected values.

A shortcoming in the methodology presented in Reference 4.7.2(e) is that the curves are non-dimensionalized on the basis of laminate extensional modulus only. The plate bending stiffnesses play an important role in determining the initial buckling and crippling loads of the element. Unlike in metallic plates, however, there exists no direct relationship between the extensional and bending stiffnesses of a composite plate and, therefore, laminates with equal in-plane stiffnesses may buckle at different load levels if their stacking sequences are not identical. Tests conducted by Lockheed and McDonnell Douglas under their respective Independent Research and Development (IRAD) programs have confirmed that more accurate buckling and crippling predictions may be obtained when the curves are defined in terms of the non-dimensional parameters

$$\frac{F^{cc}}{F^{cu}} \frac{E_x}{\bar{E}} \quad \text{and} \quad \frac{b}{t} \frac{\bar{E}}{E_x} \sqrt{\frac{F_{cu}}{\sqrt{E_x E_y}}} \qquad 4.7.2.3(a)$$

in which

$$\bar{E} = \frac{12 D_{11}}{t^3} \left(1 - \nu_{xy} \nu_{yx}\right) \qquad 4.7.2.3(b)$$

is an effective modulus accounting for stacking sequence effects through the bending stiffness term D_{11}.

4.7.2.4 Stiffener crippling strength determination

The commonly used procedure for predicting the crippling strength of a metallic stiffener, composed of several one-edge and no-edge-free elements, is to compute the weighted sum of the crippling strengths of the individual elements:

$$F_{ST}^{cc} = \frac{\sum_{i=1}^{N} F_i^{cc} \cdot b_i \cdot t_i}{\sum_{i=1}^{N} b_i \cdot t_i} \qquad 4.7.2.4$$

Test results appear to indicate that the same procedure can be successfully applied to composite stiffeners of uniform thickness if the element crippling strengths are determined with the aid of the non-dimensional parameters in Equation 4.7.2.3. Lockheed tests involved crippling of angles and channels made from thermoplastic (IM8/HTA) and thermoset (IM7/5250-4) materials. Tests results for one- and no-edge-free plates are presented in Figures 4.7.2.4(a) and 4.7.2.4(b). McDonnell Douglas also reported that, using this approach, predictions for carbon/epoxy stiffeners and AV-8B forward fuselage longerons have shown excellent correlation with test results.

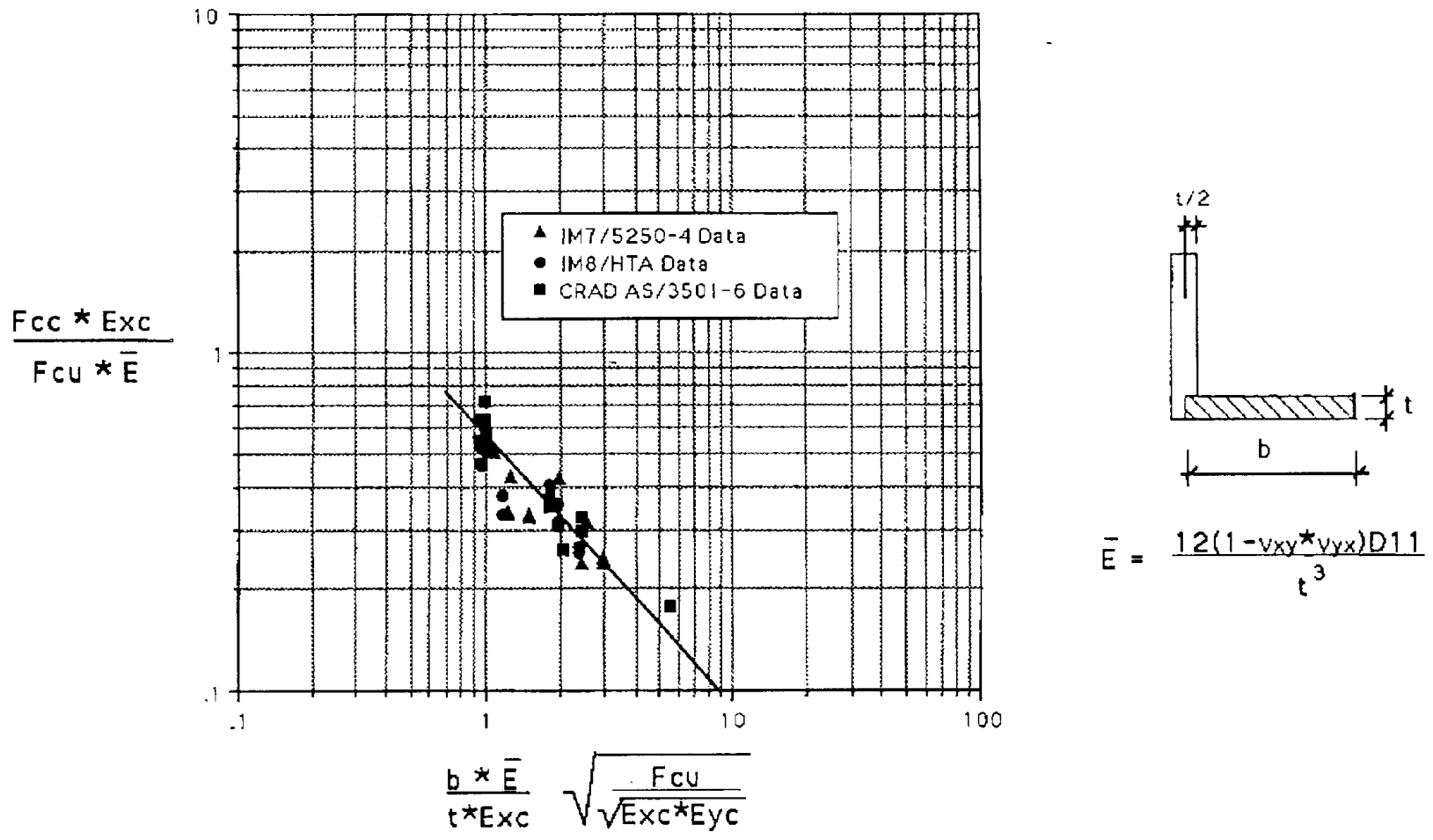

FIGURE 4.7.2.4(a) *One-edge-free crippling test results.*

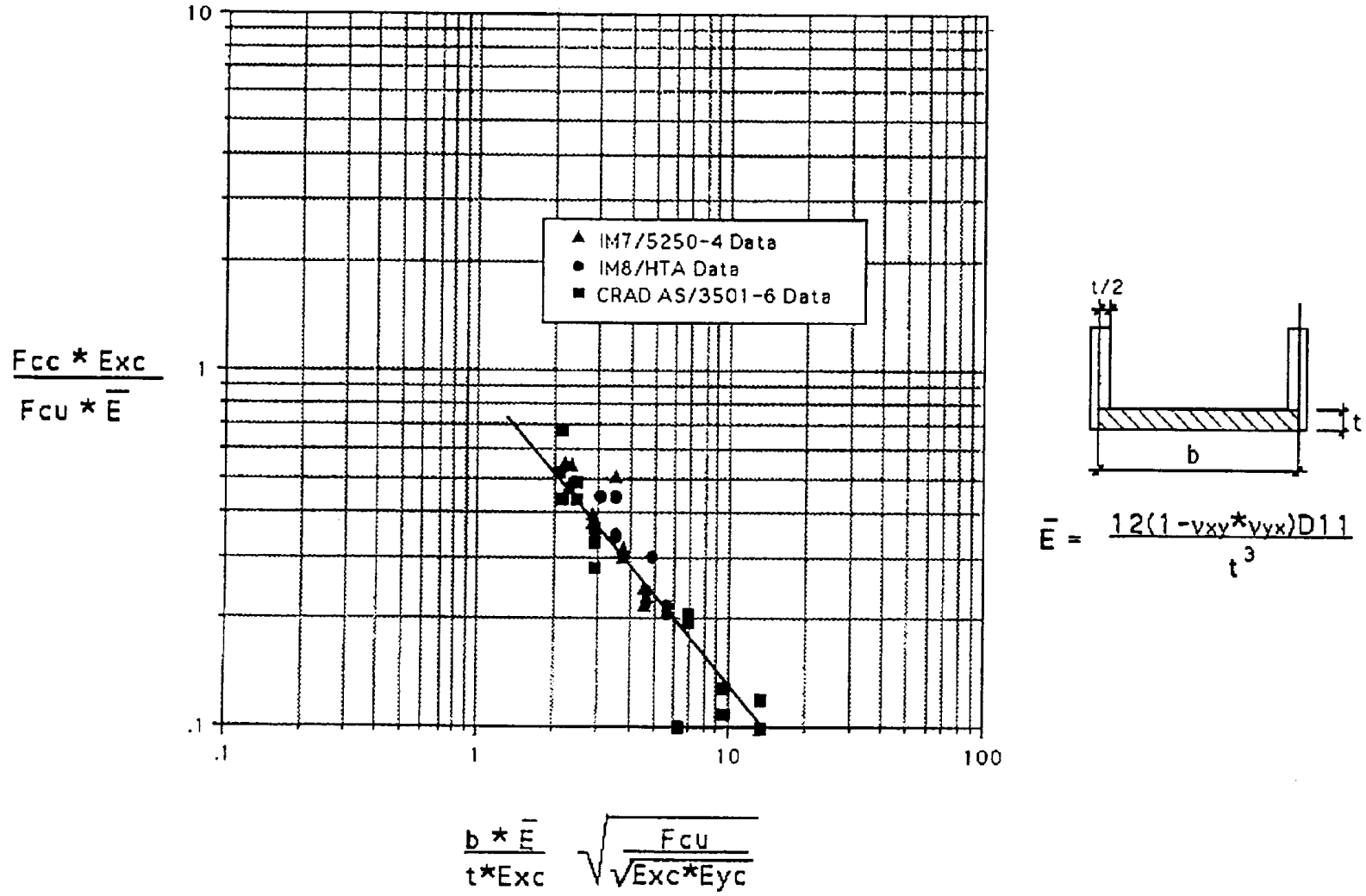

FIGURE 4.7.2.4(b) *No-edge-free crippling test results.*

Optimum design of stiffened panels made of composite materials may require the use of stiffeners of non-uniform thickness. Typical examples of frequently used stiffener configurations are shown in Figure 4.7.2.4(c). Insufficient experimental data currently exist to accurately predict the crippling strength of such stiffeners. At the juncture of two plate elements of different thickness, the thicker element will provide additional restraint to the thinner element. As a result, both the buckling and crippling strength of the thinner element will be increased while that of the thicker one will be decreased. The net effect could be an increase or decrease of the allowable stiffener stress depending on which of these two elements is more critical and thus is driving the buckling process. Equation 4.7.2.4 may be used to predict stiffener crippling but appropriate adjustments should be made to the crippling strength of the affected elements if that strength was based on data obtained from uniform thickness test specimens.

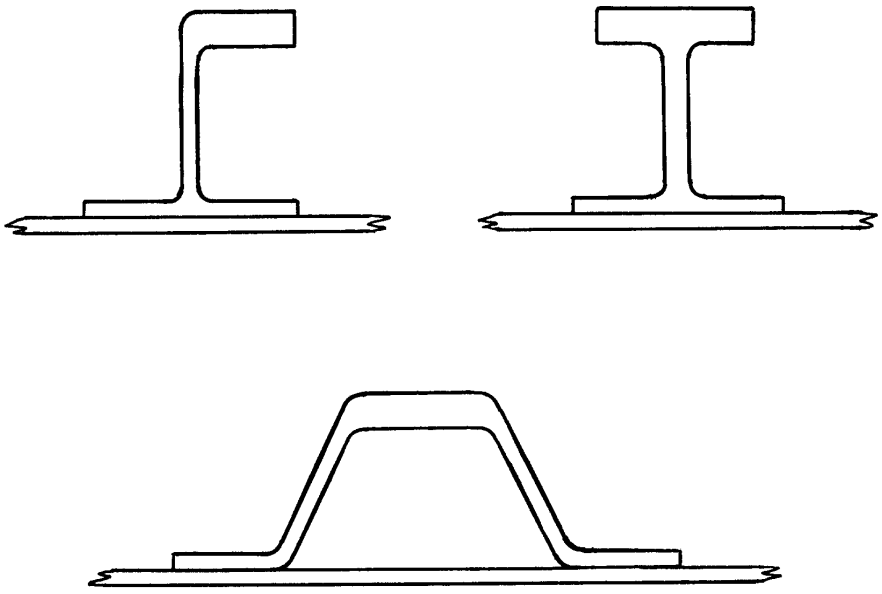

FIGURE 4.7.2.4(c) *Non-uniform thickness stiffener configurations.*

4.7.2.5 Effects of corner radii and fillets

In channel, zee, or angle section stiffeners where crippling rather than delamination is the primary mode of failure, the corner radii do not appear to have an appreciable effect on the ultimate strength of the section. The opposite is true, however, for I or J stiffeners, where the corner radii do play an important role. It has been common practice to use unidirectional tape material to fill the corners of these stiffeners, as shown in Figure 4.7.2.5. The addition of this very stiff corner material increases the crippling strength of the stiffener. Since the cross-sectional area of the fillet, and thus the amount of 0° material, is proportional to the square of the radius, the increase in crippling strength may be significant for stiffeners with large corner radii. A conservative estimate for the increase in crippling strength may be obtained from the following expression:

$$\bar{F}^{cc} = F^{cc} \frac{1 + \dfrac{E_f A_f}{\sum E_i b_i t_i}}{1 + \dfrac{A_f}{\sum b_i t_i}} \qquad 4.7.2.5$$

which is based on the assumption that the critical strain in the corner region is no greater than that for a stiffener without the additional filler material.

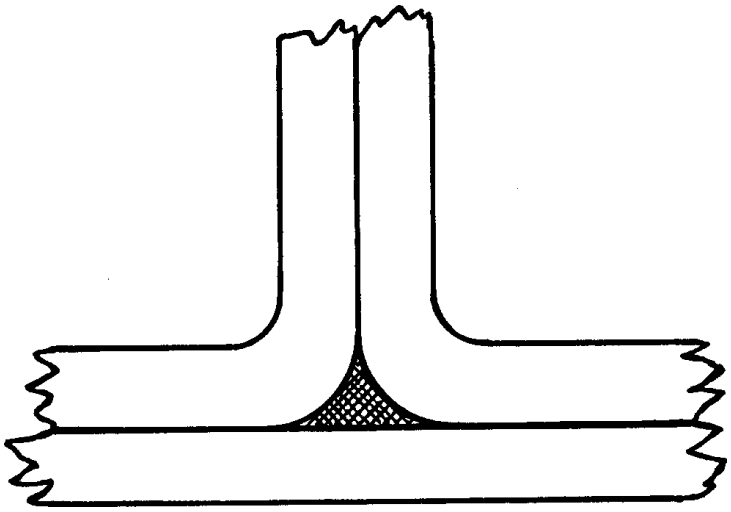

FIGURE 4.7.2.5 *Corner fillet.*

4.7.2.6 Slenderness correction

As the unsupported length increases, the stiffener may fail in a global buckling mode rather than by local crippling. The usual procedure to account for this is to apply a correction factor to the crippling strength, F_{cc}, based on the slenderness ratio (L'/ρ) of the column. The critical stress for the stiffener now becomes

$$F^{cr} \infty F^{cc}\left[1 - \frac{F^{cc}}{4\pi^2 E_x^c}\left(\frac{L'}{\rho}\right)^2\right] \qquad 4.7.2.6(a)$$

The radius of gyration for the cross-section of a composite column is defined as

$$\rho = \sqrt{\frac{(EI)_{st}}{(EA)_{st}}} \qquad 4.7.2.6(b)$$

where $(EA)_{st}$ and $(EI)_{st}$ are the extensional and bending stiffnesses of the stiffener.

4.7.3 Summary

- The buckling strength, or stability, of flat and curved composite skin panels is strongly affected by geometry, stacking sequence, boundary conditions, and loading conditions. In many cases, it may be estimated using existing closed form solutions for orthotropic plates ($r/t > 100$), such as equations 4.7.1.3 - 4.7.1.7.

4.8 CARPET PLOTS

4.9 CREEP AND RELAXATION

4.10 FATIGUE

4.11 OTHER STRUCTURAL PROPERTIES

4.11.1 Damage tolerance

4.11.1.1 Background

Damage tolerance is defined as a measure of the structure's ability to sustain a level of damage or presence of a defect and yet be able to perform its operating functions. Consequently, the concern with damage tolerance is ultimately with the damaged structure having adequate residual strength and stiffness to continue in service safely until the damage can be detected by scheduled maintenance inspection and repaired, or if undetected, for the remainder of the aircraft's life. Thus, safety is the primary goal of damage tolerance.

4.11.1.2 Types of damage and concerns

There are basically two types of damage which are categorized by their occurrence during the fabrication and use of the part, i.e., damage occurring during manufacturing or damage occurring in service. The former commonly includes consideration of defects such as porosity, microcracking, and delaminations resulting from processing discrepancies and also such items as inadvertent edge cuts, surface gouges and scratches, damaged fastener holes, and impact damage. The inadvertent (non-process) damage most commonly occurs in detail parts or components during assembly or transport.

It is expected that the occurrence of the majority of manufacturing associated damage, if beyond specification limits, will be detected by routine quality inspection. Nevertheless, some "rogue" defects or damage beyond specification limits may go undetected and consequently, their occurrence must be assumed in the design procedure. An example of such a damage tolerance design criteria would be the assumption of inadvertent delaminations existing in parts. Even though the capability to detect a 0.5 in diameter delamination by in-process ultrasonic inspection is considered typical, in designing to damage tolerance criteria, we may assume the presence of a larger delamination is missed by inspection. Quantifying the size of the "rogue" or missed flaw would be part of the contractor/customer criteria development process.

Another example of a manufacturing defect is when prepreg backing paper or separation film is inadvertently left in the laminate between plies during layup. Current inspection methods may not detect this type of discrepancy which may lead to a large delamination. Consequently, until more adequate inspection techniques are developed, in-process quality controls must be sufficiently rigid to preclude this occurrence. A damage tolerance criterion might be required to design for the occurrence of the flaw. Obviously a balance is needed between designing all possible "damage" into a part (with associated weight penalties) and what realistically can and should be eliminated from the fabrication/assembly process.

Service damage concerns are similar to those for manufacturing. Types of service damage include edge and surface gouges and cuts caused by improper tool use, or foreign object collision and blunt object impact damage caused by such incidences as dropped tools or contact with service equipment. Of these, cuts and gouges, are usually the more severe for tension loading while impact damage is generally the more severe damage type for compression, especially for thick laminates.

Delaminations can also be critical defects. However, unless they are very large, i.e., more than 2.0 inches (50 mm) in diameter, the problem is mostly with thin laminates. Effects of manufacturing defects such as porosity and flawed fastener holes are usually less severe. They are generally accounted for by the use of design allowable properties that have been obtained by testing specimens with notches, i.e., stress concentrations. Most commonly, these are specimens with a centered hole. Open holes are typically used for compression specimens while either open or filled holes (holes with an installed fastener)

are used for tension testing. (Open holes are more critical then filled holes for compression. Filled holes may be more critical in tension, especially for laminates with ply orientations with a predominate number of plies oriented in the load direction). Consequently, the design allowables thus derived may be used to account for a nominal design stress concentration caused by an installed or missing fastener, at least to a 0.25 inch (6.4 mm) diameter, as well as many manufacturing defects.

One of the primary concerns with damage tolerance of composites is detection of the damage. This is true both during manufacture and once in service. For the latter, the threshold of detectability depends on the type of inspection scheduled in service:

- walk around: long distance visual inspection to detect punctures, fiber breakage, i.e., readily detectable damage.

- visual detailed inspection using grazing light on a clean element, lens, etc., to detect barely visible impact damage. In this case the dent depth at the threshold of detectability (δ_d) should be defined.

- special detailed inspection for non-visible damage using ultrasonic, x-ray, shearography, etc.

Dent depths have been found to decay with time, aging, thermal cycling, and mechanical fatigue due to visco-elasticity phenomena. In the case of visual detailed inspections, the dent depth established should be that which after decay is at least equal to or above the threshold of detectability, (δ_d). In some cases, the initial impact indentation dent depth (δ_I) may be as much as 3 times that of δ_d.

Fortunately, most of the damage which is critical to tension loading such as cuts and gouges is, to some degree, visible. Tests have shown that for tension loading, the residual strength of a laminate with a cutout is primarily dependent on the width of the cutout and essentially independent of the cutout shape. Thus design values reduced to account for the presence of a 0.25 inch diameter hole also account for an equivalent length edge cut, however, and testing might be required to define appropriate design values. Cuts of this type that might be produced during manufacturing are a special problem since they may be filled with paint, and consequently, not detected. Sufficient testing should be done as part of design verification programs to ensure that cuts and gouges that are on the threshold of visibility will not degrade the structure enough to jeopardize its safety.

Low velocity impacts, e.g., impacts from dropped tools as opposed to ballistic impacts, present a special problem. Impacts on the laminate surface, especially those made by a blunt object, may cause considerable internal damage without producing visible indications on the surface. Damage to the resin may be particularly severe as evidenced by transverse shear cracks and delaminations. Consequently, the resin loses its ability to stabilize the fibers in compression and the local failure may initiate total structural collapse. Similarly, the impact may damage fibers and cause local stress concentrations which could result in significant loss of tensile strength. With conventional graphite/epoxy systems, which are quite brittle, losses in tension and compression strength for nondetectible impact may approach 50% and 60% respectively.

Low velocity impact damage, such as from dropped tools is a key problem in thin gage structures. The damage is characteristically different from damage in thick laminates. Laminate internal delamination is less of a problem because thin laminate damage is more typically in the form of fiber breakage and, possibly, penetration. For sandwich materials with thin faces, impact can result in visible core damage which has been shown to reduce the compressive and shear strengths. Impact damage which causes a break in the facesheet of the sandwich (as well as porosity, a manufacturing defect) also presents a long term durability problem in that it can allow water intrusion into the core.

It is considered possible that nonvisible damage might occur early in the aircraft's life and go undetected during subsequent service inspections. Thus, unless detection is ensured by more discriminating inspection procedures, the damage or defect must be assumed to be present for the entire life of the air-

craft. This "duration of damage or defect" factor is important in determining the probability that the aircraft with a defect or damage will encounter a load which might cause failure. That is, structure having undetected damage, such as low-velocity impact damage, will have a probability of encountering a particularly high load that is directly proportional to the service time during which that load may occur. In contrast, structure that has damage that is discovered and repaired in a short time period will have less chance of encountering the same high load.

4.11.1.3 Evolving military and FAA specifications

The "duration of damage or defect" factor based on degree of detectability has been the basis for establishing minimum Air Force damage tolerance residual strengths for composite structures in requirements proposed for inclusion in AFGS-87221A, "General Specification for Aircraft Structures". These strength requirements are identical to those for metal structure having critical defects or damage with a comparable degree of detectability. Requirements for cyclic loading prior to residual strength testing of test components are also identical. The nondetectable damage to be assumed includes a surface scratch, a delamination, and impact damage. The impact damage includes both a definition of dent depth, i.e., detectability, and a maximum energy cutoff. Specifically, the impact damage to be assumed is that "caused by the impact of a 1.0 inch diameter hemispherical impactor with a 100 ft-lb of kinetic energy, or that kinetic energy required to cause a dent 0.10 inch deep, whichever is least." For relatively thin structure, the detectability, i.e., the 0.1 inch (2.5 mm) depth, requirement prevails. For thicker structure, the maximum assumed impact energy becomes the critical requirement. The associated load to be assumed is the maximum load expected to occur in an extrapolated 20 lifetimes. This is a one time static load requirement. These requirements are coupled with assumptions that the damage occurs in the most critical location and that the assumed load is coincident with the worst probably environment.

In developing the requirements, the probability of encountering undetected or undetectable impact damage above the 100 ft-lb (136 J) energy level was considered sufficiently remote that when coupled with other requirements a high level of safety was provided. For the detectability requirement, it is assumed that having greater than 0.10 inch (2.5 mm) in depth will be detected and repaired. Consequently, the load requirement is consistent with those for metal structure with damage of equivalent levels of detectability. Provisions for multiple impact damage, analogous to the continuing damage considerations for metal structure, and for the lesser susceptibility of interior structure to damage are also included.

In metal structure, a major concern about damage tolerance is not only initial damage but also growth of damage prior to the time of detection. Consequently, much development testing for metals has been focused on evaluating crack growth rates associated with defects and damage, and the time for the defect/damage size to reach residual strength criticality. Typically, the critical loading mode has been in tension. Crack growth, even at comparatively low stress amplitudes, may be significant. In general, damage growth rates for metals are consistent and, after test data has been obtained, can be predicted satisfactorily. Thus, knowing the expected stress history for the aircraft, inspection intervals have been defined that confidently ensure crack detection before failure.

By contrast, the fibers in composite laminates act to inhibit tensile crack growth. Through-thickness damage growth occurs only at relatively high stress levels. Consequently, through-the-thickness damage growth in composites has generally not been a problem. In-plane damage growth associated with delaminations or impact damage, however, must be considered. Detection again, is an important consideration. Unlike cracks in metal, growth of delaminations or impact damage in composites, with probably not be detected if it does occur. Additionally, interlaminar damage growth in composites, especially that associated with impact damage, cannot be predicted satisfactorily. This has been considered in development of the referenced Air Force specification. Hence, it is required that damage be monitored for growth during cyclic tests which are conducted during development and validation. Resulting design values must be established with sufficient margins to ensure that damage growth due to repeated loads will not occur.

The damage tolerance design procedures for civil/commercial aircraft are expressed more generally but with equal effectivity. Guidelines are addressed for the BAA in Federal Aviation Regulation (FAR) 25

and in Advisory Circular AC-107A. Relative to impact damage, the FAA guidelines states "It should be shown that impact damage that can be realistically expected from manufacturing and service, but not more than the established threshold of detectability for the selected inspection procedure, will not reduce the structural strength below ultimate load capability. This can be shown by analysis supported by test evidence, or by tests at the coupon, element, or subcomponent level." The guidance is to ensure that structure with undetected damage will still meet ultimate strength requirements. Again, it assumed that more obvious damage will be detected in a timely manner and will be repaired. The difference in the Air Force specification and the FAA guideline is primarily in the residual strength value. Also, while the Air Force specification assumes visual inspection, the FAA guideline leaves the inspection method to be selected. Consequently, since specifications and guidelines differ with the type of aircraft, the manufacturer must be aware of the differences and apply those guidelines and specifications appropriate to the situation.

4.11.1.4 Material effects on damage tolerance

The ability of composite structures to resist or tolerate damage is strongly dependent on the constituent resin and fiber material properties and the material form. The properties of the resin matrix are most significant and include its ability to elongate and to deform plastically. The area under a resin's stress-strain curve indicates the material's energy absorption capability. Damage resistance or tolerance is also related to the material's interlaminar fracture toughness, G, as indicated by energy release rate properties. Depending on the application $G_{(I)}$, $G_{(II)}$, or $G_{(III)}$ may dominate the total G calculation. These parameters represent the ability of the resin to resist delamination, and hence damage, in the three modes of fracture. The beneficial influence of resin toughness on both damage resistance and tolerance, has been demonstrated by tests on new toughened thermoset laminates and with the tougher thermoplastic material systems.

Investigations have been conducted on the effect of fiber properties on impact resistance or tolerance. In general, laminates made with fabric reinforcement have better resistance to damage than laminates with unidirectional tape construction. Differences among the carbon fiber tape laminates, however, are small. Some studies have been made of composites with hybrid fiber construction, that is, composites in which two or more types of fibers are mixed in the layup. For example, a percentage of the carbon fibers are replaced with fibers with higher elongation capability, such as fiberglass or aramid. Studies in both cases have shown improvement in residual compression strength after impact. Basic undamaged properties, however, were usually reduced.

In thin gage structures such as a two- or three-ply fabric facesheet sandwich construction, materials can have a significant effect on damage tolerance. Investigations in general have shown that compression strength (both before and after impact) increases with the fiber strain-to-failure capability within a particular class of materials. Higher strain capability aramid or glass fiber structures tend to be more impact resistant than high-strength carbon fiber structure. However, the compressive strengths of the undamaged and damaged aramid and glass structures are lower than that of carbon. Structure incorporating high-modulus, intermediate-strength carbon fibers, with higher strain-to-failures offer a significant impact resistance while retaining higher strength.

In thermoset material systems, the nominal matrix toughness variations influence the impact resistance of thin gage structures but generally to a lesser extent than in thicker structures. For thermoplastic material systems, however, the generally much larger increase in the fracture toughness (G_{I_c}, G_{II_c}, etc.) of the resins do translate into significant impact resistance and residual strength improvements. For sandwich structures, where failure is not core-dependent, core density has been shown to have little effect on impact resistance. However, core density can have a significant effect on the residual strength of the sandwich if the sandwich mode is core-dependent (i.e., face wrinkling).

Methods such as through-thickness stitching have also been used to improve damage resistance. The effect has been to reduce the size of internal delaminations due to impact and similar to the hybrid high

elongation fibers, arrest damage growth. Tests involving conventional graphite/epoxies have shown increases in the residual strength of up to 15% for comparative impact energy levels. The process is quite expensive, however, and probably should be considered for application in selected critical areas only. Additionally, the stitches tend to cause stress concentrations and the tensile strength, transverse to the stitching row, is usually reduced.

There are also other properties of composites that contribute to their damage resistance/tolerance. In contrast to metals, which have a Poisson's ratio typically near 0.3, the Poisson's ratio for composite laminates may vary widely, dependent on the particular combinations of ply layup orientations. Consequently, Poisson's ratios may be unbalanced between different sets of plies within a laminate. When the laminate is stressed, these imbalances may create high internal stresses. The consequence is that these stresses may add to damage-induced stresses thereby increasing the tendency for damage growth or causing a further reduction tensile or compression strength. Hence, ply stacking sequences that produce high internal stresses when the laminate is loaded, should be avoided.

As an example consider the influence of laminate stacking sequence (LSS) on compression after impact properties. The LSS can affect compression after impact strength (CAI) in several ways. First, the bending stiffness of a laminate and failure mechanisms that occur during an impact event is strongly dependent on LSS. Load redistribution near the impact site is dependent on the distribution of damage through the laminate thickness (e.g., the LSS of sublaminates affects their stability). Finally, damage propagation leading to final failure also depends on LSS, as was the case for notched tensile strength.

When impact damage is dominated by fiber failure (e.g., Reference 4.11.1.4(a)), it is desirable to stack primary load carrying plies in locations shielded from fiber failure. Since fiber failure typically occurs first near outer surfaces, primary load carrying plies should be concentrated towards the center of the LSS.

Many of the impact damage states studied in the past have been dominated by matrix failures. The creation of matrix cracks and delaminations which combine to form sublaminates depends strongly on LSS (Reference 4.11.1.4(b)). Homogeneous sacking sequences have been found to lead to characteristic damage states which repeat through the laminate thickness. Alternatively, plies can be stacked in a sequence which concentrates damage in specific zones on the laminate.

Recent methods have been developed and verified to predict the effects of known impact damage states on CAI (References 4.11.1.4(c) - (e)). This analysis involves four steps. First, the damage state is characterized with the help of NDI and the damage is simulated as a series of sublaminates. Second, sublaminate stability is predicted with a model that includes the effects of unsymmetric LSS. Third, the in-plane load redistribution is calculated with a model that accounts for structural geometry (e.g., finite width effects). Finally, a maximum strain failure criterion is applied to calculate CAI. Figure 4.11.1.4(a) shows typical results from this analysis procedure.

Interlaminar toughness is crucial to the extent of damage created in a given impact event; however, the CAI of laminates with equivalent damage states (size and type) was found to be independent of material toughness (References 4.11.1.4(c) - (e)). The model from Reference 4.11.1.4(c), which accounts for the in-plane stress redistribution due to sublaminate buckling, has worked equally well for tough and brittle resin systems studied. Since delamination growth may be possible with some materials and LSS, a more general model would also account for out-of-plane stresses.

Experience to date suggests that a homogeneous LSS might be best for overall CAI performance dominated by matrix damage (Reference 4.11.1.4(b)). Figure 4.11.1.4(b) shows experimental data indicating that LSS has a strong effect on CAI. The combined influence of impact damage resistance and CAI performance is evident in the figure.

Basic information on laminate stacking sequence effects is found in Section 4.6.5.

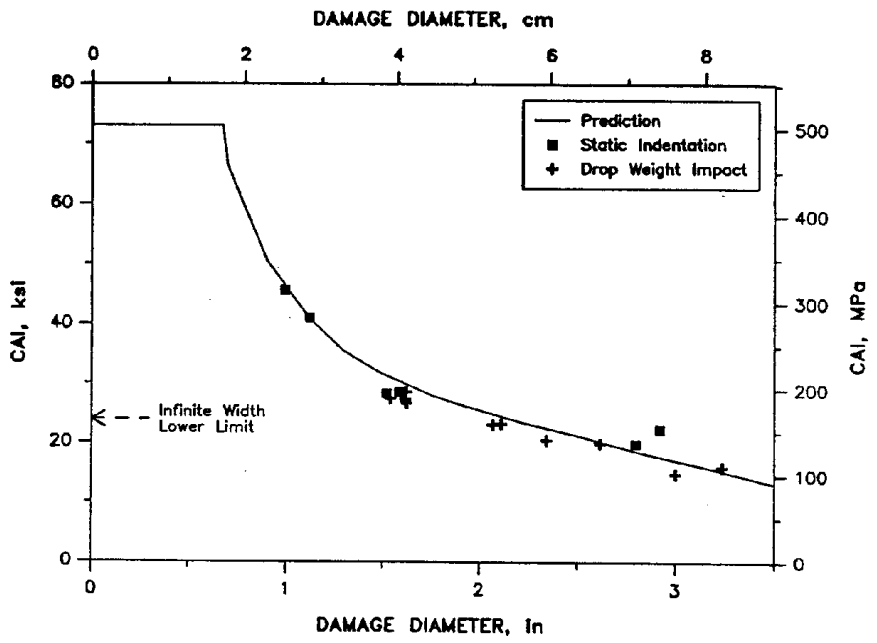

FIGURE 4.11.1.4(a) *Analysis and test results for 5 in. wide specimens, AS6/3501-6, $[45/0/-45/90]_{5S}$, and ply thickness - 0.0074 in. (from Reference 4.11.1.4(d)).*

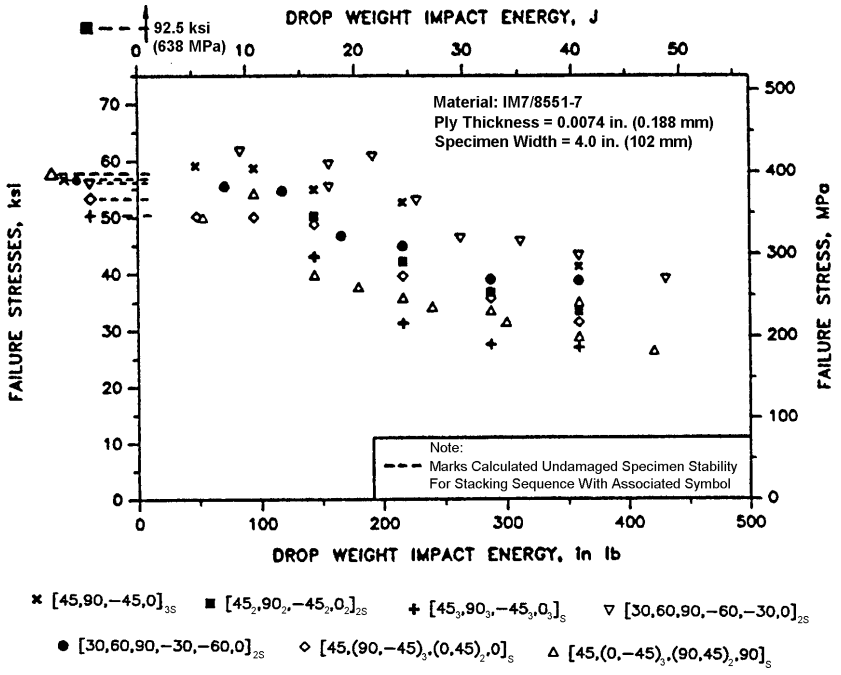

FIGURE 4.11.1.4(b) *Test data for CAI performance as a function of LSS (from Reference 4.11.1.4(e)).*

4.11.2 Durability

Durability of a structure is its ability to maintain strength and stiffness throughout the service life of the structure. A structure must have adequate durability when subjected to the expected service loads and environment spectra to prevent excessive maintenance, repair or modification costs over the service life. Thus, durability is primarily an economical consideration.

The major factors limiting the life of metallic structure are corrosion and fatigue. In composites, it has been demonstrated that one of the most common damage growth mechanisms is intercracking and fiber breakage usually occurs. Also, in three-dimensional composite structures out-of-plane loadings can either cause failure directly or induce failure indirectly. Because delamination growth is an important growth mechanism, composites are most sensitive to compression dominated fatigue loading.

A second common composite fatigue failure mode is fastener holes wear caused by high bearing stresses. In this failure mode, the hole gradually elongates may lead to a bearing failure or internal load redistribution.

Fatigue behavior of composites has been extensively investigated both experimentally and analytically. A partial list of these investigations is given as References 4.11.2(a) through 4.11.2(aa). In general, composites under in-plane loads have relatively flat fatigue stress-life (S-N) curves with high fatigue thresholds (endurance limits). This behavior is observed for various test specimen types from laminate to structural element. The fatigue threshold for a commonly used carbon/epoxy composite can be as high as 70% of the static strength under constant amplitude cyclic loading. The value of fatigue threshold is even higher when the composite is tested under applications spectra, such as that of a typical fighter aircraft spectrum (References 4.11.2(r) and (s)). Experimental data generated in Reference 19 showed that the typical fatigue failure mode was quasi-static failure when open hole specimens were tested under compression dominated fatigue spectrum loading. However, in high-cycle applications such as rotorcraft, fatigue structure endurance limits at 10^7 to 10^9 cycles must be established and these data are not readily available.

Accompanying the flat S-N curve is the significantly higher fatigue life scatter for composites compared to metals. Extensive statistical data analyses were conducted in References 4.11.2(ab) through (ae) to characterize the fatigue life data scatter of composites. The data compiled in these references included a variety of test variables such as geometry, environment and loading mode. The results of these analyses showed that the mean Weibull shape parameter for carbon/epoxy coupon data is approximately 2. This value is compared to 4.4 for commonly used aluminum alloys under constant amplitude fatigue loading and 7.7 under spectrum loading. This high variability in fatigue life is considered typical to most carbon fiber resin matrix composites and must be fully realized in order to assure adequate durability.

Traditionally, metal airframe structures are fatigue tested under spectrum loading to a minimum of two lifetimes to assure adequate durability. Based on the material variability observed in a commonly used aluminum alloys, a 2-4 lifetime fatigue test provides a very high structural reliability (approximately 0.999). However, because of the high variability of fatigue life test data observed in composites a 2-4 lifetime life factor provides a very low reliability (approximately 0.333). Therefore, the 2-4 lifetime fatigue test may not universally assure adequate durability for a composite structure. However, the use of significantly larger life factors in full-scale durability test programs may not be economically feasible. Alternate approaches may be used to reduce the test duration and at the same time demonstrate adequate reliability. Since these methods continue to evolve, early discussion with appropriate certification agency is recommended.

The load enhancement factor approach, evaluated in References 4.11.1 (ac) and (ad), is one of several alternative durability testing approaches. The objective of this approach is to increase the applied loads in the fatigue test so that the same high level of reliability can be achieved with a shorter test duration. In this approach, the fatigue life data variability, the residual strength scatter and the characteristics of composite fatigue S-N curves are integrated into a mathematical relationship. The required load enhancement factor and the test duration are then determined based on the material variability parameters

and the number of tests. A simple method for determining the load enhancement factor for any composite material and failure mode is described in Reference 4.11.2.(ae).

A second approach, the ultimate strength approach, takes advantage of the excellent fatigue response of composites and assuming no damage growth during the lifetime of the structure. The objective of the ultimate strength approach is to have operating stresses below the fatigue threshold or endurance limit, depending upon application. This is possible in practice because composites have flat S-N curves where fatigue threshold is a high proportion of ultimate strength. This approach and other durability testing approaches, such as residual strength approach, are described in detail in References 4.11.2(ac) and (ad).

4.11.2.1 Design development/certification implications

The high cost of full-scale structural test prohibits generation of sufficient data for reliability analysis. Thus, for meaningful interpretation of full-scale tests, a building-block approach is desirable for certification of composite structures. This approach fully utilized coupon, element, subcomponent and component level test data so that limited full-scale structural test data can be interpreted statistically. Use of a building-block approach is discussed in References 4.11.2.1(a) through (d). The number of tests decreases from the coupon level to the component level. A relatively large number of tests is required at the coupon level to establish the data scatter and design allowables for different loading modes, failure modes and environments. A smaller number of tests is required at the element and subcomponent level to determine failure mode interaction and to demonstrate the variability in structural response. This information is then used for design and interpretation of the full-scale structural test program. The three levels of fatigue tests--allowable, design development and full-scale--are discussed in the following paragraphs.

The purpose of design allowable tests is to evaluate the material scatter and to establish fatigue life parameters for structural design. Laminate lay-up, stacking sequence effects, ply drop-offs, out-of-plane loadings, fastener holes, cutouts, etc. should be addressed at this level. Because composites are environmentally sensitive, design allowables should be obtained for structure. In planning the fatigue allowable tests, the main consideration is the test environment. The test environment depends on the relationship between the load/temperature spectrum and the material operation limit. The proper approach is to use simple, conservative constant temperature tests with a constant moisture level. A minimum of three stress levels for each test condition is required to fully characterize the fatigue behavior within the fatigue sensitive stress range. Fatigue tests should be conducted until fatigue failure occurs, except at the lowest stress level. At this stress level, because the fatigue threshold is approached, long life is expected. To reduce the test time on extremely long fatigue tests (greater than 10^6 cycles of 24000 flight hours), test may be censored at a specified lifetime. The stress level used in the fatigue tests should be selected so that the fatigue threshold can be established. For common carbon/epoxy composites under typical spectra, the threshold stress level would be approximately 60% of the mean static strength. This may not be true for rotorcraft high cycle (10^7 - 10^9) fatigue structures which require special evaluation to establish thresholds. The test data should be interpreted for B-basis life/stress relationship (see for example Reference 4.11.2(q)).

Several factors determine the test complexity of composite design development tests. These are: structural geometry complexity, hygrothermal environment simulation, fatigue load spectrum simulation including load rates, and mixed composite/metal structure interaction. The levels of complexity in the design development testing should be functions of the design feature being validated and the failure mode. Special attention should be given to correct failure mode simulation since failure modes are frequently dependent on the test environment. In particular, the influence of complex loading on the local stress at a given design feature must be evaluated. In composites, out-of-plane stresses can be detrimental to structural integrity and, therefore, require careful evaluation.

The environmental complexity necessary for fatigue design development testing will depend on the structural hygrothermal history. Three factors must be considered. These are: structural temperature for each mission profile, the load/temperature relationships for the aircraft, and the moisture content as a

function of the aircraft usage and structure thickness. In order to obtain these data, it is necessary to derive the real time load-temperature profiles for each mission in the aircraft's history, unless a simple end-of-lifetime moisture content and applicable temperature can be used. These relationships will have a significant influence on the environmental fatigue test requirements.

An example of this testing philosophy is given in Reference 4.11.1.1(e). These relationships strongly depend on the aircraft type, configuration and mission requirements and must be carefully developed on a case by case basis. The structural material should be selected to meet these mission requirements without exceeding the material operating limit.

No significant load sequence effect on fatigue life has been observed in composite materials. However, studies on fixed wing aircraft structural load spectrum variations have shown that carbon/epoxy composites are extremely sensitive to variation in the number of high loads in the fatigue spectrum (Reference 4.11.2(r)). In contrast, truncation of low load does not significantly affect fatigue life. Therefore, high loads in the fatigue spectrum must be carefully simulated in developing load spectrum for fatigue testing. Low loads may be truncated to save test time. It has been observed that the temperature spectrum has not significant effects on fatigue life, however, temperature spectrum truncation should be a consideration in planning fatigue tests. Rotorcraft exception from this generalization. Fatigue testing of mixed metal/composite structure may introduce conflicting requirements and should be evaluated on an individual basis.

The number of replicates for each design development test should be sufficient to verify the critical failure mode and provide a reasonable estimate of the required fatigue reliability. The test effort should be concentrated on the most critical design features of the structure. The number of replicates should be increased for these areas of concern.

Full-scale durability test may not always be necessary for structures with non-fatigue critical metal parts, provided the design development testing and full-scale static test are successful. For mixed composite/metal structures, with fatigue critical metal parts, a two lifetime ambient test should be required to demonstrate durability validation of the metal parts.

4.11.3 Damage resistance

In its normal operation, the aircraft can be expected to be subjected to potential damage from sources such as maintenance personnel and tools, runway debris, service equipment, exposure to hail and lightning, etc. Even during initial manufacturing and assembly, parts are subject to dropped tools, bumps during transportation to assembly locations, etc. The aircraft structure must be able to endure a reasonable level of such incidents without requiring costly rework or downtime. Providing this necessary damage resistance is an important design function. Unfortunately for the designer, providing adequate damage resistance may not always be the most popular task. Resistance to damage requires robustness. This requirement commonly necessitates the addition of extra material above that necessary to carry the structural loads. As a result, there are many pressures to compromise because of competing goals for minimum weight and cost.

In order to establish minimum levels of damage resistance, various requirements for aircraft structure have been identified. The Air Force requirements are defined in their General Specification for Aircraft Structures, AFGS-87221A. In general, the Specification defines the type and level of low energy impact which must be sustained without structural impairment, moisture ingestion or a requirement for repair. It provides provision for such incidents as dropped tools, hail, and impact from runway debris. The aircraft is zoned depending on whether the region has high or low susceptibility to damage and its required damage resistance defined by other government agencies, industry companies and the Aerospace Industries Association (AIA).

In defining the requirements for damage resistance, the type of structure is pertinent. For example, the level of impact energy which typically must be sustained by honeycomb sandwich control surfaces

without requiring repair or allowing moisture ingestion is quite low, e.g., 4 to 6 in-lb (0.5 to 0.7 J). This is partially because these parts must be kept very light, consequently, damage resistance has admittedly been compromised. Repair is facilitated somewhat because these parts can usually be readily replaced with spares while repairs are being accomplished in the shop. Because of their light construction, however, they must be handled carefully to prevent further damage during processing or transport. By contrast, the damage resistance requirement for primary laminate structure, which is not normally readily removable from the aircraft, is much higher, e.g., 48 in-lb (5.4 J). In addition to such impact induced loads, there also needs to be requirements of resistance to damage from normal handling and step loads that might be encountered in manufacturing and airline environments. Suggested for these have been the following:

Handling loads:

Difficult access	50 lb (23 kg) over a 4 sq-in (26 cm^2) area
Overhead easy access	150 lb (68 kg) over a 4 sq-in (26 cm^2) area

"Difficult access" is interpreted as finger tips only.
"Overhead access" is interpreted as the ability to grip and hang by one hand.

Step loads:

Difficult access	300 lb (140 kg) over a 20 sq-in (130 cm^2) area
Easy access from above	600 lb (270 kg) over a 20 sq-in (130 cm^2) area

"Difficult access" is interpreted as allowing a foothold on a structure with difficulty.
"Easy access from above" is interpreted as allowing a 2g step or "hop" onto the structure.
The area of 20 square inches (130 square centimeters) represents a single foot pad.

There are certain damage susceptible regions of the airplane that require special attention. Examples of these are the lower fuselage and adjacent fairings, lower surfaces of the inboard flaps and areas around doors. These need to be reinforced with heavier structure and perhaps fiberglass reinforcement, i.e., in lieu of graphite. In addition to the above, structure in the wheel well area needs special attention because of damage susceptibility from tire disintegration. Similarly, structure in the vicinity of the thrust reversers is damage prone due to ice or other debris thrown up from the runway.

Minimum weight structure, such as that used for fairings, can cause excess maintenance problems if designed too light. For example, sandwich with honeycomb core that is too low density is unacceptable for commercial aircraft application. Also, face sheets must have a minimum thickness to prevent moisture entrance to the core. The design should not rely on the paint to provide the moisture barrier. Experience has shown that too often the paint erodes or is abraded and then moisture enters.

Honeycomb sandwich areas with thin skins adjacent to supporting fittings are particularly vulnerable to damage during component installation and removal. Consequently, use solid laminate construction within a reasonable working distance of fittings.

Trailing edges of control panels are most vulnerable to damage. The aft four inches are especially subject to ground collision and handling and also to lightning strike. Repairs in this region can be difficult because both the skins and the trailing edge reinforcement may be involved. A desirable approach for the design is to provide a load carrying member to react loads forward of the trailing edge, and material for the trailing edge, itself, that will be easily repairable and whose damage will not compromise the structural integrity of the component.

In general, damage resistance is improved by thicker laminates and, in the case of sandwich, by the use of denser core. The use of a core with some minimum thickness is also desirable. The reason is that this provides a degree of protection of the inner face, which if it does become damaged, is difficult to repair. The use of reinforcement fibers with higher strain, such as fiberglass or aramid as opposed to

graphite in laminates, also provides improved damage resistance. Similarly, improvement is gained by the use of higher modulus, higher strain graphite fibers.

A most effective method for obtaining improved damage resistance is by the use of tougher resin systems. Notable demonstrations have been made comparing tough thermoplastic resin laminates with less tough conventional thermosets. The energy required to initiate damage in the thermoplastics, as measured by instrumented impactors, was much higher. Additionally, when damage did occur, the damaged region was much smaller. Likewise, in service demonstrations, the thermoplastics have shown marked damage resistance improvement. An example is the tests on comparative landing gear doors conducted on F-5 and T-38 aircraft by Northrop. Similarly, substantial improvements are expected from the use of toughened epoxy or bismaleimide systems as opposed to the untoughened resins.

Other items that either improve damage resistance or aid in the repair include having a layer of fabric as the exterior ply of tape laminates. The outer fabric ply is more resistant to scratches and abrasion and allows drilling of the laminate without the otherwise occurrence of fiber breakout.

Laminate edges should not be positioned so they are directly exposed to the air stream since they are then subject to delamination. Options include:

a) Provide non-erosive edge protection such as a cocured metal edge member.
b) Provide an easily replaceable sacrificial material to wrap the edges.
c) Locate the forward edge below the level of the aft edge of the next panel forward.

High energy lightning strikes can cause substantial damage to composite surface structure. Resistance at fasteners and connections, in particular, generates heat that causes burning and delaminations. Minor attachments, also, can cause significant damage, particularly to the tips and trailing edges. The following are guidelines to reduce the repair requirement:

a) At critical locations, provide easily replaceable conductive material with adequate conductive area.
b) Provide protection at tips and along trailing edge spans.
c) Make all conductive path attachments easily accessible.

Another item, although not directly damage resistance, involves the judicious use of blind fasteners. Such fasteners that must be drilled out for removal result in a high percentage of damaged holes. A suggestion is to use nut plates with reusable screws for closeout panel attachment, where access to the far side of a panel is restricted or otherwise where use of a normal type fastener is prevented.

4.11.4 Summary

- Damage is categorized as having occurred during manufacture or in-service.

- Routine quality inspections should uncover manufacturing-related damage. However, "rogue defects" will escape detection and should be accounted for in the design process.

- Draft manufacturing and in-service impact damage tolerance requirements typically address both minimum detection measured by dent depth, and impact energy. Given that damage can go undetected, it is important to demonstrate by both analysis and test that the maximum realistic undetectable damage will not reduce the structural strength below design ultimate load.

- A composite material's delamination damage tolerance can be determined, qualitatively, by its laminate matrix fracture toughness properties, G_I, G_{II}, and G_{III}.

- High strain-to-failure aramid and glass fiber composites typically exhibit greater damage tolerance than carbon fiber composites, but also exhibit lower strengths. Integrating glass surface plies or through thickness stitching represent two means of increasing a laminate's damage tolerance.

In general, organic matrix composites exhibit different durability characteristics compared to metals:

- Composite laminates, loaded in-plane, are less fatigue insensitive; they exhibit greater lives at stresses closer to ultimate strength.

- They are more sensitive to compression-dominated fatigue or reversed loading ($R<0$).

- In-plane fatigue damage usually begins with matrix cracking and ends with fiber breakage leading eventually to catastrophic failure.

4.12 VIBRATION

4.12.1 Introduction

4.12.2 Stacking sequence effects

Vibration characteristics of laminated plates are also sensitive to laminate stacking sequence (LSS). As was the case with bending and buckling of laminated plates, complex interactions between LSS, plate geometry and boundary conditions will not allow simple rules relating LSS to vibrations. Instead, such rules must be established for specific structure and boundary conditions. This indicates a need to use proven analysis methods as design tools for predicting dimensional stability of composite structure subjected to dynamic load conditions.

Figure 4.12.2 is one example of the complex interactions between LSS, plate geometry, and the natural frequency in the first vibrational mode.[1] A design equation from Reference 4.7.1.9(c) which was based on analysis from Reference 4.12.2 was used to make the predictions shown in the figure. Note that the relative difference in fundamental frequencies for various LSS changes with plate geometry. Higher frequencies occur for square plates with preferential stacking of ±45° plies in outer layers. The strongest effect of LSS occurs for rectangular plates in which preferential stacking of outer plies oriented perpendicular to the longest plate dimension have the highest fundamental frequencies. Basic information on laminate stacking sequence effects is found in Section 4.6.5.

4.13 COMPUTER PROGRAMS

Numerous programs for finite element analysis and prediction of composite material properties are available. Information on many of these programs can be found in Reference 4.13. In addition, there are programs available from NASA through COSMIC, Computer Software Management Information Center, 112 Barrow Hall, The University of Georgia, Athens, Georgia, 30602, (404) 542-3265. It should be noted that the use of and the results from these computer codes rely on the model developed, the material properties selected, and the experience of the user.

4.14 CERTIFICATION REQUIREMENTS

[1] The LSS used in Figure 4.12.2 were chosen for illustrative purposes only and do not represent optimal LSS for a given application.

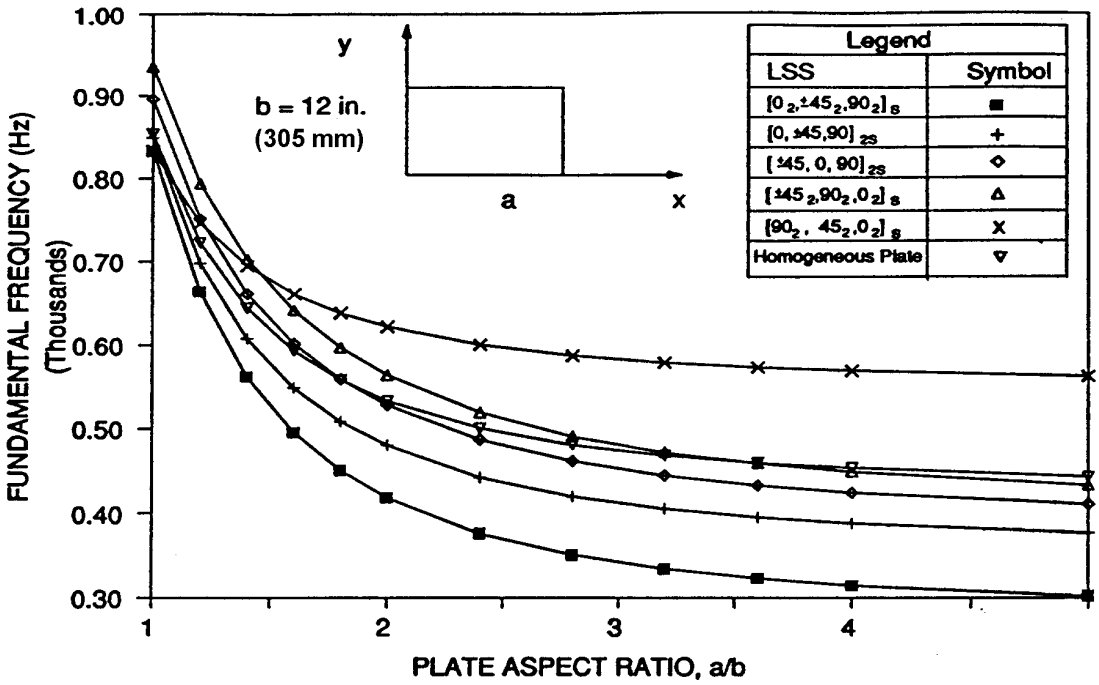

FIGURE 4.12.2 *Vibration analysis results for four sides simply-supported plates with variable aspect ratio.*

REFERENCES

4.2.2(a) Hashin, Z., "Theory of Fiber Reinforced Materials," NASA CR-1974, 1972.

4.2.2(b) Christensen, R.M., *Mechanics of Composite Materials*, Wiley-Interscience, 1979.

4.2.2.1(a) Pickett, G., AFML TR-65-220, 1965.

4.2.2.1(b) Adams, D.F., Doner, D.R., and Thomas, R.L., *J. Composite Materials*, Vol 1, 1967, pp. 4, 152.

4.2.2.1(c) Sendeckyj, G.P., "Elastic Behavior of Composites," *Mechanics of Composite Materials*, Vol. II, ed. Sendeckyj, G.P., Academic Press, 1974.

4.2.2.1(d) Hashin, Z. and Rosen, B.W., "The Elastic Moduli of Fiber-Reinforced Materials," *J. Appl. Mech.*, Vol 31, 1964, p. 223.

4.2.2.1(e) Hashin, Z., "Analysis of Properties of Fiber Composites with Anisotropic Constituents," *J. Appl. Mech.*, Vol 46, 1979, p. 543.

4.2.2.2(a) Christensen, R.M., *Theory of Viscoelasticity*, Academic Press, 1971.

4.2.2.2(b) Hashin, Z., "Viscoelastic Behavior of Heterogeneous Media," *J. Appl. Mech.*, Vol 32, 1965, p. 630.

4.2.2.2(c) Hashin, Z., "Viscoelastic Fiber Reinforced Materials," *AIAA Journal*, Vol 4, 1966, p. 1411.

4.2.2.2(d) Schapery, R.A., "Viscoelastic Behavior of Composites," in *Mechanics of Composite Materials*, Vol. II, ed. Sendeckyj, G.P., Academic Press, 1974.

4.2.2.3(a) Levin, V.M., "On the Coefficients of Thermal Expansion of Heterogeneous Materials," *Mekh. Tverd. Tela*, Vol 1, 1967, p. 88. English translation: *Mechanics of Solids*, Vol 2, 1967, p. 58.

4.2.2.3(b) Schapery, R.A., "Thermal Expansion Coefficients of Composite Materials Based on Energy Principles," *J. Composite Materials*, Vol 2, 1968, p. 380ff.

4.2.2.3(c) Rosen, B.W., "Thermal Expansion Coefficients of Composite Materials," Ph.D. Dissertation, Univ. of Pennsylvania, 1968.

4.2.2.3(d) Springer, G.S., "Environmental Effects on Epoxy Matrix Composites," ASTM STP 674, ed. Tsai, S.W., 1979, p. 291.

4.2.2.3(e) Tsai, S.W. and Hahn, H.T., *Introduction to Composite Materials*, Technomic, 1980.

4.2.3.1.1(a) Gucer, D.E. and Gurland, J., "Comparison of the Statistics of Two Fracture Modes," *J. Mech. Phys. Solids*, 1962, p. 363.

4.2.3.1.1(b) Zweben, C., "Tensile Failure Analysis of Composites," *AIAA Journal*, Vol 2, 1968, p. 2325.

4.2.3.1.2 Rosen, B.W., "Tensile Failure Analysis of Fibrous Composites," *AIAA Journal*, Vol 2, 1964, p. 1982.

4.2.3.1.3(a) Zweben, C., "A Bounding Approach to the Strength of Composite Materials," *Eng. Frac. Mech.*, Vol 4, 1970, p. 1.

4.2.3.1.3(b) Harlow, D.G. and Phoenix, S.L., "The Chain-of-Bundles Probability Model for the Strength of Fibrous Materials. I. Analysis and Conjectures, II. A Numerical Study of Convergence," *J. Composite Materials*, Vol 12, 1978, pp. 195, 300.

4.2.3.1.4 Rosen, B.W. and Zweben, C.H., "Tensile Failure Criteria for Fiber Composite Materials," NASA CR-2057, August 1972.

4.2.3.2(a) Dow, N.F. and Grundfest, I.J., "Determination of Most Needed Potentially Possible Improvements in Materials for Ballistic and Space Vehicles," GE-TIS 60SD389, June 1960.

4.2.3.2(b) Rosen, B.W., "Mechanics of Composite Strengthening," *Fiber Composite Materials*, Am. Soc. for Metals, Metals Park, Ohio, 1965.

4.2.3.2(c) Schuerch, H., "Prediction of Compressive Strength in Uniaxial Boron Fiber-Metal Matrix Composite Materials," *AIAA Journal*, Vol 4, 1966.

4.2.3.2(d) Rosen, B.W., "Strength of Uniaxial Fibrous Composites," in *Mechanics of Composite Materials,* Pergamon Press, 1970.

4.2.3.2(e) Chen, C.H. and Cheng, S., "Mechanical Properties of Fiber Reinforced Composites," *J. Composite Materials*, Vol 1, 1967, p. 30.

4.2.3.3(a) Drucker, D.C., Greenberg, H.J., and Prager, W., "The Safety Factor of an Elastic-Plastic Body in Plane Strain," *J. Appl. Mech.*, Vol 18, 1951, p. 371.

4.2.3.3(b) Koiter, W.T., "General Theorems for Elastic-Plastic Solids," *Progress in Solid Mechanics*, Sneddon and Hill, ed., North Holland, 1960.

4.2.3.3(c) Shu, L.S. and Rosen, B.W., "Strength of Fiber Reinforced Composites by Limit Analysis Method," *J. Composite Materials*, Vol 1, 1967, p. 366.

4.2.4(a) Tsai, S.W., "Strength Characteristics of Composite Materials," NASA CR-224, 1965.

4.2.4(b) Ashkenazi, E.K., *Zavod. Lab.*, Vol 30, 1964, p. 285; *Mezh. Polim*, Vol 1, 1965, p. 60.

4.2.4(c) Tsai, S.W. and Wu, E.M., "A General Theory of Strength for Anisotropic Materials," *J. Composite Materials*, Vol 5, 1971, p. 58.

4.2.4(d) Wu, E.M., "Phenomenological Anisotropic Failure Criterion," *Mechanics of Composite Materials*, ed. Sendeckyj, G.P., Academic Press, 1974.

4.2.4(e) Hashin, Z., "Failure Criteria for Unidirectional Fiber Composites," *J. Appl. Mech.*, Vol 47, 1980, p. 329.

4.3.2(a) Agarwal, B.D. and Broutman, L.J., *Analysis and Performance of Fiber Composites*, John Wiley & Sons, New York, NY, 1980.

4.3.2(b) Ashton, J.E. and Whitney, J.M., *Theory of Laminated Plates*, Technomic Publishing Co., Inc., Westport, CT, 1970.

4.3.2(c) Hussein, R.M, *Composite Panels/Plates: Analysis and Design*, Technomic Publishing Co., Inc., Westport, CT, 1986.

4.3.2(d) Jones, R.M., *Mechanics of Composite Materials*, Scripta Book Co., Washington, DC, 1975.

4.3.2(e) Tsai, S.W. and Hahn, H.T., *Introduction to Composite Materials*, Technomic Publishing Co., Inc., Westport, CT, 1980.

4.3.4 Shen, C. and Springer, G.S., "Moisture Absorption and Desorption of Composite Materials," *J. Composite Materials*, Vol 10, 1976, p. 1.

4.3.4.2(a) Chamis, C.C., "A Theory for Predicting Composite Laminate Warpage Resulting From Fabrication," 30th Anniversary Technical Conf., Reinforced Plastics/Composites Institute, The Society of Plastics Industry, Inc., Sec 18-C, 1975, pp. 1-9.

4.3.4.2(b) Hyer, M.W., "Some Observations on the Cured Shape of Thin Unsymmetric Laminates," *J. Composite Materials*, Vol. 15, 1981, pp. 175-194.

4.3.4.2(c) Hyer, M.W., "Calculations of Room Temperature Shapes of Unsymmetric Laminates," *J. Composite Materials*, Vol. 15, 1981, pp. 296-310.

4.3.5.5 Hashin, Z., Bagchi, D., and Rosen, B.W., "Nonlinear Behavior of Fiber Composite Laminates," NASA CR-2313, April 1974.

4.4 Flaggs, D.L. and Kural, M.H., "Experimental Determination of the In Situ Transverse Lamina Strength in Graphite/Epoxy Laminates", *Journal of Composite Materials*, Vol. 16, March, 1982, pp. 103-115.

4.4.1.1(a) Hashin, Z., "Failure Criteria for Unidirectional Fiber Composites", *Journal of Applied Mechanics*, Vol. 47, June, 1980, pp. 329-334.

4.4.1.1(b) Fiber Composite Analysis and Design, Federal Aviation Administration, DOT/FAA/CT-85/6)

4.4.4(a) Savin, G.N., "Stress Distribution Around Holes," NASA TT-F-607, November, 1970.

4.4.4(b) Whitney, J.M. and Nuismer, R.J., "Stress Fracture Criteria for Laminated Composites Containing Stress Concentrations," *J. Composite Materials*, Vol 8, 1974, p. 253.

4.4.4(c) Daniel, I.M., Rowlands, R.E., and Whiteside, J.B., "Effects of Material and Stacking Sequence on Behavior of Composite Plates With Holes," *Experimental Mechanics*, Vol. 14, 1974, pp. 1-9.

4.4.4(d) Walter, R.W. Johnson, R.W. June, R.R., and McCarty, J.E., "Designing for Integrity in Long-Life Composite Aircraft Structures," *Fatigue of Filamentary Composite Materials*, ASTM STP 636, pp. 228-247, 1977.

4.4.4(e) Aronsson, C.G., "Stacking Sequence Effects on Fracture of Notched Carbon Fibre/Epoxy Composites," *Composites Science and Technology*, Vol. 24, pp. 179-198, 1985.

4.4.4(f) Lagace, P.A., "Notch Sensitivity and Stacking Sequence of Laminated Composites," ASTM STP 893, pp. 161-176, 1986.

4.4.4(g) Harris C.E. and Morris, D.H., "A Fractographic Investigation of the Influence of Stacking Sequence on the Strength of Notched Laminated Composites," ASTM STP 948, 1987, pp. 131-153.

4.4.5(a) Murthy P.L.N, and Chamis, C.C., "Free-Edge Delamination: Laminate Width and Loading Conditions Effects," *J. of Composites Technology and Research*, JCTRER, Vol. 11, No. 1, 1989, pp. 15-22.

4.4.5(b) O'Brien, T.K., "The Effect of Delamination on the Tensile Strength of Unnotched, Quasi-isotropic, Graphite/Epoxy Laminates," *Proc. of the SESA/JSME International Conf. on Experimental Mechanics*, Honolulu, Hawaii, May, 1982.

4.4.5(c) Bjeletich, J.G., Crossman F.W., and Warren, W.J., "The Influence of Stacking Sequence on Failure Modes in Quasi-isotropic Graphite-Epoxy Laminates," *Failure Modes in Composites IV*, AIME, 1977, pp. 118.

4.4.5(d) Crossman, F.W., "Analysis of Delamination," *Proc. of a Workshop on Failure Analysis and Mechanisms of Failure of Fibrous Composite Structures*, NASA Conf. Publ. 2278, 1982, pp. 191-240.

4.4.5(e) O'Brien, T.K., "Analysis of Local Delaminations and Their Influence on Composite Laminate Behavior," *Delamination and Debonding of Materials*, ASTM STP 876, 1985, pp. 282-297.

4.4.5(f) Sun C.T. and Zhou, S.G., "Failure of Quasi-Isotropic Composite Laminates with Free Edges," *J. Reinforced Plastics and Composites*, Vol. 7, 1988, pp. 515-557.

4.4.5(g) O'Brien, T.K., "Characterization of Delamination Onset and Growth in a Composite Laminate," *Damage in Composite Materials*, ASTM STP 775, 1982, pp. 140-167.

4.4.5(h) Whitcomb J.D. and Raju, I.S., "Analysis of Free-Edge Stresses in Thick Composite Laminates," *Delamination and Debonding of Materials*, ASTM STP 876, 1985, pp. 69-94.

4.4.5(i) Lekhnitskii, S.G., *Anisotropic Plates*, Gordon and Breach Science Publ., 1968.

4.4.5(j) Garg, A.C., "Delamination-A Damage Mode In Composite Structures," *Eng. Fracture Mech.*, Vol. 29, No. 5, 1988, pp. 557-584.

4.4.5(k) Lagace, P.A., "Delamination in Composites: Is Toughness the Key?" *SAMPE J.*, Nov/Dec, 1986, pp. 53-60.

4.4.5(l) Soni S. R. and Kim, R.Y., "Delamination of Composite Laminates Stimulated by Interlaminar Shear," *Composite Materials: Testing and Design (Seventh Conf.)*, ASTM STP 893, 1986, pp. 286-307.

4.4.5(m) Chan, W.S., Rogers, C., and Aker, S., "Improvement of Edge Delamination Strength of Composite Laminates Using Adhesive Layers," *Composite Materials: Testing and Design (Seventh Conf.)*, ASTM STP 893, 1986, pp. 266-285.

4.4.5(n) Chan W.S. and Ochoa, O.O., "Suppression of Edge Delamination in Composite Laminates by Terminating a Critical Ply near the Edges," Presented at the AIAA/ASMR/ASCE/AHS 29th Structures, Structural Dynamics and Materials Conf., AIAA Paper #88-2257, 1988, pp. 359-364.

4.4.5(o) Vizzini, A.J., "Prevention of Free-Edge Delamination via Edge Alteration," Presented at the AIAA/ASME/ASCE/AHS 29th Structures, Structural Dynamics and Materials Conference, AIAA Paper #88-2258, 1988, pp. 365-370.

4.4.5(p) Sun, C.T., "Intelligent Tailoring of Composite Laminates," *Carbon*, Vol. 27, No. 5, 1989, pp. 679-687.

4.4.5(r) Lagace P.A. and Cairns, D.S., "Tensile Response of Laminates to Implanted Delaminations," *Proc. of 32nd Int. SAMPE Sym.*, April 6-9, 1987, pp. 720-729.

4.4.5.1(a) Shivakumar K.N. and Whitcomb, J.D., "Buckling of a Sublaminate in a Quasi-Isotropic Composite Laminate," NASA TM-85755, Feb, 1984.

4.4.5.1(b) Chai H. and Babcock, C.D., "Two-Dimensional Modelling of Compressive Failure in Delaminated Laminates," *J. of Composite Materials*, 19, 1985, pp. 67-98.

4.4.5.1(c) Vizzini A.J. and Lagace, P.A., "The Buckling of a Delaminated Sublaminate on an Elastic Foundation," *J. of Composite Materials*, 21, 1987, pp. 1106-1117.

4.4.5.1(d) Kassapoglou, C., "Buckling, Post-Buckling and Failure of Elliptical Delaminations in Laminates Under Compression," *Composite Structures*, 9, 1988, pp. 139-159.

4.4.5.1(e) Yin, W.L., "Cylindrical Buckling of Laminated and Delaminated Plates," Presented at the AIAA/ASMR/ASCE/AHS 27th Structures, Structural Dynamics and Materials Conference, AIAA Paper #86-0883, 1986, pp. 165-179.

4.4.5.1(f) Slomiana, M., "Fracture Mechanics of Delamination in Graphite-Epoxy Laminates Under Compression," PhD. Thesis, Drexel University, Philadelphia, PA, 1984.

4.4.5.1(g) Whitcomb, J.D., "Strain-Energy Release Rate Analysis of Cyclic Delamination Growth in Compressively Loaded Laminates," *Effects of Defects in Composite Materials*, ASTM STP 836, 1984, pp. 175-193.

4.4.5.1(h) Whitcomb, J.D., "Predicted and Observed Effects of Stacking Sequence and Delamination Size on Instability-Related Delamination Growth," *Proc. of American Society for Composites: 3rd Tech Conf*, 1988, pp. 678-687.

4.4.6.1.1(a) Jamison, R.D., "On the Interrelationship Between Fiber Fracture and Ply Cracking in Graphite/Epoxy Laminates," *Composite Materials: Fatigue and Fracture*, ASTM STP 907, 1986, pp. 252-273.

4.4.6.1.1(b) Kim, R.Y., "In-plane Tensile strength of Multidirectional Composite Laminates," UDRI-TR-81-84, University of Dayton Research Institute, Aug, 1981.

4.4.6.1.1(c) Ryder J.T. and Crossman, F.W., "A Study of Stiffness, Residual Strength and Fatigue Life Relationships for Composite Laminates," NASA CR-172211, Oct, 1983.

4.4.6.1.1(d) Sun C.T. and Jen, K.C., "On the Effect of Matrix Cracks on Laminate Strength," *J. Reinforced Plastics and Composites*, Vol. 6, 1987, pp. 208-222.

4.4.6.1.1(e) Bailey, J.E., Curtis, P.T., and Parvizi, A., "On the Transverse Cracking and Longitudinal Splitting Behavior of Glass and Carbon Fibre Reinforced Epoxy Cross Ply Laminates and the Effect of Poisson and Thermally Generated Strain," *Proc. R. Soc. London*, series A, 366, 1979, pp. 599-623.

4.4.6.1.1(f) Crossman, F.W. and Wang, A.S.D., "The Dependence of Transverse Cracking and Delamination on Ply Thickness in Graphite/Epoxy Laminates," *Damage in Composite Materials*, ASTM STP 775, American Society for Testing and Materials, 1982, pp. 118-139.

4.4.6.1.1(g) Flaggs, D.L. and Kural, M.H., "Experimental Determination of the In situ Transverse Lamina Strength in Graphite/Epoxy Laminates," *J. of Composite Materials*, Vol. 16, Mar. 1982, pp. 103-116.

4.4.6.1.1(h) Narin, J.A., "The Initiation of Microcracking in Cross-Ply Laminates: A Variational Mechanics Analysis," *Proc. Am Soc for Composites: 3rd Tech. Conf.*, 1988, pp. 472-481.

4.4.6.1.1(i) Flaggs, D.L., "Prediction of Tensile Matrix Failure in Composite Laminates," *J. Composite Materials*, 19, 1985, pp. 29-50.

4.4.6.1.1(j) Ilcewicz, L.B., Dost, E.F., McCool, J.W., and Grande, D.H., "Matrix Cracking in Composite Laminates With Resin-Rich Interlaminar Layers," Presented at 3rd Symposium on Composite Materials: Fatigue and Fracture, Nov. 6-7, Buena Vista, Fla., ASTM, 1989.

4.4.6.2(a) Shuart, M.J., "Short-Wavelength Buckling and Shear Failures for Compression-Loaded Composite Laminates," NASA TM-87640, Nov, 1985.

4.4.6.2(b) Shuart, M.J., "Failure of Compression-Loaded Multi-Directional Composite Laminates," Presented at the AIAA/ASME/ASCE/AHS 19th Structures, Structural Dynamics and Materials Conf, AIAA Paper No. 88-2293, 1988.

4.4.6.2(c) Hahn, H.T. and Williams, J.G., "Compression Failure Mechanisms in Unidirectional Composites," *Composite Materials: Testing and Design (Seventh Conf.)*, ASTM STP 893, 1986, pp. 115-139.

4.4.6.2(d) Hahn H.T. and Sohi, M.M., "Buckling of a Fiber Bundle Embedded in Epoxy," *Composites Science and Technology*, Vol 27, 1986, pp. 25-41.

4.6.2(a) Manson, J. A. and Seferis, J. C., "Internal Stress Determination by Process Simulated Laminates," *ANTEC '87 Conference Proceedings*, SPE, May 1987.

4.6.2(b) Kays, A.O., "Exploratory Development on Processing Science of Thick-Section Composites," AFWAL-TR-85-4090, October 1985.

4.6.3(a) Chan, W.S., Rogers, C. and Aker, S., "Improvement of Edge Delamination Strength of Composite Laminates Using Adhesive Layers," *Composite Materials: Testing and Design*, ASTM STP 893, J.M. Whitney, ed., American Society for Testing and Materials, 1986.

4.6.3(b) Chan, W.S. and Ochoa, O.O., "An Integrated Finite Element Model of Edge-Delamination Analysis for Laminates due to Tension, Bending, and Torsion Loads," *Proceedings of the 28th Structures, Dynamics, and Materials Conference*, AIAA-87-0704, 1987.

4.6.3(c) O'Brien, T.K. and Raju, I.S., "Strain Energy Release Rate Analysis of Delaminations Around an Open Hole in Composite Laminates," *Proceedings of the 25th Structures, Structural Dynamics, and Materials Conference*, 1984, pp. 526-536.

4.6.3(d) Pagano, N.J. and Soni, S.R., "Global - Local Laminate Variational Method," International *Journal of Solids and Structures*, Vol 19, 1983, pp. 207-228.

4.6.3(e) Pipes, R.B. and Pagano, N.J., "Interlaminar Stresses in Composites Under Uniform Axial Extension," *J. Composite Materials*, Vol 4, 1970, p. 538.

4.7.1.1(a) Almroth, B. O., Brogan, F. W., and Stanley, G. W., "User's Manual for STAGS," NASA Contractor Report 165670, Volumes 1 and 2, March 1978.

4.7.1.1(b) Ashton, J. E. and Whitney, J. M., *Theory of Laminated Plates*, Technomic Publishers, 1970, pp. 125-128.

4.7.1.2 *Advanced Composites Design Guide, Volume II - Analysis,* Air Force Materials Laboratory, Advanced Development Division, Dayton, Ohio, January 1973, Table 2.2.2-1, pp. 2.2.2-12.

4.7.1.3(a) Spier, E. E., "On Experimental Versus Theoretical Incipient Buckling of Narrow Graphite/Epoxy Plates in Compression," AIAA-80-0686-Paper, published in *Proceedings of AIAA/ASME/ASCE/AHS 21st Structures, Structural Dynamics, & Materials Conference*, May 12-14, 1980, pp. 187-193.

4.7.1.3(b) Spier, E. E., "Local Buckling, Postbuckling, and Crippling Behavior of Graphite-Epoxy Short Thin Walled Compression Members," Naval Air Systems Command Report NASC-N00019-80-C-0174, June 1981, p. 22.

4.7.1.3(c) Arnold, R. R., "Buckling, Postbuckling, and Crippling of Materially Nonlinear Laminated Composite Plates," Ph.D. Dissertation, Stanford University, March 1983, p. 65.

4.7.1.3(d) Arnold, R. R. and Mayers, J., "Buckling, Postbuckling, and Crippling of Materially Nonlinear Laminated Composite Plates," *Internal Journal of Solids and Structures*, Vol 20, pp. 863-880. 82-0779-CP, AIAA/ASME/ASCE/AHS, published in the *Proceedings of the 23rd Structures, Structural Dynamics, and Materials Conference*, New Orleans, Louisiana, May 1982, pp. 511-527.

4.7.1.8(a) Chamis, C.C., "Buckling of Anisotropic Composites," *Journal of the Structural Division*, Am. Soc. of Civil Engineers, Vol. 95, No. 10, 1969, pp. 2119-2139.

4.7.1.8(b) Whitney, J.M., *Structural Analysis of Laminated Anisotropic Plates*, Technomic Publishing Co., Inc., Westport, CT, 1987.

4.7.1.8(c) "DOD/NASA Advanced Composites Design Guide, Volume II Analysis," Structures/Dynamics Division, Flight Dynamics Laboratory, Air Force Wright Aeronautical Laboratories, Wright-Patterson Air Force Base, OH, 1983.

4.7.1.8(d) Davenport, O.B., and Bert, C.W., "Buckling of Orthotropic, Curved, Sandwich Panels Subjected to Edge Shear Loads," *Journal of Aircraft*, Vol. 9, No. 7, 1972, pp. 477-480.

4.7.1.8(e) Spier, E.E., "Stability of Graphite/Epoxy Structures With Arbitrary Symmetrical Laminates," *Experimental Mechanics*, Vol. 18, No. 11, 1978, pp. 401-408.

4.7.2(a) Spier, E.E., "On Experimental Versus Theoretical Incipient Buckling of Narrow Graphite/Epoxy Plates in Compression," AIAA-80-0686-Paper, published in Proceedings of AIAA/ASME/ASCE/AHS 21st Structures, Structural Dynamics, & Materials Conference, May 12-14, 1980, pp. 187-193.

4.7.2(b) Spier, E.E., "Local Buckling, Postbuckling, and Crippling Behavior of Graphite-Epoxy Short Thin Walled Compression Members," Naval Air Systems Command Report NASC-N00019-80-C-0174, June 1981.

4.7.2(c) Spier, E.E., "On Crippling and Short Column Buckling of Graphite/Epoxy Structure with Arbitrary Symmetrical Laminates," Presented at SESA 1977 Spring Meeting, Dallas, TX, May 1977.

4.7.2(d) Spier, E.E. and Klouman, F.K., "Post Buckling Behavior of Graphite/Epoxy Laminated plates and Channels," Presented at Army Symposium on Solid Mechanics, AMMRC MS 76-2, Sept. 1976.

4.7.2(e) Renieri, M.P. and Garrett, R.A., "Investigation of the Local Buckling, Postbuckling and Crippling Behavior of Graphite/Epoxy Short Thin-Walled Compression Members," McDonnell Aircraft Report MDC A7091, NASC, July 1981.

4.7.2(f) Bonanni, D.L., Johnson, E.R., and Starnes, J.H., "Local Crippling of Thin-Walled Graphite-Epoxy Stiffeners," AIAA Paper 88-2251.

4.7.2(g) Spier, E.E., "Postbuckling Fatigue Behavior of Graphite-Epoxy Stiffenersm," AIAA Paper 82-0779-CP, AIAA/ASME/ASCE/AHS, published in the Proceedings of the 23rd Structures, Structural Dynamics, & Materials Conference, New Orleans, LA, May 1982, pp. 511-527.

4.7.2(h) Deo, R.B., et al, "Design Development and Durability Validation of Postbuckled Composite and Metal Panels," Air Force Flight Dynamics Laboratory Report, WRDC-TR-89-3030, 4 Volumes, November 1989.

4.11.1.4(a) Cairns, D.S., "Impact and Post-Impact Response of Graphite/Epoxy and Kevlar/Epoxy Structures," PhD Dissertation, Telac Report #87-15, Dept. of Aeronautics and Astronautics, Massachusetts Institute of Technology, Aug, 1987.

4.11.1.4(b) Gosse J.H. and Mori, P.B.Y., "Impact Damage Characterization of Graphite/Epoxy Laminates," *Proc. of the American Society for Composites: 3rd Tech Conf*, 1988, pp. 344-353.

4.11.1.4(c) Dost, E.F., Ilcewicz, L.B., and Gosse, J.G., "Sublaminate Stability Based Modeling of Impact-Damaged Composite Laminates," *Proc. of the American Society for Composites: 3rd Tech Conf*, 1988, pp. 354-363.

4.11.1.4(d) Ilcewicz, L.B., Dost, E.F., Coggeshall, R.L., "A Model for Compression After Impact Strength Evaluation," *Proc. of 21st International SAMPE Tech. Conf.*, 1989, pp. 130-140.

4.11.1.4(e) Dost, E.F., Ilcewicz, L.B., and Avery, W.B., "The Effects of Stacking Sequence On Impact Damage Resistance and Residual Strength for Quasi-Isotropic Laminates," Presented at 3rd Symposium on Composite Materials: Fatigue and Fracture, Nov. 6-7, Buena Vista, Fla., ASTM, 1989.

4.11.2(a) Broutman, L.J., and Sahu, S., "A New Theory to Predict Cumulative Fatigue Damage in Fiberglass Reinforced Plastics," *Composite Materials: Testing and Design,* ASTM STP 497, 1972, pp. 170-188.

4.11.2(b) Halpin, J.C., Jerina, K.L., and Johnson, T.A., "Characterization of Composites for the Purpose of Reliability Prediction," *Analysis of Test Methods for High Modulus Fibers and Composites*, ASTM STP 521, 1973, pp. 5-65.

4.11.2(c) McLaughlin, P.V., Jr., Kulkarni, S.V., Huang, S.N., and Rosen, B.W., "Fatigue of Notched Fiber Composite Laminates: Part I-Analysis Model," NASA Contract Report No. CR-132747, March 1975.

4.11.2(d) Hahn, H.T., and Kim, R.Y., "Proof Testing of Composite Materials," *Journal of Composite Materials*, Vol 2, No. 3, July 1975, pp. 297-311.

4.11.2(e) Yang, J.N., and Liu, M.D., "Residual strength Degradation Model and Theory of Periodic Proof Tests for Graphite/Epoxy Laminates," AFML-TR-76-225, 1976.

4.11.2(f) Kulkarni, S.V., McLaughlin, P.V., Jr., and Pipes, R.B., "Fatigue of Notched Fiber Composite Laminates: Part II - Analytical and Experimental Evaluation," NASA Contract Report No. CR-145039, April 1976.

4.11.2(g) Ryder, J.T., and Walker, E.K., "Ascertainment of the Effect of Compression Loading on the Fatigue Lifetime of Graphite/Epoxy Laminates for Structural Applications," AFML-TR-76-241, December 1976.

4.11.2(h) Sendeckyj, G.P., and Stalnaker, H.D., "Effect of Time at Load on Fatigue Response of $[(0/\pm45/90)_s]_2$ T300/5208 Graphite-Epoxy Laminate," *Composite Materials: Testing and Design*, ASTM STP 617, 1977.

4.11.2(i) Grimes, G.C., "Structures Design Significance of Tension-Tension Fatigue Data on Composites," *Composite Materials: Testing and Design*, ASTM STP 617, 1977, pp. 106-119.

4.11.2(k) Williams, R.S., and Reifsnider, K.L., "Strain Energy Release Rate Method for Predicting Failure Modes in Composite Materials," ASTM STP 677, 1979, pp. 629-650.

4.11.2(l) Ratwani, M.M., and Kan, H.P., "Compression Fatigue Analysis of Fiber Composites," Report No. NADC-78049-60, September 1979.

4.11.2(m) Ryder, J.T., and Walker, E.K., "The Effect of Compressive Loading on the Fatigue Lifetime of Graphite/Epoxy Laminates," AFML-TR-79-4128, October 1979.

4.11.2(n) Rotem, Al, "Fatigue Mechanism of Multidirectional Laminate Under Ambient and Elevated Temperature," *Proceedings, Third International Conference on Composite Materials*, Paris, 1980, pp. 146-161.

4.11.2(o) Saff, C.R., "Compression Fatigue Life Prediction Methodology for Composite Structures-Literature Survey," Report No. NADC-78203-60, June 1980.

4.11.2(p) Lauraitis, K.N., Ryder, J.T., and Pettit, D.E., "Advanced Residual Strength Degradation Rate Modeling for Advanced Composite Structures," Vol. I, II, and III, AFWAL-TR79-3095, July 1981.

4.11.2(q) Sendeckyj, G.P., "Fitting Models to Composite Materials Fatigue Data," ASTM STP 734, 1981, pp. 245-260.

4.11.2(r) Badaliance, R., and Dill, H.D., "Effects of Fighter Attack Spectrum on Composite Fatigue Life," AFWAL-TR-81-3001, March 1981.

4.11.2(s) Ratwani, M..M. and Kan, H.P., "Development of Analytical Techniques for Predicting Compression Fatigue Life and Residual Strength of Composites," Report No. NADC-82104-60, March 1982.

4.11.2(t) Liechti, K.M., Reifsnider, K.L., Stinchcomb, W.W., and Ulman, D.A., "Cumulative Damage Model for Advanced Composite Materials: Phase I Final Report," AFWAL-TR-82-4094, July 1982.

4.11.2(u) Chou, P.C., Wang, A.S.D., and Miller, H.R., "Cumulative Damage Model for Advanced Composite Materials: Phase I Final Report," AFWAL-TR-82-4083, September 1982.

4.11.2(v) Badaliance, R., and Dill, H.D., "Compression Fatigue Life Prediction Methodology for Composite Structures, Volume I-Summary and Methodology Development," Report No. NADC-78203-60, September 1982.

4.11.2(w) Baldini S.E., and Badaliance, R., "Compression Fatigue Life Prediction Methodology for Composite Structures, Volume II-Test Data and Damage Tracking," Report No. NADC-78203-60, September 1982.

4.11.2(x) Ryder, J.T., and Crossman, F.W., "A Study of Stiffness, Residual Strength and Fatigue Life Relationships for Composite Laminates," NASA Contract No. CR-172211, October 1983.

4.11.2(y) Wang, A.S.D., Chou, P.C., and Lai, C.S., "Cumulative Damage Model for Advanced Composite Materials: Phase II Final Report," AFWAL-TR-84-4004, March 1984.

4.11.2(z) Miller, H.R., Reifsnider, K.L., Stinchcomb, W.W., Ulman, D.A., and Bruner R.D., "Cumulative Damage Model for Advanced Composite Materials: Final Report," AFWAL-TR-85-4069, June 1985.

4.11.2(aa) Wang, A.S.D., Chou, P.C., Lai, C.S., and Bucinell, R.B., "Cumulative Damage Model for Advanced Composite Materials," Final Report, AFWAL-TR-85-4104, October 1985.

4.11.2(ab) Whitehead, R.S., and Schwarz, M.G., "The Role of Fatigue Scatter in the Certification of Composite Structures," presented at ASTM Symposium on the Long Term Behavior of Composites, Williamsburg, Virginia, March 1982.

4.11.2(ac) Whitehead, R.S., Kan, H.P., Cordero, R., and Saether, E.S., "Certification Testing Methodology for Composite Structures," Report No. NADC-86132-60, January 1986.

4.11.2(ad) Sanger, K.B., "Certification Testing Methodology for Composite Structures," Report No. NADC-86132-60, January 1986.

4.11.2(ae) Wong, R. and Abbot, R., "Durability and Damage Tolerance of Graphite/Epoxy Honeycomb Structures," *SAMPE 35th International Symposium and Exhibition*, April 1990.

4.11.2(af) Rogers, Chan, and Martin, "Design Criterion for Damage Tolerance Helicopter Primary Structure of Composite Materials," Volume I-Final Design Criteria, USAAVSCOM-TR-87-D-3A, June 1987.

4.11.2.1(a) Whitehead, R.S., "A Review of the Rationale for Durability Validation of Composite Structures," Proceedings of the 5th DoD/NASA Conference on Fibrous Composites in Structural Design, New Orleans, Louisiana, January 1981.

4.11.2.1(b) Whitehead, R.S., "Durability Certification Data for Composite Structures," presented at the 6th DoD/NASA Conference on Fibrous Composites in Structural Design, New Orleans, Louisiana, January 1983.

4.11.2.1(c) Whitehead, R.S., Ritchie, G.L., and Mullineaux, J.L., "Durability of Composites," presented at 9th Mechanics of Composites Review, Dayton, Ohio, October 1983.

4.11.2.1(d) Whitehead, R.S. and Deo, R.B., "Wing/Fuselage Program Durability Methodology," presented at the 6th Mechanics of Composites Review, Dayton, Ohio, November 1980.

4.11.2.1(e) Whitehead, R.S., et al, "Composite Wing Fuselage Program," Contract No. F33615-79-C-3203, Interim Reports 1-11, October 1979 - October 1984.

4.12.2 Lackman, L.M., Lin, T.H., Konishi, D.Y., and Davidson, J.W., "Advanced Composites Data for Aircraft Structural Design - Volume III," AFML-TR-70-58, Vol. III, Los Angeles Div/Rockwell, Dec, 1970.

4.13 Brown, R. T., "Computer Programs for Structural Analysis," *Engineered Materials Handbook, Volume 1 Composites*, ASM International, Metals Park, Ohio, 1987, pp. 268 - 274.

This page intentionally left blank

Index Worksheet